

The Anatomy of *Asilisaurus kongwe*, a Dinosauriform from the Lifua Member of the Manda Beds (~Middle Triassic) of Africa

STERLING J. NESBITT ^{1*}, MAX C. LANGER,² AND MARTIN D. EZCURRA ³

¹Department of Geosciences, Virginia Tech, Blacksburg, Virginia

²Departamento de Biologia, Universidade de São Paulo, Ribeirão Preto, Brazil

³Sección Paleontología de Vertebrados CONICET—Museo Argentino de Ciencias Naturales “Bernardino Rivadavia”, Buenos Aires, Argentina

ABSTRACT

The diagnosis of Dinosauria and interrelationships of the earliest dinosaurs relies on careful documentation of the anatomy of their closest relatives. These close relatives, or dinosaur “precursors,” are typically only documented by a handful of fossils from across Pangea and nearly all specimens are typically missing important regions (e.g., forelimbs, pelvis, skulls) that appear to be important to help resolving the relationships of dinosaurs. Here, we fully describe the known skeletal elements of *Asilisaurus kongwe*, a dinosauriform from the Middle Triassic Manda Beds of the Ruhuhu Basin of Tanzania. The taxon is known from many disarticulated and partially articulated remains and, most importantly, from a spectacularly preserved associated skeleton of an individual containing much of the skull, pectoral and pelvic girdles, forelimb and hindlimb, and parts of the vertebral column including much of the tail. The unprecedented detail of the anatomy indicates that *Asilisaurus kongwe* had a unique skull that was short and had both a premaxillary and dentary edentulous margin, but retained a number of character states plesiomorphic for Archosauria, including a crocodylian-like ankle configuration and a rather short foot with well-developed metatarsals I and V. Additionally, character states present across the skeleton of *Asilisaurus kongwe* suggest it is more closely related to *Silesaurus opolensis*

ABBREVIATIONS: CMNH = Carnegie Museum of Natural History, Pittsburgh, Pennsylvania, USA; CRILAR-Pv = Centro Regional de Investigaciones Científicas y Transferencia Tecnológica, Anillaco, Argentina; GR = Ghost Ranch Ruth Hall Museum of Paleontology, Ghost Ranch, New Mexico, USA; ISI = Indian Statistical Institute, Kolkata, India; MACN-Pv = Museo Argentino de Ciencias Naturales “Bernardino Rivadavia,” Paleontología de Vertebrados, Buenos Aires, Argentina; MB = Museum für Naturkunde der Humboldt Universität, Berlin, Germany; MCN = Museu de Ciências Naturais, Fundação Zoobotânica do Rio Grande do Sul, Porto Alegre, Brazil; MCP = Museu de Ciências e Tecnologia da Pontifícia Universidade Católica do Rio Grande do Sul, Porto Alegre, Brazil; MCZ = Museum of Comparative Zoology, Harvard University, Cambridge, Massachusetts, USA; MNA = Museum of Northern Arizona, Flagstaff, Arizona, USA; NHMUK PV = Natural History Museum, London, Palaeontology Vertebrates, London, UK; NMT = National Museum of Tanzania, Dar es Salaam, Tanzania; PEFO = Petrified Forest National Park, Arizona, USA; PULR = Paleontología, Universidad Nacional de La Rioja, La Rioja, Argentina; PVL = Instituto Miguel Lillo, Tucumán, Argentina;

PVSJ = División de Paleontología de Vertebrados del Museo de Ciencias Naturales y Universidad Nacional de San Juan, San Juan, Argentina; SAM = Iziko South African Museum, Cape Town, South Africa; UCMP = University of California Museum of Paleontology, Berkeley, California, USA; ULBRA = Museu de Ciências Naturais, Universidade Luterana do Brasil, Canoas, Brazil; ZPAL = Institute of Paleobiology of the Polish Academy of Sciences, Warsaw, Poland

Grant sponsor: National Geographic Society; Grant number: NGS 7787-05; Grant sponsor: National Science Foundation; Grant numbers: NSF, NSF EAR-1337291, NSF EAR-1337569.

*Correspondence to: Sterling J. Nesbitt, Department of Geosciences, Virginia Tech, Blacksburg, VA 24061.

E-mail: sjn2104@vt.edu

Received 2 November 2018; Revised 21 March 2019; Accepted 12 April 2019.

DOI: 10.1002/ar.24287

Published online 00 Month 2019 in Wiley Online Library (wileyonlinelibrary.com).

than to dinosaurs; thus suggesting high homoplasy and parallel trends within Silesauridae and within lineages of early dinosaurs. The anatomy of *Asilisaurus kongwe* and detailed description of early members of clades found outside Dinosauria are clearly needed to untangle the seemingly complex character evolution of the skeleton within avemetatarsalians. *Anat Rec*, 00:000–000, 2019. © 2019 American Association for Anatomy

Key words: Dinosauria; evolution; Dinosauromorpha; Tanzania; dinosaur “precursor”; Mesozoic

The origin and early evolution of dinosaurs was critical in vertebrate evolution and the radiation of the group in the Triassic Period set the stage for their global takeover either at the end of the period or the beginning of the Jurassic Period (Langer et al., 2010; Brusatte et al., 2010a, 2010b). Why dinosaurs rose to prominent ecological roles in this critical time in Earth History has been hotly debated (Irmis, 2011). These debates have focused on the timing of the diversification of dinosaur groups and extinctions of various terrestrial vertebrate “competitors” (Bakker, 1968, 1971; Tucker and Benton, 1982; Benton, 1983; Brusatte et al., 2008) and the innate features of dinosaurs themselves (Langer et al., 2010; Brusatte et al., 2010a, 2010b; Langer, 2014). Dinosaurs appeared to be unique with respect to their contemporaries: they had unique anatomy throughout their skeleton (Gauthier, 1986; Novas, 1996), rates of growth faster than their contemporaries (Padian et al., 2001, 2004), and different biomechanical strategies (Bonaparte, 1984; Charig, 1984). These observations were largely based on comparing the earliest dinosaurs to other archosaurs, particularly purported “dinosaur precursors” such as *Lagerpeton chañarensis* (Romer, 1971; Sereno and Arcucci, 1994a), *Marasuchus* (= *Lagosuchus*) *lilloensis* (Romer, 1971; Bonaparte, 1984; Sereno and Arcucci, 1994b) and later, *Pseudolagosuchus major* (Arcucci, 1987). Unfortunately, all of these “precursors came from a single stratigraphic unit, the Chañares Formation, in Argentina (Ezcurra et al., 2017), were relatively incomplete (skulls and hands are largely unknown), and their small size made identification of anatomical features difficult or open to interpretation.

A great leap in our knowledge of “dinosaur precursors” came with the discovery of *Silesaurus opolensis* (Dzik, 2003; Dzik and Sulej, 2007; Fostowicz-Frelik and Sulej, 2010; Piechowski and Dzik, 2010; Piechowski et al., 2014; Piechowski et al., 2018) from the Carnian stage of Poland. The anatomy of articulated and well preserved skeletons of *Silesaurus opolensis* lead to the discovery of similar taxa from across Pangea from either reinterpreted material or new discoveries (Ezcurra, 2006; Parker et al., 2006; Ferigolo and Langer, 2007; Nesbitt et al., 2007, 2010; Irmis et al., 2007a; Small, 2009; Kammerer et al., 2012; Martínez et al., 2013; Peacock et al., 2013). Combined, these recognitions and discoveries showed that the “dinosaur precursors” were more abundant, taxonomically diverse, and came temporally before and lived with the earliest dinosaurs for more than 20 millions of years (Ezcurra, 2006; Irmis et al., 2007a; Nesbitt et al., 2010; Langer et al., 2013;

Marsh and Rowe, 2018). These discoveries were a breakthrough for understanding the origin of dinosaurs given that the origin of dinosaurian “uniqueness” could now be traced more easily through their close relatives. It was found that dinosaurs did have a number of unique anatomical and growth characteristics (Langer et al., 2010, 2013; Brusatte et al., 2014), but the once long-list of unique dinosaurian attributes, was whittled down to a remaining few.

The key to understanding how dinosaurs acquired their anatomy, physiology, and behavior lies in the relationships of their closest relatives, the silesaurids. A number of phylogenetic analyses including *Silesaurus*-like taxa found a “core clade” of these forms just outside Dinosauria to the exclusion of *Marasuchus lilloensis* and Lagerpetidae (Ezcurra, 2006; Irmis et al., 2007a; Nesbitt et al., 2010; Nesbitt, 2011; Kammerer et al., 2012; Martínez et al., 2013; Peacock et al., 2013; Bittencourt et al., 2015; Baron et al., 2017; Langer et al., 2017) and this groups was named Silesauridae (Langer et al., 2010; Nesbitt et al., 2010). Other phylogenetic analyses (Langer and Ferigolo, 2013; Cabreira et al., 2016) still found a “core” Silesauridae, but this clade fell into Dinosauria at the base of Ornithischia.

One of the key taxa that lies at the heart of resolving the position of silesaurids as a whole and the relationship within the Silesauridae is *Asilisaurus kongwe* (Nesbitt et al., 2010), one of the oldest and more complete dinosauriforms known to date (Fig. 1). *Asilisaurus kongwe* was first described based on an isolated dentary from a bonebed of many individuals of different ontogenetic stages (Nesbitt et al., 2010). All *Silesaurus*-like material from the type locality was assigned to that species, but, as pointed out by some authors (Langer et al., 2010), the material could pertain to more than one species. Here, we present an exceptionally well preserved skeleton of a single individual that unambiguously ties the holotype and the referred material from the holotype locality to a single taxon—*Asilisaurus kongwe*. In this contribution, we detail the anatomy of *Asilisaurus kongwe* from representative material from the holotype locality and referred material, including an exceptional skeleton, from other localities within the Manda Beds across the Ruhuhu Basin of Tanzania. From this description we score all of the *Asilisaurus kongwe* remains into the most recent and largest phylogenetic dataset and comment on the impact of the morphology of *Asilisaurus kongwe* on understanding archosaurs as a whole, avemetatarsalian, dinosauriform, and dinosaur trends and character transformations.



Fig. 1. Reconstruction of the skeleton of *Asilisaurus kongwe* in lateral view. Reconstruction of skeleton completed by Scott Hartman. Scale bar equals 10 mm.

Systematic Paleontology

ARCHOSAURIA Cope (1869) *sensu* Gauthier and Padian (1985)

DINOSAURIFORMES Novas, 1992 *sensu* Sereno et al. (2005)

SILESAURIDAE Langer et al. (2010), Nesbitt et al. (2010)

ASILISAURUS KONGWE Nesbitt et al. (2010)

Holotype—NMT RB9, the anterior portion of a left dentary with associated tooth.

Paratypes—Anterior cervical vertebra (NMT RB21), left scapulocoracoid (NMT RB10), sacrum (NMT RB11), proximal portion of an ischium (NMT RB12), ilium (NMT RB13), proximal portion of a pubis (NMT RB14), anterior portion of a skull (NMT RB15), proximal portion of a left humerus (NMT RB16), left astragalus (NMT RB17), right calcaneum (NMT RB18), proximal portion of a left femur (NMT RB19), right tibia (NMT RB20).

Referred Specimens—The following description relies heavily on NMT RB159, a large and associated individual directly referable to the holotype based on overlapping material of the dentary. Specifically, the holotype and NMT RB159 completely overlap and share all of the character states present in the diagnosis, including: the anterior portion of the dentary tapers to a sharp point; teeth absent from the anterior portion of the dentary; teeth ankylosed into the alveoli; distinctly convex dorsal margin of the anterior portion of the dentary; Meckelian groove positioned at the dorsoventral midpoint of the medial surface of the dentary. NMT RB159 contains a disarticulated cranium (premaxilla, maxillae, prefrontal fragments, frontals, squamosals, jugals, quadrate, dentary, ectopterygoid, articular, and other fragments), vertebrae (one presacral, second sacral, most caudals, fragments), rib fragments, pectoral girdle (scapulocoracoid), forelimb (humerus, ulna, radii, metacarpals), pelvic girdle (ilium, ischium, pubis), and hindlimb (femora, tibiae, fibulae, astragali, calcaneum, 4th tarsal, metatarsals, phalanges).

Locality and Horizon—The holotype specimen is from locality Z34 (see Sidon and Nesbitt, 2018 for a description of Ruhuhu Basin localities; Fig. 2), detailed in Smith et al. (2018) and other specimens are from across the Lifua Member of the Manda Beds (Figs. 2 and 3). Overall, the holotype and referred specimens come from a fluvio-

lacustrine mudstone–sandstone sequence in the Lifua Member of the Manda Beds, across the Ruhuhu Basin, Tanzania (Nesbitt et al., 2010; Smith et al., 2018). The Lifua Member is considered Middle Triassic in age based on correlating the taxa present (e.g., *Cynognathus* and other cynodonts, and dicynodonts) with other areas with similar taxa and better age constraint (e.g., Karoo Basin; for details, see Smith et al., 2018; Wynd et al., 2017; Peacock et al., 2018). No radiometric dates are known from the Manda Beds at this time, so the Middle Triassic age must be considered our best estimate based on the currently available evidence.

Revised Diagnosis—Based solely on the holotype dentary and associated tooth (NMT RB9), *Asilisaurus kongwe*

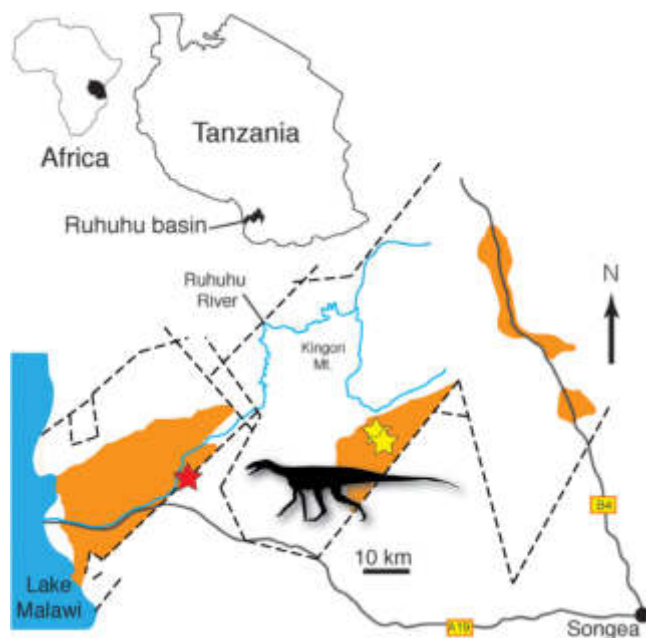


Fig. 2. Geographic position of the type locality of *Asilisaurus kongwe* (red star) and other areas where referred specimens were found (yellow stars) (modified from Nesbitt et al., 2014). Dash lines represent major faults. Orange color indicates mapped Manda Beds. Reconstruction of skeleton completed by Scott Hartman.

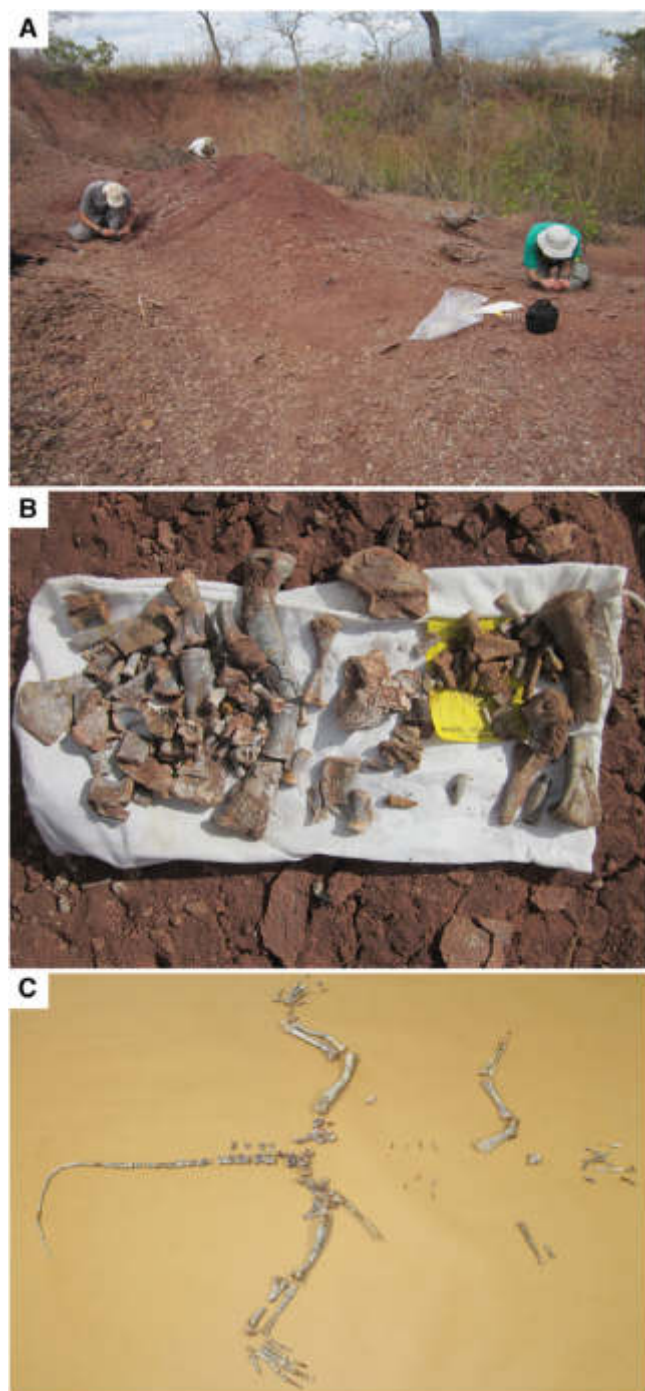


Fig. 3. The discovery locality [Z137] of a partial skeleton (NMT RB15) referred to *Asilisaurus kongwe*. (A), first collection of the skeleton just after discovery (B), and the fully prepared skeleton (NMT RB159) referred to *Asilisaurus kongwe* (C). Photographs in A and B by Roger Smith.

differs from all other archosaurs in possessing the following unique combination of traits: anterior portion of the mandible tapers to a sharp point; teeth absent from the anterior portion of the mandible; dentary teeth ankylosed into the alveoli; distinctly convex dorsal margin of the

dentary; Meckelian groove positioned at the dorsoventral midpoint of the medial surface of the dentary; peg-like teeth with small, poorly developed serrations.

Asilisaurus kongwe can be further diagnosed based on morphological data gathered from the skeleton of a single individual (NMT RB159; Fig. 3), given that the anterior portion of its associated mandible shares all of the features of the holotype (NMT RB9). As such, *Asilisaurus kongwe* can be diagnosed based on the following combination of traits, in addition to those discussed above (possible autapomorphies indicated by an asterisk): premaxilla mostly edentulous with a single tooth located at the posterior margin*; anterior portion of the premaxilla tapered; maxilla with a weakly defined antorbital fossa that extends posteroventrally to nearly contacting the ventral margin; vertically oriented palatal process of the maxilla; anteriorly tapered jugal; frontal with a well-defined supratemporal fossa on the dorsal surface of the posterior part; laterally exposed quadrate head in articulation with the squamosal; humerus with a nearly straight shaft; a broad, proximodistally oriented groove on the anterolateral surface of the ulna*; closed acetabulum; ischial distal expansion present; femur longer than the tibia; femora with a facies articularis antitrochanterica, equally developed anterolateral, anteromedial, and posteromedial tubera, a proximally pointed anterior trochanter and trochanteric shelf in large individuals; an astragalus with a short anterior ascending process; calcaneum with a convex fibular facet and a clear posteriorly-pointing calcaneum tuber; metatarsal III is just shorter than 50% the length of the tibia; metatarsals I and V are well developed but still shorter than metatarsals II–IV; unguals with ventrally flat bases with no clear ventral tubercle.

Taphonomic Comments—Remains of *Asilisaurus kongwe* are rather common across the middle to upper portions of the Lifua Member of the Manda Beds (Nesbitt et al., 2010, 2017) and occur either as isolated bones, associated skeletons (e.g., NMT RB159), or in nearly monotonous bone accumulations (e.g., the holotype and originally referred specimens; Nesbitt et al., 2010). The holotype locality (NMT RB34) of *Asilisaurus kongwe* contained isolated bones, either partial or complete, and a partially articulated skeletal portion (e.g., NMT RB15, partially articulated skull, vertebrae). Unfortunately, at the type-locality, all bones were found on the surface, none of them *in situ*. Nearly all of the bones found here are hypothesized to be from *Asilisaurus kongwe*, but a few remains of cynodonts (NMT RB153), a proximal end of a femur that is similar to those of aphanosaurs (NMT RB148), and a tooth of a large archosauriform (NMT RB150) were also found here; it is not clear if they are from the same layer given that they were found out of stratigraphic context. Another locality (Z90) that produces material possibly assignable to small *Asilisaurus kongwe* individuals (or at least a dinosauriform with identical hindlimb morphology) contains tens to possibly one hundred individuals (Griffin and Nesbitt, 2016a). This taphonomically biased sample contains dozens of proximal ankle bones, braincase elements, phalanges, limb bone ends, and hundreds of vertebrae from all over the column, but lacks most cranial bones and larger limb bones. These data will be mostly presented elsewhere but a few observations of tarsals from Z90 are presented below.

Skeletal Maturity—The skeletal maturity of *Asilisaurus kongwe* was assessed based on a variety of

different sized femora and histological analysis of limb bones by Griffin and Nesbitt (2016a). Briefly, this study showed that the femur of *Asilisaurus kongwe* has high variation in appearance of ontogenetically variable traits and that the taxon has a similar sequential polymorphism as that also found in some early dinosaurs (Griffin and Nesbitt, 2016b). No growth marks were found in any of the histologically sampled bones of *Asilisaurus kongwe* (Griffin and Nesbitt, 2016a). Specimen NMT RB159, featured heavily in the description below, is one of the largest and most mature individuals recovered based on the analysis of Griffin and Nesbitt (2016a). Although histology was not obtained from NMT RB159, the bone scars of the femora and other parts of the limbs are consistent with the larger specimens of *Silesaurus opolensis* (ZPAL ab III/361) and *Coelophysis bauri* (see Griffin and Nesbitt, 2016b). Therefore, NMT RB159 represents one of the most complete skeletons of any Triassic dinosauriform that was nearly or completely skeletally mature.

A much larger femur from a silesaurid was also described from the Manda Beds (Barrett et al., 2015). Although much of this large femur is missing, the morphology of the femur is nearly identical to that of *Asilisaurus kongwe* and the bone scars on the larger femur are consistent with an old ontogenetic age. We still do not know if this femur can be assigned to *Asilisaurus kongwe* and the taxon grew to much larger sizes that are rarely sampled in the Manda Beds, or this is another silesaurid taxon. A parallel situation where there are two size classes of silesaurids is present in the near co-eval beds (Peacock et al., 2018) in the Ntawere Formation in Zambia.

DESCRIPTION

Skull

The skull of *Asilisaurus kongwe* is represented by both isolated elements and partially articulated sections from the holotype locality and other localities across the Manda Beds (Fig. 4). Other than a partially articulated anterior portion of the skull (NMT RB15; Fig. 5) and the holotype, the description of the skull below largely relies on the associated, but disarticulated, and well preserved skull of a single individual (NMT RB159). A partial braincase (NMT RB846) and many disarticulated elements of the braincase (e.g., basioccipital, otoccipital, parabasisphenoid) will be described in a subsequent paper.

Overall, the reconstruction of the skull (Fig. 4) has similar proportions to that of *Silesaurus opolensis* (Dzik and Sulej, 2007). The antorbital region is short, where the preorbital portion of the skull is predicted to be shorter than the region posterior to the anterior margin of the orbit. The estimated size of the naris is smaller than that of the antorbital fenestra. The orbit is circular in lateral view and possibly represents the largest opening of the skull. The supra- and infratemporal openings are present, but there is currently little constraint on the size of the openings.

Premaxilla—A right premaxilla (NMT RB159; Fig. 6) is nearly complete, but with broken posterior portions of the posterodorsal (= maxillary), anterodorsal (= narial) and palatal processes. The premaxilla is strikingly different from those of all other Triassic dinosauriforms, including those of *Silesaurus opolensis* (Dzik, 2003) and a specimen referred to *Lewisuchus admixtus* (CRILAR-Pv 552).

The ventral margin of the beak-like premaxilla of *Asilisaurus kongwe* is edentulous for much of its length (Fig. 6), but bears teeth throughout its entire length in *Silesaurus opolensis*. The premaxilla of *Asilisaurus kongwe* forms much of the external naris and a shallow narial fossa is present on the lateral surface of the element. The anterior margin of the bone is gently convex in lateral view and this curvature continues onto the short anterodorsal process. The anterodorsal process tapers posterodorsally and is D-shaped in cross-section, suggesting that the process contacts its antimerie on the midline. Two dorsoventrally aligned and anteriorly opening foramina (Fig. 6A) are located between the base of the anterodorsal process and the ventral margin of the premaxilla. The more ventral foramen has a defined channel leading from the opening toward the anteroventral margin of the bone. The convex anterior margin of the premaxilla meets its ventral margin at a near right angle. Here, dozens of tiny foramina dot the lateral surface of the bone.

The premaxilla has a nearly straight ventral margin in lateral view, but a distinctly convex lateral margin in dorsal view. The posterior portion of the ventral margin gently curves dorsally to form the ventral margin of posterodorsal process, similar to that of *Silesaurus opolensis* (ZPAL Ab III 361/34) and a specimen referred to *Lewisuchus admixtus* (CRILAR-Pv 552). The base of the posterodorsal process originates near the posteroventral margin of the premaxillary body and the dorsal margin forms the posteroventral margin of the narial fossa, similar to that of *Silesaurus opolensis* (ZPAL Ab III/361/34).

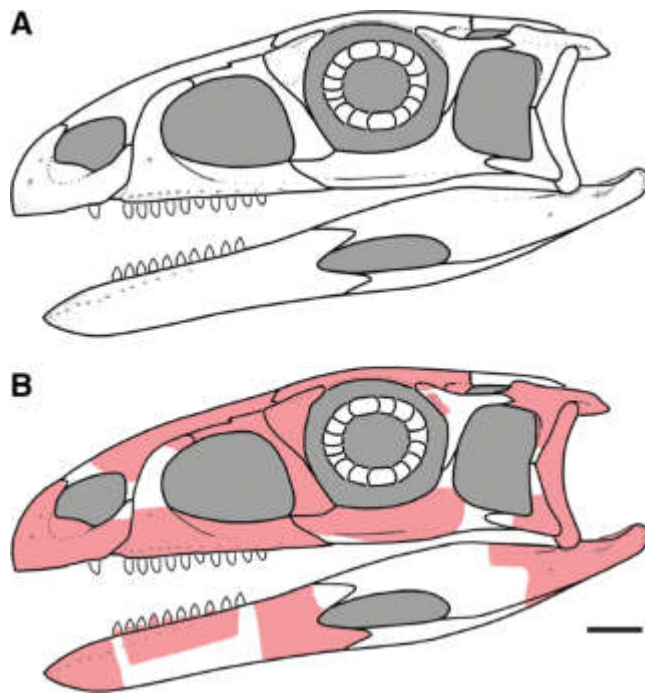


Fig. 4. Reconstruction of the skull of *Asilisaurus kongwe* based on all known parts (A) and (B) skull reconstruction illustrating the bones (in red) recovered from NMT RB15 and NMT RB130 from the holotype locality and the most complete individual (NMT RB159). Part of the skull that are not represented in the *Asilisaurus kongwe* specimens are modeled from *Sacisaurus agudoensis*, *Silesaurus opolensis*, and early dinosaurs (e.g., *Coelophysis bauri*). Scale bar equals 10 mm.

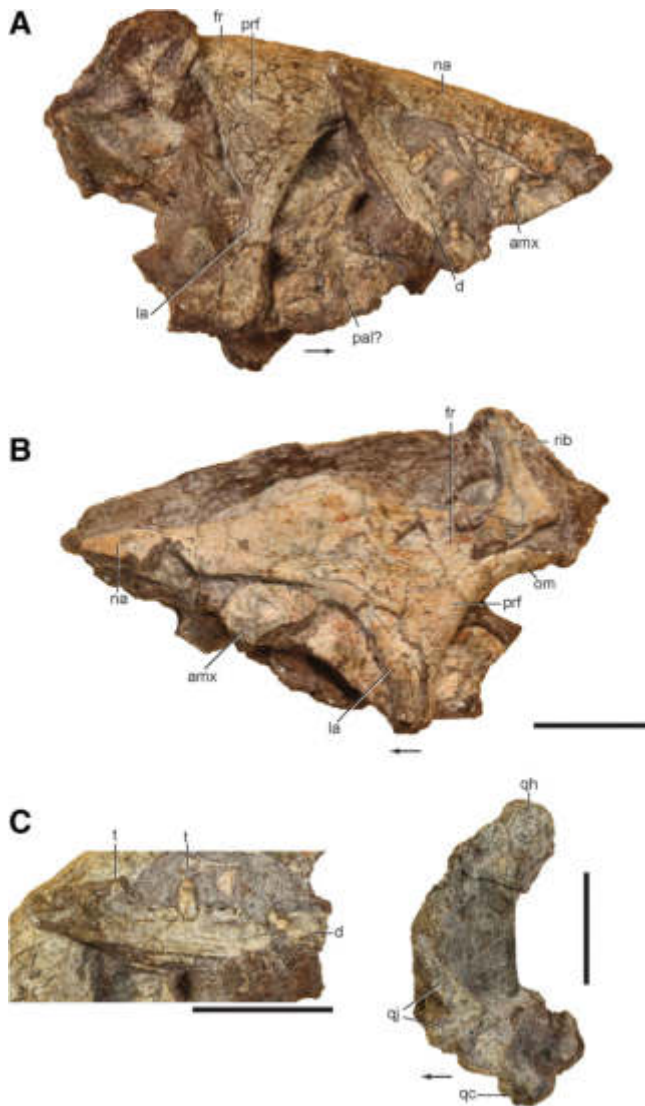


Fig. 5. Partially articulated and associated skull referred to *Asilisaurus kongwe* (NMT RB15) from the right (A) and left (B) sides, a close-up of the dentary (C) and a complete left quadrate and articulated quadratojugal in lateral (D) view. Abbreviations: amx, ascending process of the maxilla; d, dentary; fr, frontal; la, lacrimal; na, nasal; om, orbital margin; pal, palatine; prf, prefrontal; qc, quadrate condyles; qh, quadrate head; qj, quadratojugal; rib, rib; t, tooth. Arrows indicate anterior direction. Scale bars equal 10 mm.

The lateral surface of the process is slightly concave. Much of the process is broken, so that it is not clear if the maxilla contributed to the external naris or not.

In ventral view, the lateral surface is defined by a sharp, cutting ridge (Fig. 6C). Just medial to the sharp lateral margin, the ventral surface is largely mediolaterally concave and this surface continues posteriorly to form the ventral surface of the palatal process. A series of ventrally opening foramina lie near the lateral margin and larger foramina are located in an anteroposterior line near the medial margin. A single round alveolus is located at the posterior end of the ventral edge of the premaxilla, medial to the base of the posterodorsal process. Although a tooth is not present, thin laminae on the edges of the alveolus

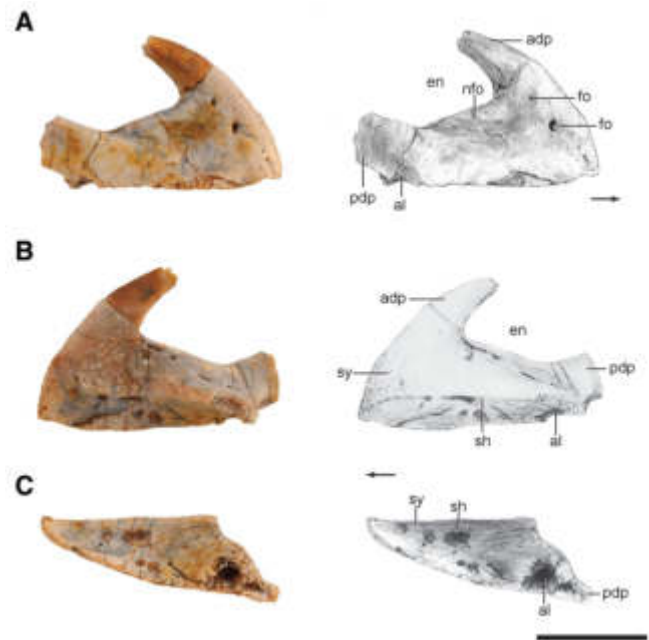


Fig. 6. Photographs and drawings of the right premaxilla of a partial skeleton referred to *Asilisaurus kongwe* (NMT RB159) in lateral (A), medial (B), and occlusal (C) views. Abbreviations: adp, anterodorsal process; al, alveolus; en, external naris; fo, foramen; nfo, narial fossa; pdp, posterodorsal process; sh, shelf; sy, symphysis. Arrows indicate anterior direction. Scale bar equals 10 mm.

(Fig. 6C) suggest that the implantation was likely ankylothecondont like that in the maxillae and dentaries.

Most of medial surface of the premaxilla (Fig. 6B) is flat and generally smooth. The surface bears tiny ridges and foramina, but these are not similar to the larger ridges that indicate a tight contact between the left and right premaxillae. A similar midline contact is also present in *Silesaurus opolenis* (ZPAL Ab III/361/34) and a specimen referred to *Lewisuchus admixtus* (CRILAR-Pv 552). More posteriorly, anteroposteriorly elongated foramina are present just ventral to the external naris. The preserved portion of the palatal process is dorsoventrally compressed and its dorsal surface lacks a clear facet for articulation with the palatal process of the maxilla, even though these processes fit when the two elements are in articulation.

Maxilla—The maxilla is represented by right and left bones from NMT RB159 (Fig. 7) and a fragment of the ascending process of NMT RB15 (Fig. 5). The left and right maxillae of NMT RB159 are missing the anterior portion of the palatal process, most of the ascending process and the posterior tip of the posterior process.

A series of anteroposteriorly aligned nutrient foramina lie just dorsal to the ventral margin of the maxilla. The anterior foramina open anteroventrally, those in the anteroposterior middle of the bone open ventrally, and the posterior foramina open posteroventrally. The lateral surface of the maxilla is flat ventral to the base of the ascending process. A sharp ridge (Fig. 7A, D) divides this lateral surface from the lateral surface of the dorsoventrally tall palatal process. Here the latter is nearly flat dorsoventrally and is medially depressed relative to the lateral surface of the maxillary body. A large anteriorly

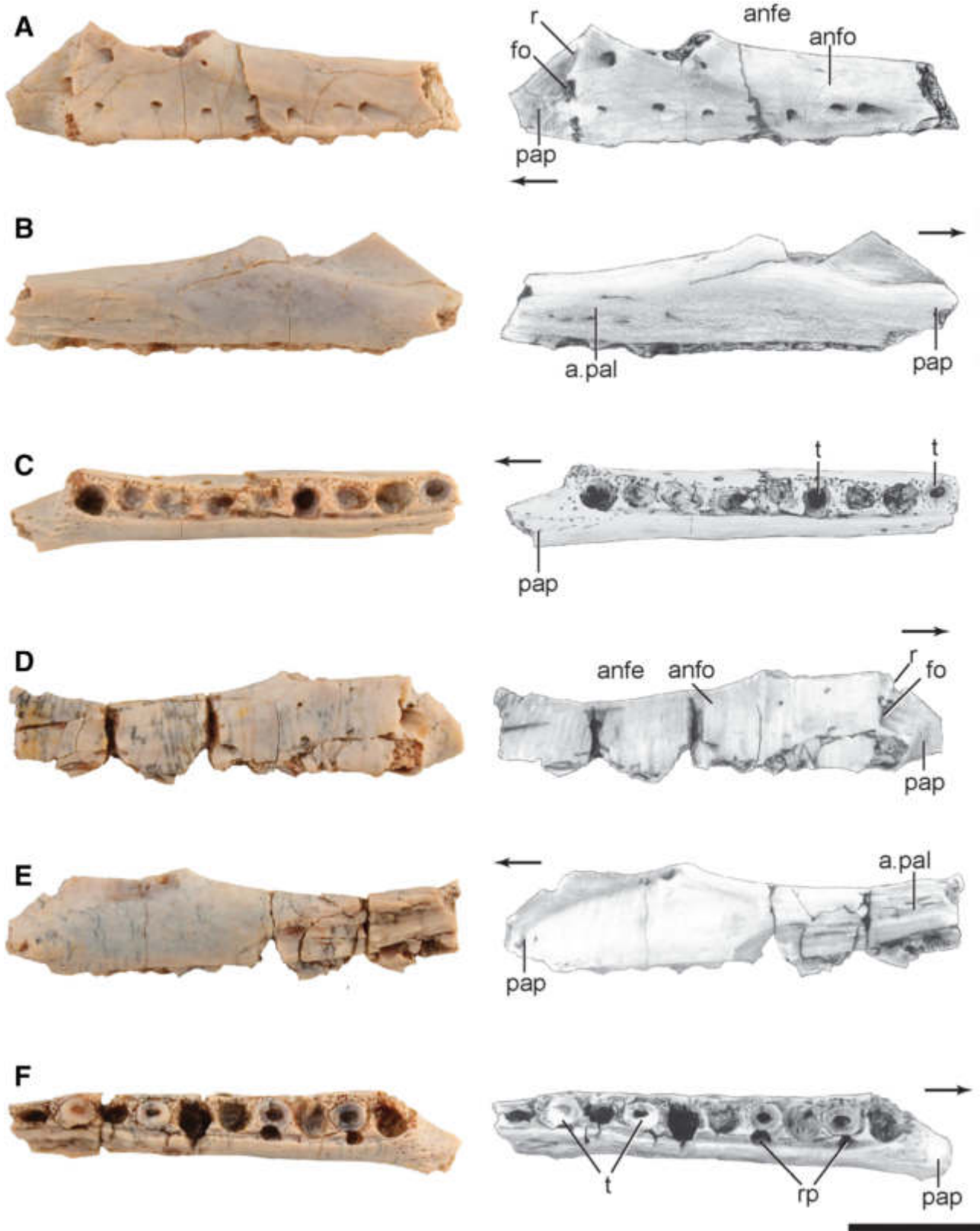


Fig. 7. Photographs and drawings of the maxillae of a partial skeleton referred to *Asilisaurus kongwe* (NMT RB159). Left maxilla in lateral (A), medial (B), and occlusal (C) views. Right maxilla in lateral (D), medial (E), and occlusal (F) views. Abbreviations: a., articulates with; anfe, antorbital fenestra; anfo, antorbital fossa; fo, foramen; pal, palatine; pap, palatal process; r, ridge; rp, reabsorption pits; t, tooth. Arrows indicate anterior direction. Scale bars equal 10 mm.

directed foramen lies just anterior to the ridge and is partially hidden in lateral view by the lateral surface of the maxillary body. Similar dividing ridge, foramen, and laterally flat palatal process are found in *Silesaurus opolensis* (ZPAL Ab III/361/26; Dzik, 2003) and *Sacisaurus agudoensis* (Langer and Ferigolo, 2013), and likely represent a synapomorphy of the group uniting these taxa (see below). However, the ridge is oriented more vertically in *Asilisaurus kongwe* (Fig. 7) in comparison with those of *Silesaurus opolensis* and *Sacisaurus agudoensis*. The depressed surface accommodates the posterodorsal process of the premaxilla and, when the two skull elements are in articulation, there is little to no gap in their ventral margin and dentition. In contrast, *Lewisuchus admixtus* lacks a depressed anterior lateral surface and the respective dividing ridge (PULR 01, CRILAR-Pv 552). The anterodorsal margin of the palatal process of *Asilisaurus kongwe* slants anteroventrally and is straight in lateral view.

What we interpret as the posterodorsal tip of the ascending process of the maxilla in NMT RB15 (Fig. 5) is in near articulation with the lacrimal. It is mediolaterally compressed and dorsoventrally tapering. The dorsal margin is straight in lateral view and it appears that the large antorbital fossa excavates the entire surface of the ascending process. In contrast, the antorbital fossa is more restricted to the ventral margin of the process in *Sacisaurus agudoensis* (MCN PV10050; Langer and Ferigolo, 2013) and this region is not known in other silesaurids.

The lateral surface of the posterior process of the maxilla is marked by shallow and poorly defined antorbital fossa that slants posteroventrally; the antorbital fossa deepens (dorsoventrally) posteriorly until it becomes parallel with the ventral margin of the bone at the posterior end of its preserved portion, just dorsal to an antero-posterior oriented line of nutrient foramina (Fig. 7). A similarly shallow antorbital fossa is present in *Silesaurus opolensis* (ZPAL Ab III/361/26; Dzik, 2003); however, in that species, the fossa nearly contacts the ventral border of the maxilla. Additionally, a *Silesaurus*-like morphology seems to also be present in *Sacisaurus agudoensis* (MCN PV10050), although the antorbital fossa was originally interpreted as shorter and lying in parallel with the ventral margin (Langer and Ferigolo, 2013). No distinct ridge separates the antorbital fossa from the rest of the lateral surface of the maxilla in these forms, unlike the distinct ridge present in a specimen referred to *Lewisuchus admixtus* (CRILAR-Pv 552) and many dinosaurs (e.g., *Coelophysis bauri*, AMNH FR 7224). The posterior portion of the maxilla slightly expands dorsally at its posterior end (Fig. 7D, E). In dorsal view, this expanded portion is mediolaterally compressed. In contrast, the maxilla of *Sacisaurus agudoensis* (MCN PV10050), *Silesaurus opolensis* (ZPAL Ab III/361/26) and *Lewisuchus admixtus* (PULR 01) taper posteriorly. A large, posterodorsally opening foramen is located at the dorsal margin of the posterior process within the antorbital fossa. The foramen opens into a long and well defined groove that shallows posteriorly. The groove is much better defined on the left side than on the right side of NMT RB159. The ventral margin of the maxilla is straight in lateral view and lies in the horizontal plane.

Most of the medial surface of the maxilla is convex dorsoventrally (Fig. 7B, D). From the posterior portion of the

base of the ascending process, the maxilla tapers anteriorly. Dorsal to this surface, a deep, but broad fossa lies medial to much of the base of the ascending process and to the dorsal portion of the palatal process. Although broken, it appears that the anterior portion of the palatal process is located on the horizontal plane, as in *Lewisuchus admixtus* (Bittencourt et al., 2015), and is not anteroventrally deflected. It is not clear if the palatal process of the maxillae met on the midline as in most archosaurs (Nesbitt, 2011). The medial surface of the posterior process bears an anteroposteriorly long and concentric scar for articulation with the palatine (Fig. 7).

The maxilla bears at least 10 alveoli (nine preserved in the left and 10 preserved in the right elements of NMT RB159; Fig. 7C, F). Based on the size and shape of the alveoli and the preservation of most of the maxillary length (in the right side), we hypothesize that *Asilisaurus kongwe* would have had 10–12 maxillary teeth. This is far fewer than that present in *Lewisuchus admixtus* (~20; Bittencourt et al., 2015), but more comparable to *Sacisaurus agudoensis* (~eight, Langer and Ferigolo, 2013) and *Silesaurus opolensis* (11, Dzik, 2003). It is not clear if the posterior portion of the maxilla of *Asilisaurus kongwe* lacked teeth as in *Sacisaurus agudoensis* (Langer and Ferigolo, 2013) and *Silesaurus opolensis* (Dzik, 2003). The size of the alveoli remains the same throughout the series and the first tooth is present directly posterior to the articulation surface with the premaxilla. Interdental plates separate each of the alveoli and are easily visible in the medial side of the maxilla.

Most teeth have fallen out of the sockets prior to preservation. However, tooth position nine of the left maxilla and positions, two, four, seven, and nine of the right maxilla preserve the base of broken crowns (Fig. 7C, F). Each base is firmly attached to the maxilla through fusion of the tooth to alveolar bone. This condition is characterized by small ridges of bone that connect the bone of attachment to the base of the tooth. Thus, there is no gap around the tooth in *Asilisaurus kongwe* like in fully thecodont taxa, resembling the condition in *Lewisuchus admixtus* (PULR 01, CRILAR-Pv 552), *Silesaurus opolensis* (Nesbitt et al., 2010) and *Sacisaurus agudoensis* (Langer and Ferigolo, 2013). Circular foramina are present directly medial to the bases of the teeth, but are not present in the tooth positions that are empty. The cross-section of each tooth is circular. Only one maxillary crown is preserved and it is located in the 6th alveolus of the left maxilla (Fig. 7C; tooth is within the socket and not observable in the figure). The crown is labiolingually expanded, similar to those in the dentary (see below). Fine serrations (~6 per mm) are seen on both the mesial and distal carinae and they extend to the tip of the crown. The tip is pointed and slightly posteriorly recurved.

Nasal—Left and right nasals are partially preserved in NMT RB15 (Fig. 5A, B). They are wide posteriorly and narrow anteriorly in dorsal view. The dorsal surface is flat. Posteriorly, the nasal dorsally overlaps the frontal in an interdigitating suture. A small sliver of nasal may split the frontals on the midline based on the morphology of the anterior portion of the frontals of NMT RB159, but this region is not well preserved. It is clear that a posterior prong of the nasal slips in between the lateral edge of the anterior extent of the frontal and the medial edge of the prefrontal. Laterally, the nasal contacts the prefrontal and the lacrimal. It appears that the nasal and

lacrimal have an interdigitating suture at the contact between the anterior end of the lacrimal and the nasal. In this arrangement, the nasal has a short posterior prong that fits into a slot of the lacrimal. This contact resembles that of saurischians (Langer and Benton, 2006; character 9), but the prong of the nasal is relatively shorter than in those forms. The dorsoventrally convex lateral margin of the nasal anterior to the articulation with the lacrimal did not contribute to the antorbital fossa, but the contact between the nasal and the maxilla may have marked the maximal anterior extent of the antorbital fossa, given that the fossa appears to cover the entire lateral surface of the ascending process of the maxilla. The anterior portion of the nasal bifurcates around the posterodorsal limits of the external naris; the anterior process tappers medially and the lateral process stretches anterolaterally. Overall, the nasal of *Asilisaurus kongwe* is similar to that of *Silesaurus opolensis* (ZPAL Ab III 361/31).

Lacrimal—The morphology of the lacrimal can be reconstructed from the left and right bones of NMT RB15 (Fig. 5A, B) and possible fragments from the referred specimen NMT RB159 (Fig. 8A, B). The lacrimal forms the dorsal, posterodorsal, and posterior borders of the antorbital fossa and fenestra. The dorsal margin of the lacrimal meets the nasal medially and anteriorly in a complex articulation (see above). The lateral portion of the dorsal half of the lacrimal is laterally rounded like that of the prefrontal. A similar lateral expansion is present in *Silesaurus opolensis* (ZPAL Ab III/1930). Posterior of this expansion, the lacrimal is bordered by the prefrontal. The contact gently arcs anteriorly in lateral view. The vertical ventral process of the lacrimal has a sharp anterior margin—the margin that defines the posterior extent

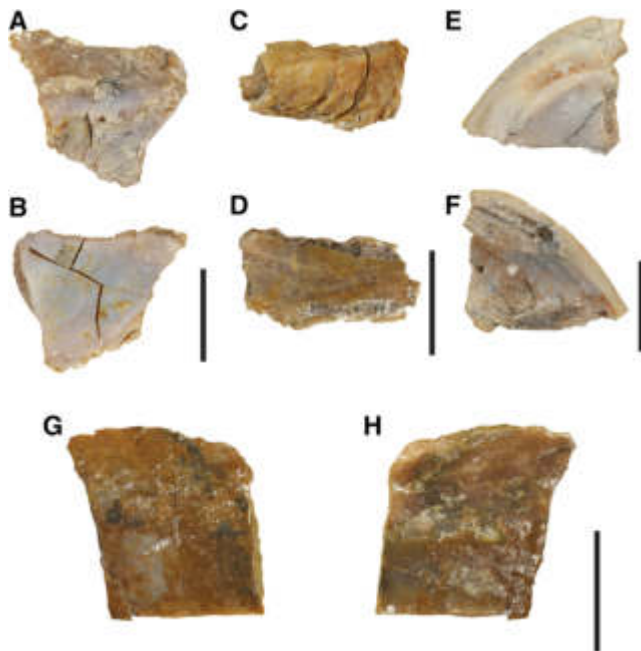


Fig. 8. Skull fragments of an associated skeleton referred to *Asilisaurus kongwe* (NMT RB159). (A, B) possible fragment of a lacrimal, (C, D) possible portion of the postorbital, (E, F), possible fragment of a pterygoid, and splenial fragment in medial (G) and lateral (H) views. Scale bar equals 10 mm.

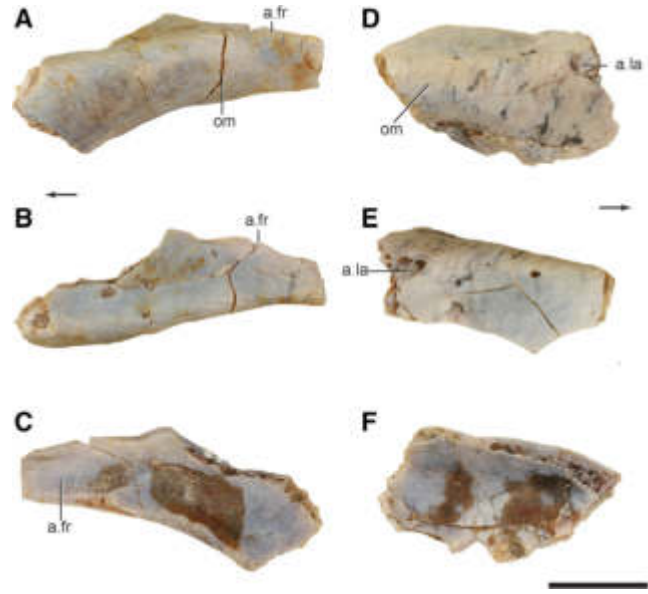


Fig. 9. Left and right partial prefrontals of a partial skeleton referred to *Asilisaurus kongwe* (NMT RB159). Left prefrontal in lateral (A), dorsal (B), and medial (C) views. Right prefrontal in lateral (D), dorsal (E), and medial (F) views. Abbreviations: a., articulates with; fr, frontal; la, lacrimal; om, orbital margin. Arrows indicate anterior direction. Scale bar equals 5 mm.

of the antorbital fossa. Posterior to this margin, the lacrimal slopes posteromedially where it meets the ventral process of the prefrontal. A piece of bone we interpret as the ventral end of the lacrimal (Fig. 5) is flat laterally but expands anterior and posteriorly. Anterior to the ventral process, a mediolaterally thin sheet of bone from the lacrimal forms an extensive antorbital fossa (Fig. 5), which expands as a pocket at its posterodorsal margin. This pocket is not completely visible in lateral view, but most of it can be seen; this is in contrast to the deeper pockets in this region in dinosaurs (Langer and Benton, 2006).

Prefrontal—The complete prefrontal is known from the right and left sides of NMT RB15 in articulation with the surrounding elements (Fig. 5) and from isolated partial right and left elements of NMT RB159 (Fig. 9). The prefrontal of *Asilisaurus kongwe* is large compared with the lacrimal and forms much of the dorsal and anterior margins of the orbit. Its lateral surface, at the anterodorsal margin of the orbit, is expanded in a lateral “swelling” much like, but larger than, that of the lacrimal. This “swelling” is not present in *Silesaurus opolensis* (ZPAL Ab III/1930) and its lateral surface bears a rugose pattern of anteroventrally directed grooves and ridges that also extend to the posterior end of the element (Fig. 9); these ridges are located on the lateral margin of the bone and define the lateral margin of the skull.

Posteriorly, the prefrontal has a complex articulation with the frontal. A posterior prong of the prefrontal fits, via an interdigitating suture, into the frontal, just ventral to the dorsal rim of the orbit. More anteriorly, the concave medial surface of the prefrontal fits onto the lateral surface of a complementary convex surface of the frontal. Just dorsal to this concave-convex articulation, the prefrontal butts up against the lateral side of frontal in an anteroposteriorly oriented contact. A small ridge in the

frontal, just ventral to this contact, fits into a corresponding groove on the medial side of the prefrontal. Such a complex articulation appears to be also present in *Silesaurus opolensis* (ZPAL Ab III 361/37). A posteriorly tapering slot on the dorsal surface of the frontal medial to the contact surface between the frontal and the prefrontal (Fig. 10) may also pertain to the prefrontal-frontal contact, but it may also pertain to the nasal-frontal articulation. The orbital fossa on the ventral surface of the frontal continues anteriorly onto the prefrontal. Here, the medial process of the prefrontal is dorsoventrally compressed into a thin lamina of bone (Fig. 9; NMT RB15).

Medially, the prefrontal may contact the nasal, but this is not clear in any of the specimens. The dorsal surface of the prefrontal is nearly flat with a few dorsally opening foramina. Anteriorly, the prefrontal contacts the lacrimal. The suture between the elements curves more anteriorly at its dorsal portion than at the ventral portion. The ventral process parallels the ventral process of the lacrimal and the two elements meet at a dorsoventrally oriented contact. The ventral process twists medially to form the anterior margin of the orbit, so that the ventral portion of the bone is less visible in lateral view toward the ventral termination. The ventral process of NMT RB15 (Fig. 9A) appears to be complete and to expand medially at the ventral termination, relative to more dorsal portions. Due to breakage of NMT RB15, it is not clear what percentage of the anterior margin of the orbit is formed by the prefrontal, but it is likely more than 50%.

Frontal—The frontal is represented by well preserved and nearly complete right and left bones from NMT RB159 (Fig. 10). In dorsal view (Fig. 10A, D), its width slightly tapers anteriorly, resembling the condition in the early avemetatarsalian *Teleocrater rhadinus* (NMT RB496). This contrast with the condition in the sauropodomorph *Panphagia protos* (Martínez et al., 2013), in which the posterior portion of the frontal expands much more laterally than the rest of the bone. The frontal of *Asilisaurus kongwe* is proportionally much wider and less waisted near the anteroposterior mid-point of the orbit than that of *Panphagia protos* (PVSJ 874). Its dorsal surface is nearly flat anteriorly, dorsally expanded in the lateral portion across the orbital margin, and ventrally depressed in the posterior third of the element. The dorsal surface is generally smooth, but with a few anterolaterally directed grooves that originate as foramina close to the midline. Anteriorly, the frontal meets the nasal and the prefrontal. The anteriormost end is not complete in either specimen, but it is clear that the nasal partially overlapped the dorsal surface of the frontal where the two elements meet, and the posterior extent of this contact suggests that the suture was interdigitating. The complex (see above) prefrontal contact takes place at the anterolateral margin of the frontal.

In dorsal view, the lateral margin that contributes to the orbit is nearly anteroposteriorly straight and is highly rugose (Fig. 10A, D), with small and laterally projecting tubercles; the same is present in *Silesaurus opolensis* (ZPAL Ab III 361/37). More posteriorly, the frontal curves laterally to contact the postorbital or postfrontal (see below). This contact is also anteroposteriorly oriented in *Asilisaurus kongwe*, but deeply invades the body of the frontal in *Silesaurus opolensis* (ZPAL Ab III/361/37). The contact with the postorbital or postfrontal is slightly medially sloped at its ventral margin, so that the sutural contact is not visible in dorsal view. The articulation surface with the postorbital

or postfrontal is rugose, with deep grooves and pits and thin ridges, and is deepest in the anteroposterior center, with tapering anterior and posterior sides.

The dorsal surface of the frontal is depressed on the posterior third relative to the rest of the bone (Fig. 10A, D), as also seen in *Silesaurus opolensis* (ZPAL Ab III/361/37; ZPAL Ab III/1223). A deep and rimmed supratemporal fossa is present on the posterolateral edge of the frontal—a condition present in all dinosaurs (Gauthier, 1986; Langer and Benton, 2006; Nesbitt, 2011). In *Teleocrater rhadinus*, the supratemporal fossa is also present on the frontal but it is not well-rimmed (Nesbitt et al., 2018). The rimmed depression is clearly absent in the other silesaurid with a known frontal, *Silesaurus opolensis* (ZPAL Ab III/1223). The anterior and medial rims of the supratemporal fossa are well-marked as in *Panphagia protos* (Martínez et al., 2013). Such a well defined rim fails to reach the midline in *Asilisaurus kongwe* and the fossae are clearly separated by the parietals. Within the supratemporal fossa, the anterior portion expands into the body of the frontal, so that the anterior extent of the fossa is not visible in dorsal view. The supratemporal fossa continues onto the dorsal surface of the postorbital or postfrontal. The articulation with the parietal is restricted to the surface medial to the supratemporal fossa. Thus, the frontal did not, or only slightly participated in the supratemporal fenestra, similar to *Herrerasaurus ischigualastensis* (Serenó and Novas, 1994). The frontals and parietals meet at an interdigitating suture that stretches anteriorly as it approaches the midline.

The frontal midline articulation consists of grooves and ridges radiating from near the anteroposterior middle of the element (Fig. 10G). Here, the frontal is thickest, but only marginally thicker than the rest of the bone. Ventrally, the frontal bears a well-developed orbital fossa with a deep, ventrally expanded rim that defines its medial margin. The surface of the orbital fossa has shallow and wide grooves. Anterior to the fossa, the ventral surface is depressed, and more so near the midline. A shallow groove is located medial and parallel to the rim that defines the medial edge of the orbital fossa, as also seen in *Silesaurus opolensis* (ZPAL Ab III/361/37). Overall, the surface medial to that rim is depressed and covered in shallow, posteromedially directed grooves and represents the mold of the passage of the olfactory tract. A few tiny, ventrally opening foramina are also present in this region. The articulation surface with the parietal barely expands anteriorly, unlike the condition in *Silesaurus opolensis* (ZPAL Ab III/361/37), where this articulation surface extends much further anteriorly.

Postfrontal/Postorbital—The right frontal of NMT RB159 (Fig. 10D–F) preserves a small fragment of a cranial element in articulation at its posterolateral edge. It is unclear if this element pertains to the postfrontal or the postorbital, given the restricted morphology that is preserved and the phylogenetic position of *Asilisaurus kongwe*. Dinosaurs lack postfrontals (Gauthier, 1986), whereas stem archosaurs and pseudosuchians retain the element; the paucity of skull material for non-dinosaur avemetatarsalians does not allow us to pinpoint where the postfrontal was lost within early Avemetatarsalia.

Squamosal—The squamosal is represented by nearly complete right and partial left elements from NMT RB159 (Fig. 11). It has distinct anterior, posterior, ventral and anteromedial processes. All of those are nearly complete in the right side, except for the anteromedial process, which is broken in both specimens. The body of

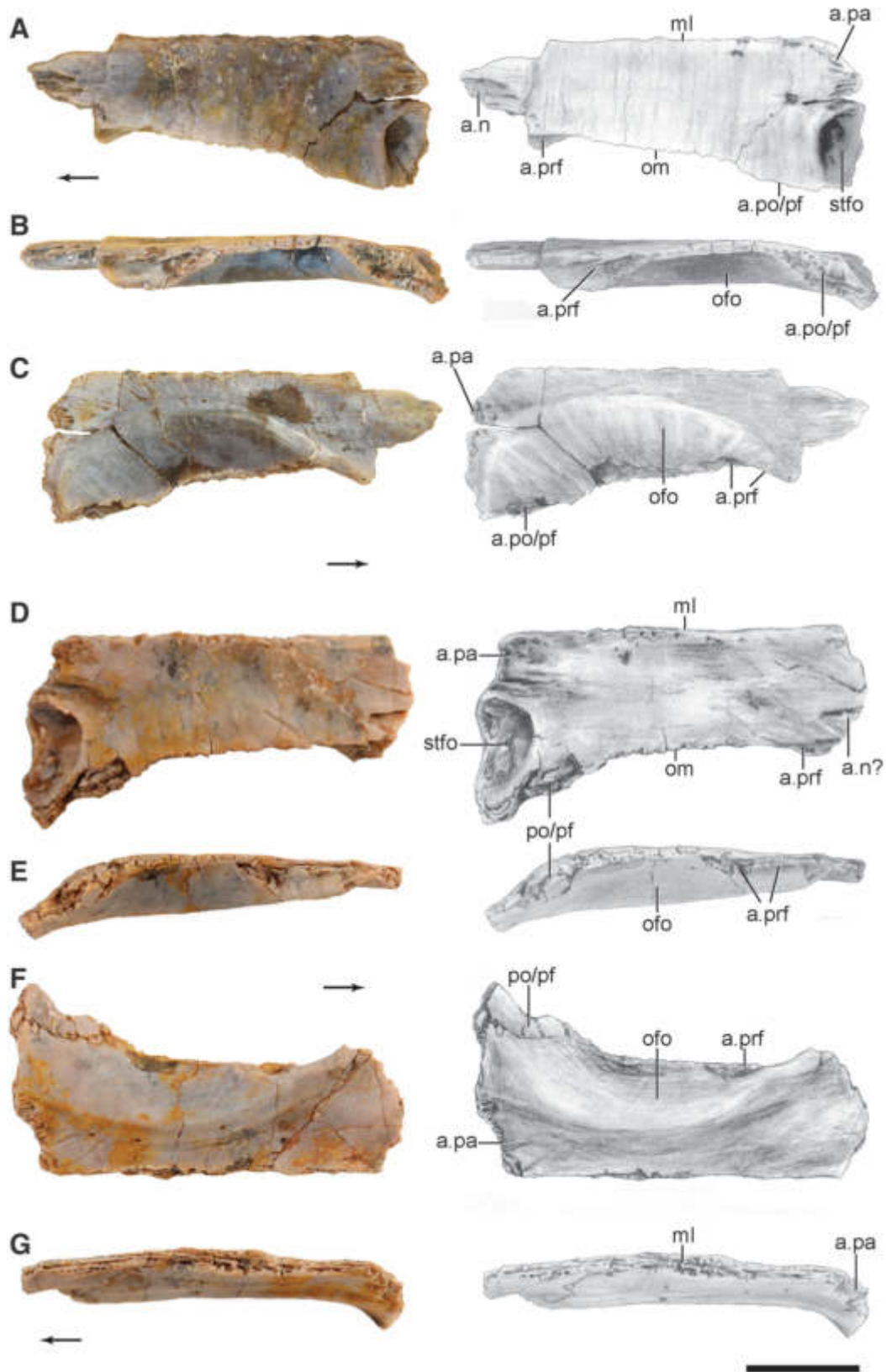


Fig. 10. Nearly complete frontals of a partial skeleton referred to *Asilisaurus kongwe* (NMT RB159). Photographs and drawings of the left frontal in dorsal (A), lateral (B), and ventral (C) views. Photographs and drawings of the right frontal in dorsal (D), lateral (E), ventral (F), and medial (G) views. Abbreviations: a., articulates with; ml, midline; n, nasal; ofo, orbital fossa; om, orbital margin; pa, parietal; pf/po, postfrontal or postorbital; prf, prefrontal; stfo, supratemporal fossa. Arrows indicate anterior direction. Scale bar equals 10 mm.

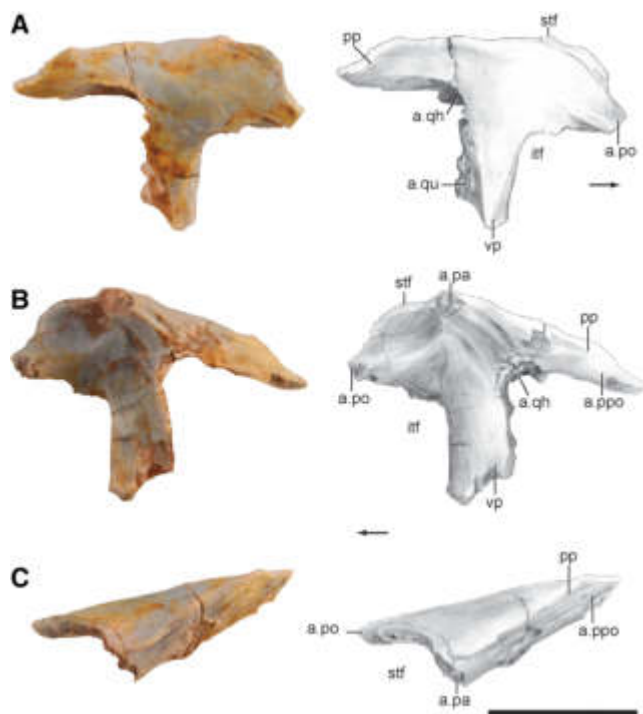


Fig. 11. Partial right squamosal of a partial skeleton referred to *Asilisaurus kongwe* (NMT RB159) in lateral (A), medial (B), and dorsal (C) views. Abbreviations: a. articulates with; itf, infratemporal fenestra; pa, parietal; po, postorbital; pp, posterior process; ppo, paroccipital process of the opisthotic; qh, quadrate head; qu, quadrate; stf, supratemporal fenestra; vp, ventral process. Arrows indicates anterior direction. Scale bar equals 10 mm.

the anterior process is dorsoventrally tall, but narrows to a point on the ventral half of the anteriormost extension of element. This pointed process likely fitted into a groove on the lateral surface of the posterior portion of the postorbital, and a medial slot just opposite to the pointed process likely accepted a posterior prong of the postorbital as in early dinosaurs (*Coelophysis bauri*, CMNH 31374; *Eoraptor lunensis*, Sereno et al., 2013). The area ventral to the slot is broken away. The ventral edge of the anterior process meets the ventral process at a near right angle (Fig. 11). A thin ridge located on the lateral surface of the ventral process originates at its junction to the anterior process and trends ventrally, subparallel to the posterior border of the infratemporal fenestra. The ventral process is wider dorsally than ventrally, because its posterior part bears a mediolaterally compressed lamina of bone that occupies a larger portion of the process as it proceeds ventrally. This lamina partially covers the lateral surface of the quadrate in lateral view. Ventral to this lamina of bone, the process tapers to a point, but its length is not known, because the ventral tip is not preserved. The posterior lamina of bone also expands somewhat medially, so that the medial surface of the ventral process bears a posteriorly directed, longitudinally elongate concavity that fits the dorsal portion of the quadrate.

The ventral and the posterior processes of the squamosal meet at a rounded, near right angle, dorsally shifted compared to the contact between the anterior and ventral processes. The point where the ventral and posterior

processes meet defines the dorsal articulation surface for the quadrate head. Thus, the head of the quadrate is visible in lateral view, similar to dinosaurs (Sereno and Novas, 1994; Langer and Benton, 2006). This articulation surface is concave with a longer anteroposterior than mediolateral axis. Posterior to this articulation surface, the posterior process of the squamosal tapers. Its medial surface angles dorsomedially and is nearly flat, with a few anteroposteriorly trending ridges. This surface likely contacted the paroccipital processes of the braincase. A distinct ridge defines the dorsal edge of the posterior process and this ridge continues anteriorly to define the dorsal edge of the anteromedial process. The anteromedial process is dorsoventrally compressed, with small parallel ridges on the dorsal surface and a thin ridge that marks the posteromedial edge of the element. The medial surface bears an anteromedially opening fossa at the base of the medial process. Ventral and posterior of this fossa, at the medial extension where the medial and posterior processes meet, two parallel grooves are present and contain small foramina (Fig. 11).

Jugal—The jugal is represented by the anterior half of the left element and a fragment of the right jugal body that lies ventral to the orbit (Fig. 12). The latter is low and tapers anteriorly. The bone is the mediolaterally thickest where it forms the ventral margin of the orbit. Here it is dorsally convex and marked by shallow grooves. The anterior process only slightly expands dorsally; this suggests that the lacrimal almost contacted the ventral margin of the orbit, as in some dinosaurs (e.g., *Coelophysis bauri*, Colbert, 1989; *Eoraptor lunensis*, Sereno et al., 2013). The articulation surface with the lacrimal is only visible in medial view; the ventral end of the lacrimal sits in a shallow depression near the dorsal margin and the posterior margin of this articulation surface suggests that there may have been some interdigitization between the two elements. The anteriormost portion of the jugal tapers and it does not appear that the jugal contributed to the antorbital fenestra or fossa like in *Silesaurus opolensis* (ZPAL Ab III/1930). A shallow but clear shelf,

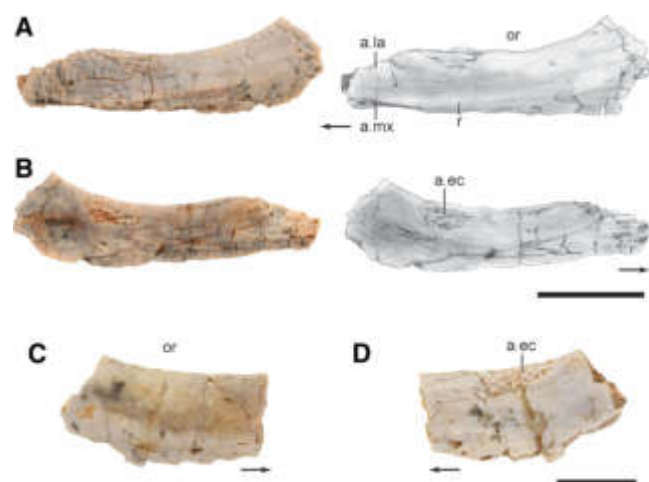


Fig. 12. Photographs and drawings of the jugals of a partial skeleton referred to *Asilisaurus kongwe* (NMT RB159). Left jugal in lateral (A) and medial (B) view. Fragmentary left jugal in lateral (C) and medial (D) views. Abbreviations: a., articulates with; ec, ectopterygoid; la, lacrimal; mx, maxilla; or, orbit; r, ridge. Arrows indicate anterior direction. Scale bar equals 10 mm in A, B and 5 mm in C, D.

with a dorsally bounded ridge, on the lateral surface of the anterior termination, marks the articulation surface with the posteriormost portion of the maxilla, thus indicating that the posterior end of the maxilla terminated posterior of the anterior margin of the orbit, as in most early dinosaurs (Nesbitt et al., 2009b; Martínez et al., 2011), and probably also in *Silesaurus opolensis* (Dzik, 2003). This articulation surface terminates into a point and then it continues on the lateral surface of the jugal as a distinct, but low anteroposteriorly oriented ridge. This ridge, which is also in *Silesaurus opolensis* (ZPAL Ab III/1930), fades posteriorly and disappears ventral to the base of the dorsal (= ascending) process. A distinctly more laterally developed ridge is present in *Lewisuchus admixtus* (PULR 01, CRILAR-Pv 552). The lateral surface of the jugal of *Asilisaurus kongwe* ventral to the anteroposteriorly oriented ridge has a number of small anteriorly opening foramina.

The medial surface of the jugal is nearly flat, with low and small anteroposteriorly oriented ridges (Fig. 12B, D). A distinct and rugose scar on its dorsal margin, near the base of the dorsal process, represents the articulation surface with the ectopterygoid. This facet indicates that the ectopterygoid lacked a contact with the maxilla. Posterior and ventral to this, the lateral surface of the jugal is depressed.

Quadratojugal—The quadratojugal is only represented by a small fragment still in articulation with the quadrate in NMT RB15 (Fig. 5D). Its posterior portion is L-shaped in lateral view with equally sized dorsal and anterior processes. The processes meet at an expanded posteroventral portion with a rounded posterior termination in lateral view. The dorsal process is thin in lateral view, anterodorsally directed, and expands medially to articulate with the lateral edge of the quadrate. No quadrate-quadratojugal foramen can be seen, but it is not certain that it was absent. The anterior process is dorsoventrally short, as in *Lewisuchus admixtus* (PULR 01), but unlike the much taller process in *Silesaurus opolensis* (ZPAL Ab III/1930).

Ectopterygoid—The ectopterygoid is represented by a nearly complete left element from NMT RB159 (Fig. 13). It lacks the jugal articulation surface of the lateral process and the dorsoventrally thin portions surrounding the articulation with the pterygoid. The lateral (=jugal) process is dorsally and anteriorly arched like that of dinosaurs (Gauthier, 1986) and other dinosauriforms (*Lewisuchus admixtus*; Bittencourt et al., 2015). It is overall a robust process with a rounded anterior edge on its dorsal margin. A ridge defines the posterodorsal margin of the process and its ventral surface is slightly concave dorsoventrally.

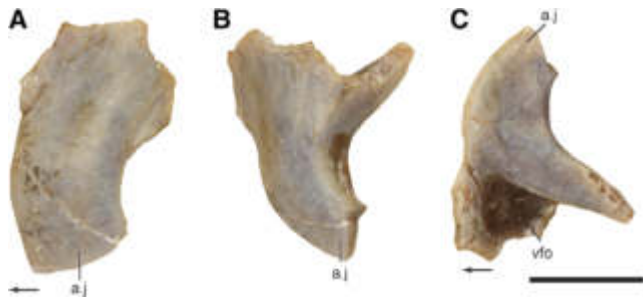


Fig. 13. Left partial ectopterygoid of a partial skeleton referred to *Asilisaurus kongwe* (NMT RB159) in dorsal (A), posterior (B), and ventral (C) views. Abbreviations: a., articulates with; j, jugal; vfo, ventral fossa. Arrows indicate anterior direction. Scale bar equals 5 mm.

The medial portion of the ectopterygoid splits into two processes, a robust posteromedial process and an anteromedial process. The posteromedial process is tapering and its ventral margin is marked by a well-developed ridge. The anteromedial process is convex on its anterior surface and concave on its posterior surface. A deep ventrally opening recess occurs between the two medial processes (Fig. 13). It excavates the medial margin of the posteromedial process to the extent that the medial expansion of the recess cannot be observed in ventral view. This ventral recess is present in a variety of theropods (Gauthier, 1986; *Liliensternus liliensterni*, MB R2175; *Allosaurus fragilis*, Madsen, 1976) and Triassic sauropodomorphs (e.g., *Plateosaurus erlenbergensis*; Prieto-Márquez and Norell, 2011; *Eoraptor lunensis*, Sereno et al., 2013), absent in ornithischians (Langer and Benton, 2006), but also in dinosauriforms outside Dinosauria (*Lewisuchus admixtus*; Bittencourt et al., 2015). The depth of the fossa in *Asilisaurus kongwe* is similar to that of theropods, which have been interpreted as pneumatic in origin (Rauhut, 2003). The dorsal surface of the medial expansion has a small triangular fossa framed by two ridges that converge anterolaterally. It appears, based on the articulation surfaces of the ectopterygoid, that the element would have attached to the dorsal surface of the pterygoid, like that of dinosaurs (Sereno and Novas, 1994; Langer and Benton, 2006) and other dinosauriforms (*Lewisuchus admixtus*; Bittencourt et al., 2015).

Quadrate—The quadrate is known from a few partial to nearly complete bones, including NMT RB15 (Fig. 5D) and NMT RB159 (Fig. 14). It has two larger processes extending anteriorly, a lateral process that articulates

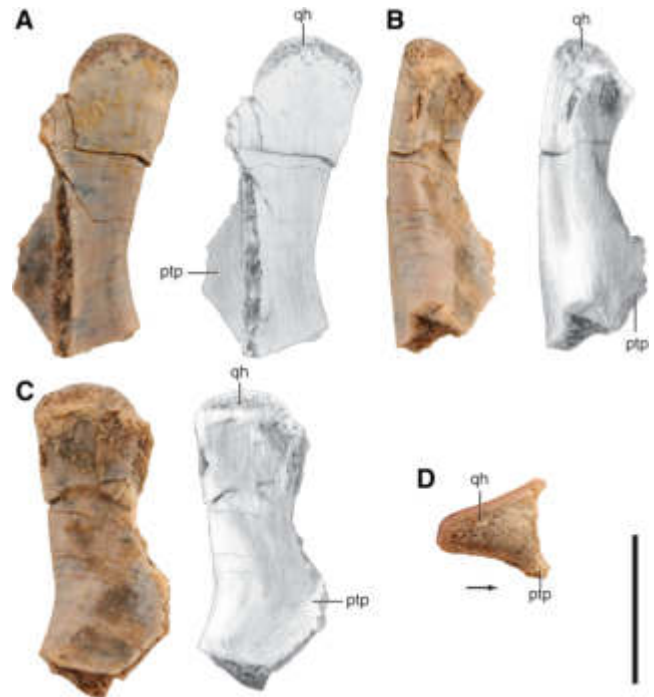


Fig. 14. Photograph and drawings of the dorsal half of the left quadrate of a partial skeleton referred to *Asilisaurus kongwe* (NMT RB159) in lateral (A), posterior (B), medial (C), and dorsal (D) views. Abbreviations: ptp, pterygoid process; qh, quadrate head. Arrow indicates anterior direction. Scale bar equals 10 mm.

with the quadratojugal ventrally and the squamosal dorsally and a more medial process that articulates with the pterygoid. Both processes are mediolaterally compressed and much of their anterior margins are not preserved in any of the specimens. The main body of the quadrate is triangular in cross section and the posterior margin is distinctly concave in lateral view. This posterior margin is gently rounded transversely. A quadratojugal-quadrate foramen, if present, would have been much smaller than that of *Teleocrater rhadinus* (Nesbitt et al., 2018).

The dorsal head of the quadrate, which articulates with the glenoid of the squamosal, is triangular to suboval in dorsal view, where the medial and the lateral edges of the head converge posteriorly and the long axis of the head is anteroposteriorly directed. In lateral and medial views, the head is convex dorsally. In posterior view, the head is canted medially in all specimens of *Asilisaurus kongwe*. Ventrally, the quadrate bears two condyles in a mediolateral plane that are separated by a small gap. The more lateral condyle has a mediolaterally oriented long axis, whereas the more medial condyle has an anteroposteriorly oriented long axis.

Dentary—The dentary is represented by many elements, including the holotype (NMT RB9; Fig. 15), a left and right pair (NMT RB837; Fig. 16), partial left and right elements from the well preserved skull (NMT RB159; Figs. 17, 18), among others (e.g., NMT RB15, Fig. 5; NMT RB130, Fig. 19). All of the referred anterior portion of the dentaries, including NMT RB159, share the unique character states of the holotype (see above). The new specimens also help to clarify and enrich the anatomy of the covered or missing portions of the holotype.

The anterior portion of the dentary tapers in lateral view, where the dorsal edge bends anteroventrally and the ventral edge arches anterodorsally. Additionally, it is important to note that, in medial view, that is, the surface that is exposed in the holotype (NMT RB9), the anteriormost portion of the dentary is slightly upturned. Indeed, the complete and well preserved NMT RB159 (Figs. 17 and 18) has a similar morphology in medial view, but this anterior “upturn” is a consequence of a

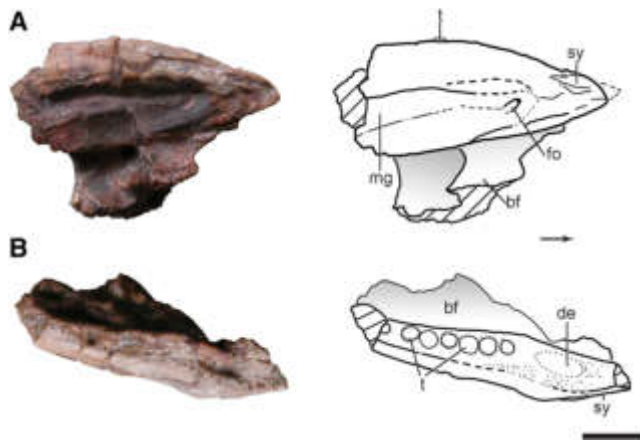


Fig. 15. Photographs and line drawings of the holotype left anterior portion of the dentary of *Asilisaurus kongwe* (NMT RB9) in medial (A) and occlusal (B) views. Abbreviations: bf, bone fragment; de, depression; fo, foramen; mg, Meckelian groove; sy, symphysis; t, tooth. Arrow indicates anterior direction. Scale bar equals 10 mm.

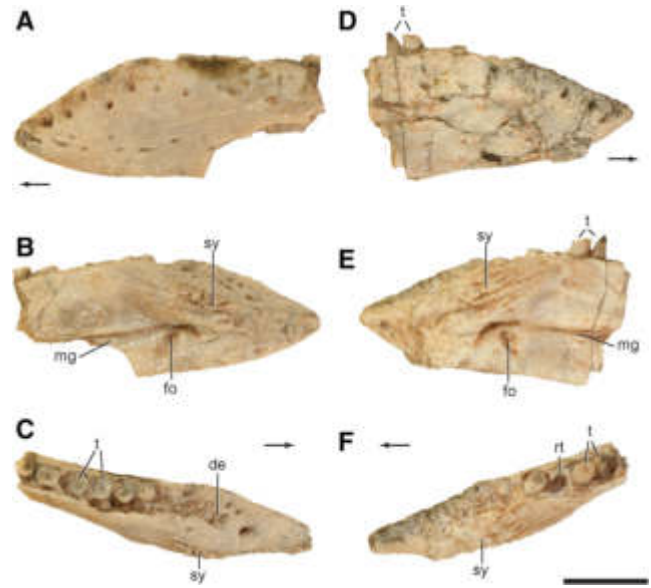


Fig. 16. Anterior portions of the left and right dentaries (NMT RB837) of an individual referred to *Asilisaurus kongwe*. Anterior portion of the right dentary in lateral (A), medial (B), and occlusal (C) views. Anterior portion of the left dentary in lateral (D), medial (E), and occlusal (F) views. Abbreviations: de, depression; fo, foramen; mg, Meckelian groove; rt, replacement tooth; sy, symphysis; t, tooth. Arrows indicate anterior direction. Scale bar equals 10 mm.

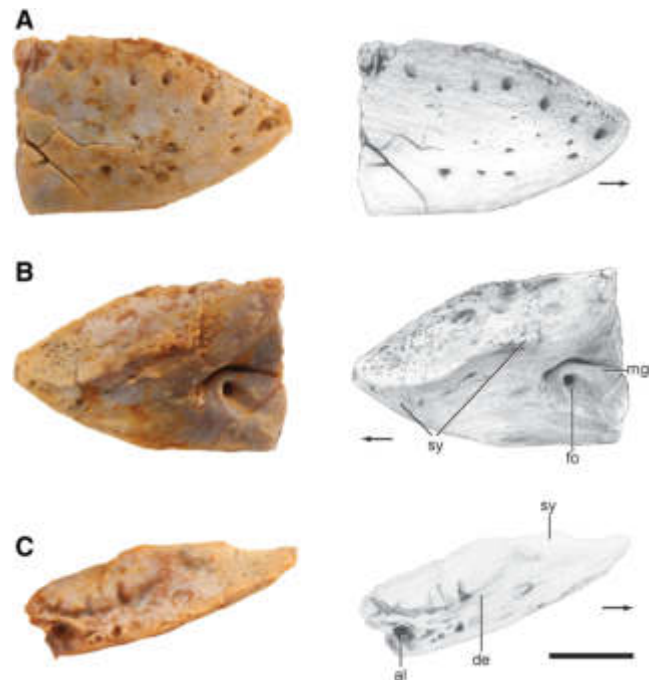


Fig. 17. Photographs and drawings of the anterior portion of the dentary of a partial skeleton referred to *Asilisaurus kongwe* (NMT RB159) in lateral (A), medial (B), and occlusal (C) views. Abbreviations: al, alveolus; de, depression; fo, foramen; mg, Meckelian groove; sy, symphysis; t, tooth. Arrows indicate anterior direction. Scale bar equals 10 mm.

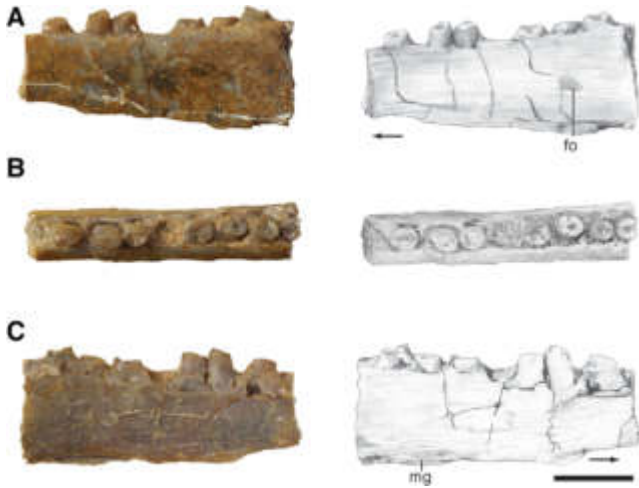


Fig. 18. Photographs and drawings of a partial left dentary of a partial skeleton referred to *Asilisaurus kongwe* (NMT RB159) in lateral (A), occlusal (B), and, medial (C) views. Abbreviations: fo, foramen; mg, Meckelian groove. Arrows indicates anterior direction. Scale bar equals 10 mm.

depression on the medial surface just adjacent to the anterior tip. The anteriormost portion of the dentary of *Asilisaurus kongwe* differs from those of all other silesaurids with a preserved dentary in that its anterior portion is anteriorly “downturned” and not anterodorsally expanded or “upturned” like that of *Silesaurus opolensis* (ZPAL Ab III 437/1) and *Sacisaurus agudoensis* (MCN PV10040, MCN PV10043; Langer and Ferigolo, 2013).

The lateral surface of the anterior portion of the dentary is smoothly dorsomedially convex, with a row of prominent dorsally and anterodorsally opening foramina that parallel the dorsal margin. A much smaller row of foramina line the dorsalmost edge. Other foramina are located on the anterior posterior of the dentary just like in *Silesaurus opolensis* (ZPAL Ab III/437/1). *Asilisaurus kongwe* lacks the prominent “sigmoidal groove” of *Sacisaurus agudoensis* (MCN PV10061; Langer and Ferigolo, 2013) and also possibly of *Silesaurus opolensis* (Langer and Ferigolo, 2013). Moreover, *Asilisaurus kongwe* also lacks the large anteriorly opening foramen near the start of the dentition seen in *Sacisaurus agudoensis* (MCN PV10041; Langer and Ferigolo, 2013) and *Silesaurus opolensis* (ZPAL Ab III 437/1). A slightly rugose surface on the anterior portion of the lateral side of the dentary may mark the area that was capped by a rhamphotheca in life (Holliday and Nesbitt, 2013), but it is clear that there is no posterior boundary as suggested for *Sacisaurus agudoensis* (Langer and Ferigolo, 2013).

Medially, the anterior portion of the dentary has a horizontal shelf that extends to the symphysis (Figs. 15–17); at the midline, the medial margin of the shelf is slightly rounded dorsoventrally. Grooves and ridges mark the dentary symphysis and these rugosities cover much of the anterior portion of the medial surface. The exact configuration of the grooves and ridges differs across the specimens and even across the left and right sides of the same individual. In general, the symphysis is divided into a horizontal portion and a more ventral portion that parallels the anteroventral margin of the dentary; both surfaces converge at the anteriormost tip of the bone. The

horizontal component turns posteriorly into a set of parallel grooves and ridges that reach the anteriormost teeth (Fig. 17). No deep groove is present on the symphysis surface as there is in *Sacisaurus agudoensis* (MCN PV10043; Langer and Ferigolo, 2013) and *Silesaurus opolensis* (ZPAL Ab III 437/1). This groove originally considered as an anterior extension of the Meckelian groove (Nesbitt et al., 2010; Nesbitt, 2011) was reinterpreted as separate from the groove by Langer and Ferigolo (2013) (see below). In articulation, the dentaries diverge from one another at a $\sim 40^\circ$ angle. Posterior to the symphysis, the Meckelian groove terminates in a rounded depression well anterior or the start of the dentary tooth row. At the anterior termination of the Meckelian groove, a rounded, medially opening foramen is located just ventral to a long, crescent shaped furrow in all of the specimens (Figs. 15–17). The posterior margin of the crescent shaped opening transforms into the dorsal margin of the Meckelian groove. *Sacisaurus agudoensis* (MCN PV10043; Langer and Ferigolo, 2013) possesses two foramina in the same region that we interpret as homologous.

The Meckelian groove divides the medial surface of the dentary in almost equal dorsal and ventral portions and the groove maintains a similar height through much of the anterior part of the dentary. This differs from the tall part dorsal to the Meckelian groove in a specimen referred to *Lewisuchus admixtus* (CRILAR-Pv 552) and in *Silesaurus opolensis* (ZPAL Ab III/437/1). The dorsal portion of the medial side of the dentary of *Asilisaurus kongwe* is gently convex dorsoventrally, whereas the ventral portion is flat, likely for articulation with a corresponding flat surface of the splenial (see below).

Dorsally, the lateral edge of the anterior end of the dentary bows laterally and forms a sharp ridge (=cutting blade) that lacks any dentition. Similarly, both *Silesaurus opolensis* (ZPAL Ab III/437/1) and *Sacisaurus agudoensis* (MCN PV10043) lack dentition in this part of the dentary. However, the dentition of *Asilisaurus kongwe* starts further posteriorly than in both *Silesaurus opolensis* (ZPAL Ab III/437/1) and *Sacisaurus agudoensis* (MCN PV10043). The medial surface of the cutting blade bears several small foramina and larger, dorsally opening foramina parallel the lateral margin. These larger foramina lie in a groove that is also present in the holotype (Fig. 15) and this groove continues medially to the anterior start of the dentition. The surface medial to the groove with foramina is gently rounded dorsoventrally.

None of the dentaries are complete; the anterior tip of the bone is much more commonly preserved than the middle (NMT RB159; Fig. 18) or posterior portions (NMT RB130; Fig. 19). In lateral view, the dorsal margin of the dentary is nearly straight, contrasting with the dorsally bowed dentary of *Lewisuchus admixtus* (PULR 01, CRILAR-Pv 552). In medial view, the dorsal margin is also straight, but it is ventrally shifted slightly compared to the lateral view. From the preserved dentary pieces, we conclude that there were a minimum of eight teeth, with the possibility of only one or two more. The dentary tooth count in *Asilisaurus kongwe* is, therefore, lower than that of *Silesaurus opolensis* (ZPAL Ab III 437/1) in which there were at least 12 teeth (Dzik, 2003) and *Sacisaurus agudoensis* (MCN PV10043) in which they are ~ 15 (Langer and Ferigolo, 2013). The posterior portion of the dentary of *Asilisaurus kongwe* lacks dentition, similar to *Silesaurus opolensis* (ZPAL Ab III 361/27). The total number of

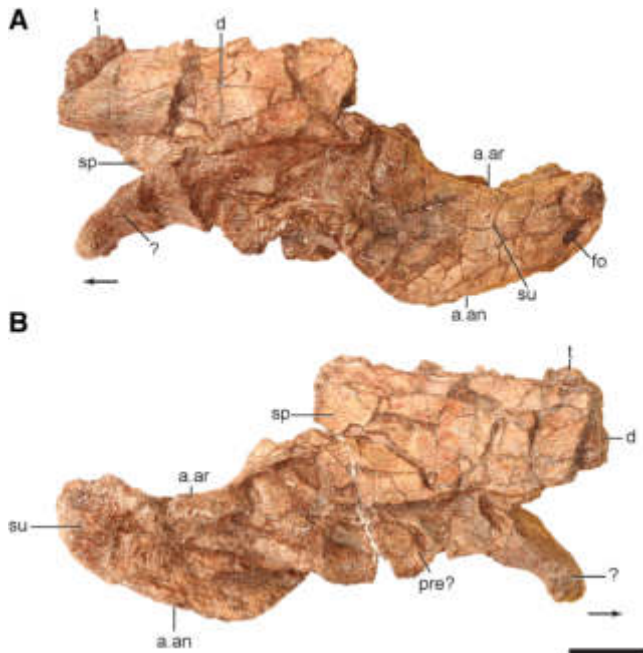


Fig. 19. Partial left hemimandible (NMT RB130) referred to *Asilisaurus kongwe* from the holotype locality in lateral (A) and medial (B) views. Abbreviations:?, unknown; a., articulates with; an, angular; ar, articular; d, dentary; fo, foramen; pre?, prearticular; sp, splenial; su, surangular; t, tooth. Arrows indicates anterior direction. Scale bar equals 10 mm.

dentary teeth of *Asilisaurus kongwe* indicates that there were fewer teeth in the dentary than in the upper tooth row (one in the premaxilla, 10+ in the maxilla).

Articular and Surangular—The articular and articulated partial surangular is known from the spectacularly preserved right side from NMT RB159 (Fig. 20), and other isolated specimens from the holotype locality (NMT RB140, NMT RB128). The articular of NMT RB159 is nearly complete, but is missing the extreme ends of the medial process of the main body and the medial process of the retroarticular process. The glenoid, as viewed in dorsal view, consist of two depressions that fit to the ventral condyles of the quadrate (see above). Here, the bone is spongy and not compact like that of the rest of the articular. A ridge, trending posterolaterally to anteromedially, divides the two condyle basins. A small dorsally opening fossa is located anterior and adjacent to the glenoid. A well-defined ridge separates the posterior margin of the glenoid from the retroarticular process. The medial portion of the ridge extends further dorsally than the lateral portion and extends medially as a short finder of bone. A small, dorsally opening foramen is present directly posterior of the medial basin and exits on the medial surface of the articular well ventral of the glenoid. This foramen likely allowed the passage of the chorda timpani.

The posterior expansion of the articular beyond the glenoid, typically referred to as the retroarticular process, is longer than the anteroposterior length of the rest of the articular, similar to that of *Lewisuchus admixtus* (as illustrated by Romer, 1972: Fig. 1; region currently lost) and *Silesaurus opolensis* (ZPAL Ab III/1930). In dorsal view, the process is triangular, with medial and lateral margins that converge posteriorly. The dorsal surface, which is composed of compact bone, is concave between the posterior

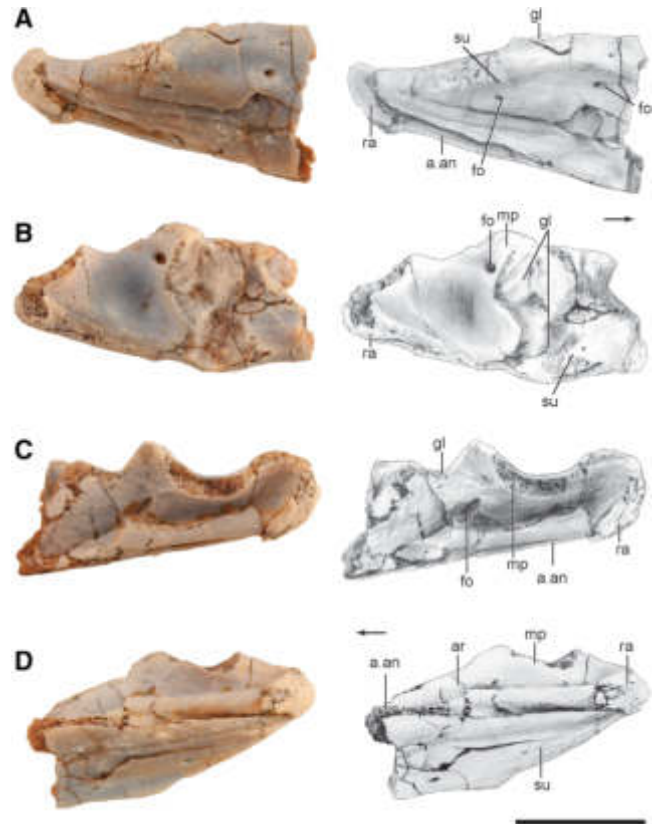


Fig. 20. Photographs and drawings of the posterior portion of the right hemimandible of a partial skeleton referred to *Asilisaurus kongwe* (NMT RB159) in lateral (A), dorsal (B), medial (C), and (D) ventral views. Abbreviations: a., articulates with; an, angular; ar, articular; fo, foramen; gl, glenoid; mp, medial process; ra, rough area; su, surangular. Arrows indicate anterior direction. Scale bar equals 10 mm.

termination and the posterior margin of the glenoid. The medial edge of this concave surface, although broken, does indicate that a medially projecting articular process was present (Fig. 20); the base of this process is crescent-shaped. The tapering posterior end expands dorsally and medially like in *Silesaurus opolensis* (ZPAL Ab III/1930), but the extent of the medial expansion in *Asilisaurus kongwe* is not known because of breakage in all specimens. However, it is clear that a medially opening fossa excavated the medial surface of the posterior end of the posterior process. The posteriormost edge of the process is “capped” by bone with a striated surface, forming clear ventral and medial margins (Fig. 20). The ventral margin of the posterior process is straight in lateral view, extends posterodorsally to anteroventrally, and is gently mediolaterally rounded. A sliver of the articular is visible in lateral view, from the posterior termination to a point ventral to the glenoid.

The surangular is mostly coossified to the articular in NMT RB159; in some places, breaks in the specimen appear to coincide with the contact between the two elements. The posterior portion of the surangular tapers posteriorly, similar to that of articular. The posteriormost portion of the surangular gently turns dorsally to form part of the dorsal expansion present in the articular. The dorsal portion of the lateral surface of the surangular is rugose between the glenoid and the posterior extent of the

element. The lateral surface is weakly dorsoventrally concave and a few small foramina are present on its dorsal half. The largest of the foramina is located just anterior of the glenoid and this is likely homologous with the surangular foramen of many archosauromorphs (Nesbitt, 2011; Ezcurra, 2016). The lateral surface of the surangular does have a low and poorly defined surangular ridge as in a specimen referred to *Lewisuchus admixtus* (CRILAR-Pv 552) and *Silesaurus opolensis* (ZPAL Ab III/451), but this is in contrast to the much more prominent ridges of most archosaurs (Nesbitt, 2011). The dorsal margin of the surangular is gently rounded mediolaterally.

A concave dorsal margin, viewed in lateral view, marks the lateral extent of the glenoid. In dorsal view, the surangular clearly forms much of the lateral basin of the glenoid. The contact between the surangular and the articular is angled anteromedially to posterolaterally through the lateral basin and stretches anterior of the medial basin of the glenoid. In anterior view, there is a deep fossa ventral to the dorsal surface and there may be a foramen in the center of the fossa, but it is not clear. The placement and orientation of the glenoid of *Asilisaurus kongwe* with respect to the rest of the hemimandible is not clear. It is not known if it is located well ventral of the dorsal margin of the dentary and the surangular arched more dorsally, like sauropodomorphs (e.g., *Plateosaurus engelhardti*; Prieto-Márquez and Norell, 2011), or if the glenoid is at a similar horizontal level as the dorsal margin of the dentary and the surangular is more horizontally oriented, like that of theropods (e.g., *Coelophysis bauri*, CMNH 31374).

Splenial—The splenial is known from just fragments of the left and possibly the right elements from NMT RB159 (Fig. 8G, H). The medial side is smooth and convex in the dorsoventral plane. The ventral and dorsal edges taper in medial view. The ventral portion of the flat lateral surface bears an articulation facet for the dentary. Dorsal to this facet, the lateral surface of the bone is slightly dorsoventrally concave.

Dentition—The dentition of *Asilisaurus kongwe* is poorly represented across the tooth bearing elements; only dentary crowns are known (Fig. 21). All dentition of *Asilisaurus kongwe* is fused to the dentary when the tooth is fully erupted like other silesaurids (Nesbitt et al., 2010; Nesbitt, 2011). In the case of the holotype dentary of *Asilisaurus kongwe*, nearly every tooth is fused and broken at its base (Fig. 15). The teeth are closely spaced at their bases and interdental plates are clearly present in the maxilla, but much less distinct in the dentary. The tooth crowns of the dentary of *Asilisaurus kongwe* bear a variable number of serrations (Fig. 21) on mesial and distal carina, but the variation pattern is not clear given the small sample size. The long axis of the serrations is oblique to the apicobasal axis of the crown and the tip of each serration is pointed in lingual and labial views. The pointed tip of the crowns are distally shifted relative to the mesiodistal middle of the tooth, but the teeth are not recurved. Each tooth has a circular root in cross section and the crown is not labiolingually compressed as the teeth of most archosauriforms from the Triassic Period (Nesbitt, 2011). No cingulum is present in *Asilisaurus kongwe*, a feature present in some teeth of *Sacisaurus agudoensis* (MCN PV10053).

Vertebral Column

Cervical Vertebrae—*Atlas-Axis*. This region of the cervical series is represented by a partial axis fused to the

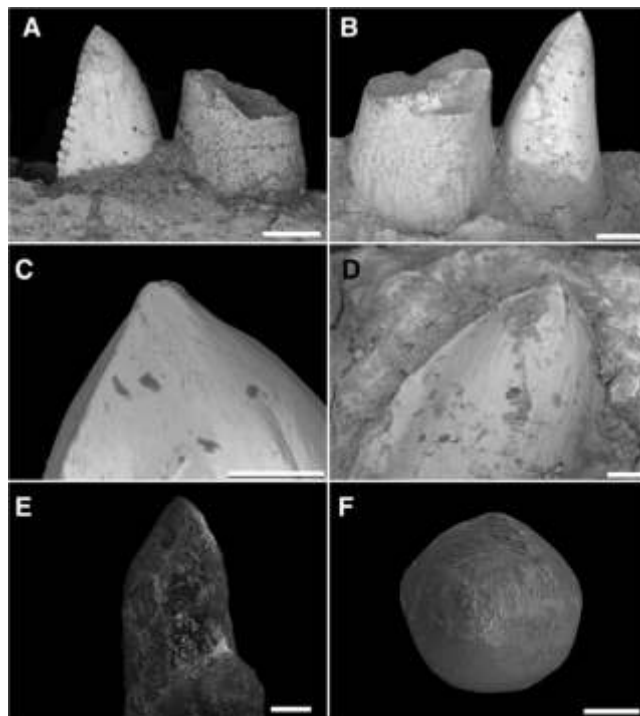


Fig. 21. Scanning electron micrographs of the dentary teeth of *Asilisaurus kongwe*. Dentary teeth positions 3 and 4 of NMT RB837 in labial (A) and lingual (B) views. (C) Tip of the 4 tooth (NMT RB837) in labial view. (D) Top of a replacement tooth in position 2 in lingual view (NMT RB837). Isolated holotype tooth of *Asilisaurus kongwe* (NMT RB9) in lingual (E) and occlusal (F) views. Scale bar equals 0.5 mm in A, B and 100 μ m in C–F.

odontoid process (atlantal centrum) and the axial inter-centrum (NMT RB147; Fig. 22A–D). The odontoid process is transversely broader than dorsoventrally tall and extends anteriorly distinctly beyond the level of the axial

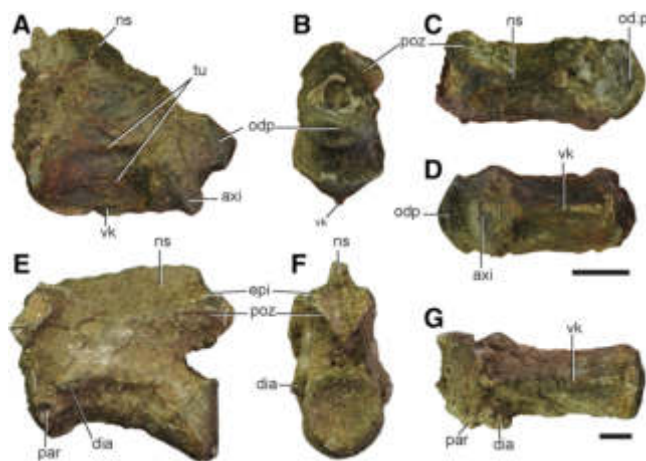


Fig. 22. Anterior cervical vertebrae referred to *Asilisaurus kongwe*. Atlas/axis (NMT RB147) in right lateral (A), anterior (B), dorsal (C), and ventral (D) views. Anterior cervical (NMT RB21) in left lateral (E), posterior (F), and ventral (G) views. Abbreviations: axi, axis intercentrum; dia, diapophysis; epi, epiphysis; ns, neural spine; odkp, odontoid process; par, parapophysis; poz, postzygapophysis; tu, tuberosity; vk, ventral keel. Scale bars equal 5 mm.

intercentrum. In lateral view, this process is sub-pentagonal, with an anteriorly facing apex and an anterodorsal margin longer than the anteroventral one. The shape of the odontoid process is highly variable in lateral view among early dinosauriforms, being trapezoidal in *Silesaurus opolensis* (ZPAL Ab III/361), subtriangular in *Herrerasaurus ischigualastensis* (PVSJ 407), *Buriolestes schultzi* (Müller et al., 2018), and *Scelidosaurus harrisonii* (NHMUK PV R1111), or ending anteriorly as a ball-like structure in *Heterodontosaurus tucki* (SAM-PK-K1332). The odontoid process of *Asilisaurus kongwe* is subtriangular in dorsal view (Fig. 22C), with a median anterior apex, and its dorsal and ventral surfaces are concave and convex, respectively. The lateral surface of the odontoid process is gently anteroposteriorly concave to receive the atlantal intercentrum, but lacks the well-defined, anteroventrally to posterodorsally oriented groove present in *Herrerasaurus ischigualastensis* (PVSJ 407) and *Buriolestes schultzi* (Müller et al., 2018).

The axial intercentrum is semilunate-shaped in anterior view and transversely broader than the axial centrum (Fig. 22A), as occurs in other dinosauriforms (e.g., *Lewisuchus admixtus*, PULR 01; *Silesaurus opolensis*, Piechowski and Dzik, 2010; *Herrerasaurus ischigualastensis*, Sereno and Novas, 1994; *Scelidosaurus harrisonii*, NHMUK PV R1111). The axial intercentrum is D-shaped in ventral view, with a gently posteriorly concave posterior margin and a strongly convex anterior margin. The length of this intercentrum is less than half the length of the axial centrum. The ventral and lateral surfaces of the intercentrum are transversely convex, whereas the anterodorsal surface, which received the atlantal intercentrum, is concave.

The axis preservationally lacks the left postzygapophysis, both prezygapophyses, and most of the neural spine (Fig. 22A–D). The neurocentral suture is closed. The centrum is moderately transversely compressed at mid-length and approximately 1.5 times longer than tall, resembling the condition in *Marasuchus lilloensis* (PVL 3870: ratio = 1.7; PVL 3872: ratio = 1.5), *Lewisuchus admixtus* (PULR 01: ratio 1.7), *Silesaurus opolensis* (ZPAL Ab III/361: ratio = 1.7), *Herrerasaurus ischigualastensis* (PVSJ 407: ratio = 1.6), *Heterodontosaurus tucki* (SAM-PK-K1332: ratio = 1.4), and *Dilophosaurus wetherilli* (UCMP 37302: ratio = 1.5). By contrast, the centrum is distinctly proportionally longer in the aphanosaurs *Yarasuchus deccanensis* (ISIR 334: ratio = 3.2) and *Teleocrater rhadinus* (NMT RB504: ratio = 2.7). The anterior and posterior articular surfaces of the axis of *Asilisaurus kongwe* are placed approximately at the same level in lateral view. The ventral surface of the centrum possesses a well-developed, longitudinal median keel, which has a mostly straight ventral margin in lateral view, as also occurs in *Teleocrater rhadinus* (Nesbitt et al., 2018), *Marasuchus lilloensis* (PVL 3872) and *Lewisuchus admixtus* (PULR 01; Bittencourt et al., 2015). The axis of *Silesaurus opolensis* (ZPAL Ab III/361) and *Herrerasaurus ischigualastensis* (PVSJ 407) also possesses a well-developed ventral keel, but it has a ventrally concave profile in lateral view. The articular facet for the axial rib cannot be confidently identified on the anterior end of the axial centrum or intercentrum. There is no diapophysis on the neural arch, as occurs in other early avemetatarsalians (e.g., *Teleocrater rhadinus*, Nesbitt et al., 2018; *Lewisuchus admixtus*, PULR 01; *Silesaurus opolensis*, Piechowski and Dzik, 2010) and several early dinosaurs (e.g., *Herrerasaurus*

ischigualastensis, PVSJ 407; *Heterodontosaurus tucki*, SAM-PK-K1332; *Lesothosaurus diagnosticus*, Baron et al., 2016; *Buriolestes schultzi*, Müller et al., 2018). The lateral surface of the centrum possesses two low longitudinal tuberosities, one placed approximately at mid-height and the other immediately ventral to the base of the neural arch. The latter tuberosity bows ventrally and extends adjacent to the posterolateral rim of the centrum, closely resembling the condition in some other dinosauriforms, such as *Lewisuchus admixtus* (PULR 01) and *Coelophysis bauri* (MCZ 4333). These tuberosities bound a dorsoventrally concave surface, as occurs in *Teleocrater rhadinus* (Nesbitt et al., 2018) and *Lewisuchus admixtus* (Bittencourt et al., 2015).

The postzygapophysis is posteriorly projected at approximately the same level as the posterior margin of the centrum and posterolaterally oriented laterally at an angle of around 50° with respect to the sagittal axis of the vertebra. There is no evidence of an epipophysis on the dorsal surface of the postzygapophysis, as occurs in other non-dinosaurian dinosauriforms (e.g., *Lewisuchus admixtus*, Bittencourt et al., 2015; *Silesaurus opolensis*, ZPAL Ab III/361) and some ornithischian dinosaurs (e.g., *Lesothosaurus diagnosticus*, Butler, 2005; Baron et al., 2016; *Heterodontosaurus tucki*: SAM-PK-K1332). By contrast, the axis of *Teleocrater rhadinus* (Nesbitt et al., 2018), *Yarasuchus deccanensis* (ISIR 334), and several dinosaurs (e.g., *Scelidosaurus harrisonii*, NHMUK PV R1111; *Herrerasaurus ischigualastensis*, Sereno and Novas, 1994; *Eoraptor lunensis*, Sereno et al., 2013; *Buriolestes schultzi*, Müller et al., 2018; *Dilophosaurus wetherilli*, UCMP 37302), possesses an epipophysis that extends posteriorly beyond the postzygapophyseal facet. The base of the axial neural spine of *Asilisaurus kongwe* extends along the entire dorsal surface of the neural arch and is connected with the postzygapophyses by laterally curved ridges.

Anterior-middle postaxial cervical vertebrae. Three anterior-middle cervical vertebrae of *Asilisaurus kongwe* are preserved. One of these vertebrae (NMT RB21; Fig. 22E–G) is more anterior than the others (probably third to fifth cervical element) because its centrum is proportionally longer and the diapophyses placed lower on the centrum than in the other available cervical vertebrae. These changes can be observed through the anterior-middle cervical series of other early avemetatarsalians with articulated or well-known cervical sequences (e.g., *Teleocrater rhadinus*, Nesbitt et al., 2018; *Lewisuchus admixtus*, PULR 01; *Silesaurus opolensis*, Piechowski and Dzik, 2010).

Anterior postaxial cervical vertebra. The anteriormost preserved cervical vertebra (NMT RB21; Fig. 22E–G) lacks most of the prezygapophyses and neural spine. It has a closed neurocentral suture. The centrum is parallelogram-shaped in lateral view, with the anterior articular facet placed dorsally to the posterior one, and the ventral margin of the centrum strongly concave in lateral view, resembling the condition in the anterior cervical vertebrae of other early avemetatarsalians (e.g., *Teleocrater rhadinus*, Nesbitt et al., 2018; *Marasuchus lilloensis*, Sereno and Arcucci, 1994b; *Lewisuchus admixtus*, Bittencourt et al., 2015; *Silesaurus opolensis*, Piechowski and Dzik, 2010; *Herrerasaurus ischigualastensis*, MACN-Pv 18060) and several non-avemetatarsalian archosauromorphs (Nesbitt et al., 2015; Ezcurra, 2016). The ventral surface of the centrum possesses a median keel that extends along its entire

length and anteriorly projects ventrally to the rim of the centrum, as occurs in the anterior cervical vertebrae of some early dinosauriforms, such as *Herrerasaurus ischigualastensis* (PVSJ 407) and *Silesaurus opolensis* (ZPAL Ab III/unnumbered). The centrum is approximately 2.3 times longer than its posterior height, closely resembling the proportions seen on the third and fourth cervical vertebrae of *Silesaurus opolensis* (ZPAL Ab III 411/7, 361: ratio = 2.3–2.4) and the third cervical vertebra of *Lewisuchus admixtus* (PULR 01: ratio = 2.3). By contrast, the postaxial anterior cervical vertebrae of aphanosaurs are considerably longer (*Teleocrater rhadinus*, Nesbitt et al., 2018, ratio = 3.0–3.1; *Yarasuchus deccanensis*, ISIR 334, ratio = 2.8) and those of *Marasuchus lilloensis* shorter (PVL 3870, ratio = 2.0; PVL 3872: ratio = 1.8). Both anterior and posterior articular surfaces of the centrum of NMT RB21 are gently concave and sub-circular. Its lateral surface is dorsoventrally convex ventral to the diapophysis. The parapophysis is placed on the anteroventral corner of the centrum, adjacent to its anterior rim. The articular facet of the parapophysis is subcircular. The diapophysis is placed posterodorsal to and closely approaching the parapophysis. The base of the diapophysis extends posteriorly as a low, ventrally concave ridge up to slightly posterior to the mid-length of the centrum, as occurs in *Lewisuchus admixtus* (PULR 01), *Marasuchus lilloensis* (PVL 3870) and early saurischians (e.g., *Herrerasaurus ischigualastensis*, PVSJ 407). A similar, but lower, posterior extension of the base of the diapophysis also occurs in the aphanosaurs *Teleocrater rhadinus* (Nesbitt et al., 2018; NMT RB505) and *Yarasuchus deccanensis* (ISIR 334). By contrast, the anteriormost postaxial cervical vertebrae of *Silesaurus opolensis* distinctly possess more laterally projected and dorsally placed diapophyses (Piechowski and Dzik, 2010; ZPAL Ab III/1930). The diapophysis of the anterior postaxial cervical vertebrae of the early ornithischians *Heterodontosaurus tucki* (Santa, 1980; SAM-PK-K1332) and *Eocursor parvus* (Butler, 2010; SAM-PK-K8025) are centrally placed on the lower end of the neural arch and do not extend posteriorly as a ridge.

The neural arch of the anteriormost preserved postaxial cervical vertebra of *Asilisaurus kongwe* (NMT RB21; Fig. 22E–G) lacks laminae, as also occurs in aphanosaurs (Nesbitt et al., 2018), *Lewisuchus admixtus* (PULR 01), *Marasuchus lilloensis* (PVL 3870), and early dinosaurs (e.g., *Herrerasaurus ischigualastensis*, PVSJ 407; *Heterodontosaurus tucki*, SAM-PK-K1332; *Eocursor parvus*, SAM-PK-K8025). By contrast, *Silesaurus opolensis* possesses well-developed posterior centrodiapophyseal and postzygodiapophyseal laminae in all the postaxial cervical vertebrae (Piechowski and Dzik, 2010; ZPAL Ab III/1930). The postzygapophyses project posteriorly to the posterior margin of the centrum and they are separated from one another by a deep, oval postspinal fossa. The postzygapophyseal articular facets are oval and face lateroventrally, forming an acute angle between one another in posterior view. The postzygapophyses contact one another on the median line and there is no hyposphene. The dorsal surface of the postzygapophysis possesses a sharp, very low prominence that is interpreted as an epipophysis, closely resembling the condition described by Bittencourt et al. (2015) for the holotype of *Lewisuchus admixtus* (although these authors did not interpret these structures as epipophyses). The neural spine is transversely narrow and extends anteroposteriorly along the entire dorsal surface of the neural arch.

Anterior-middle postaxial cervical vertebrae. The other two, more posterior, anterior-middle cervical vertebrae (NMT RB851, RB159; Fig. 23) share a very similar morphology and, as a result, are described together. One of these vertebrae (NMT RB851; Fig. 23F, G, I) lacks the right prezygapophysis, most of the right diapophysis, left postzygapophysis and neural spine; whereas the other vertebra (NMT RB159; Fig. 23A–E, H) is fairly complete, missing only most of the left diapophysis and the distal margin of the neural spine. The neurocentral sutures are closed in both vertebrae. The centra are parallelogram-shaped in lateral view, with the anterior articular facet placed dorsally to the posterior. The ventral surface of the centra possesses a longitudinal median keel that is less anteroposteriorly concave than in the anteriormost preserved postaxial cervical vertebra. The centra are approximately 2.0 times longer than their posterior height, thus being slightly proportionally shorter than the above described postaxial cervical vertebra and resembling the condition of a sixth cervical vertebra of *Silesaurus opolensis* (ZPAL Ab III/361: ratio = 1.9). Both anterior and posterior articular surfaces of the centra are gently concave, being sub-circular in NMT RB851 and slightly taller than broad in NMT RB159. The lateral surface of the centra is gently convex dorsoventrally and the parapophyses are placed on their anteroventral corner, adjacent to the anterior rim. The diapophyses are anteroposteriorly longer than in the above described vertebra, but still distinctly shorter than those of the anterior-middle postaxial cervical vertebrae of *Silesaurus opolensis* (Piechowski and Dzik, 2010). The articular facet of the diapophysis closely approaches that of the parapophysis, but is separated from that by a cleft. The articular facet of the diapophysis is subcircular and faces lateroventrally. The base of the diapophysis extends posteriorly as a short ridge, contrasting with the longer ridge present in the above described more anterior cervical vertebra. Immediately ventral to this ridge there is a raised portion of bone in NMT RB159, with a shallowly concave surface.

The neural arch of these two anterior-middle cervical vertebrae lack laminae, as occurs in the anteriormost postaxial cervical vertebra described above (Fig. 23), but contrasting with the anterior-middle postaxial cervical vertebrae of *Silesaurus opolensis* (Piechowski and Dzik, 2010). The lateral surface of the base of the neural arch, anteroventrally to the postzygapophysis, has a shallow, poorly rimmed fossa, resembling the condition in the sixth cervical vertebra of *Lewisuchus admixtus* (PULR 01). This fossa occurs in a very similar position than the much deeper postzygapophyseal centrodiapophyseal fossa of the anterior-middle cervical vertebrae of *Silesaurus opolensis* (Piechowski and Dzik, 2010). The prezygapophyses extend anteriorly distinctly beyond the level of the centrum and their articular facet is oval, slightly longer than broad, and faces mainly dorsally. There is a deep and small prespinal fossa that separates the base of both prezygapophyses and does not extend onto the neural spine (Fig. 23C). The postzygapophyses extend posteriorly to the posterior margin of the centrum and are separated from one another by a deep, oval postspinal fossa that invades the base of the neural spine in posterior view. The postzygapophysis of NMT RB159 possess a thick, blunt epipophysis that extends posteriorly slightly beyond the rim of the postzygapophyseal facet (Fig. 23D),

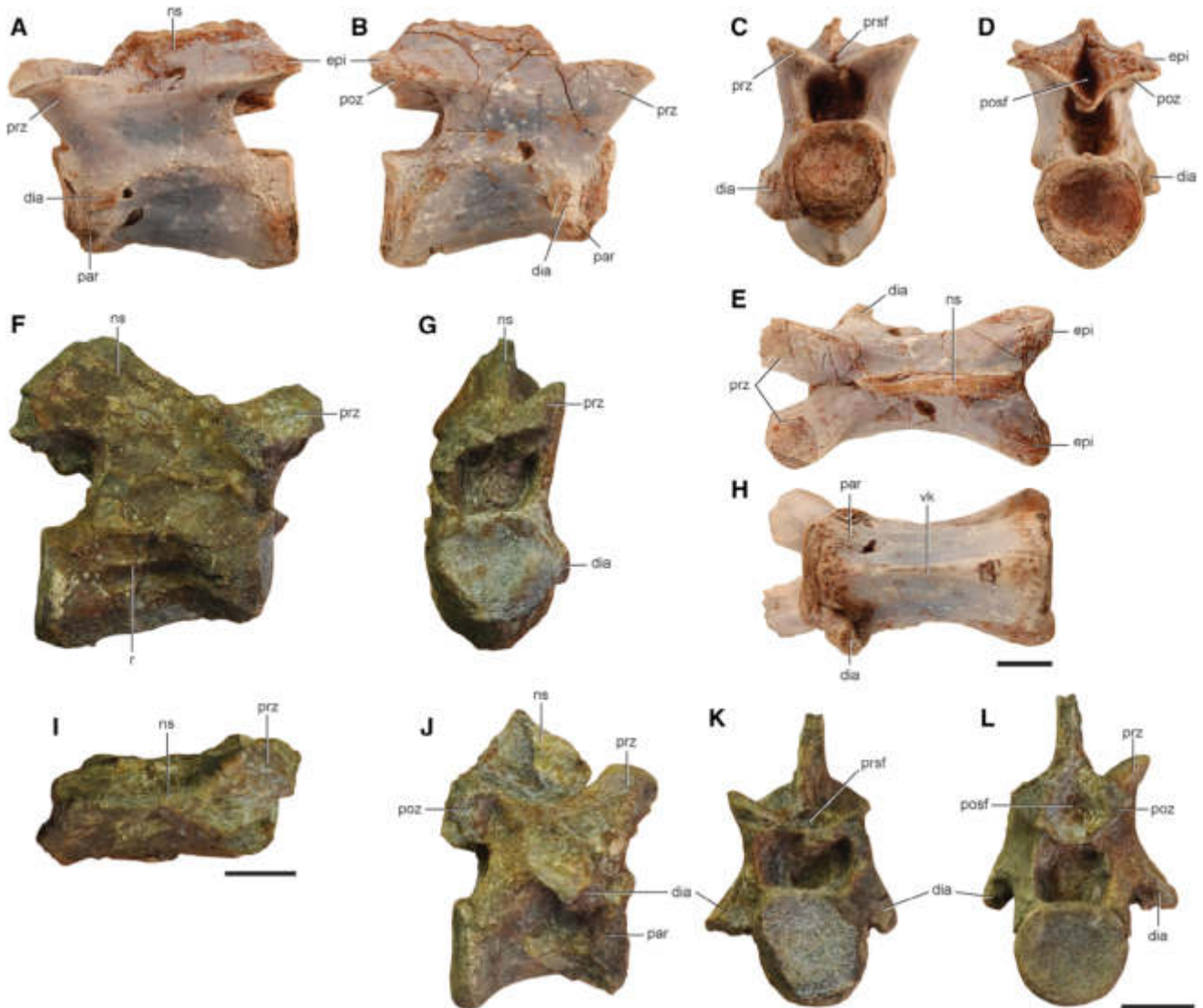


Fig. 23. Cervical vertebrae referred to *Asilisaurus kongwe*. Anterior to middle cervical vertebra of an associated skeleton referred to *Asilisaurus kongwe* (NMT RB159) in left lateral (A), right lateral (B), anterior (C), posterior (D), dorsal (E), and ventral (H) views. Anterior cervical vertebra (NMT RB851) in right lateral (F), anterior (G), and dorsal (I) views. Middle—posterior cervical vertebra (NMT RB116) in right lateral (J), anterior (K), and posterior (L) views. Abbreviations: dia, diapophysis; epi, epipophysis; ns, neural spine; par, parapophysis; posf, postspinal fossa; poz, postzygapophysis; prsf, prespinal fossa; prz, prezygapophyses; r, ridge; vk, ventral keel. Scale bars equal 5 mm.

resembling the condition in early dinosaurs (Langer and Benton, 2006). The postzygapophyses contact one another on the median line, forming a V-shaped structure in posterior view, but there is no hyposphene and neither an hypantrum in the prezygapophyses. The neural spine is transversely narrow and extends anteroposteriorly along the entire dorsal surface of the neural arch.

Posterior cervical vertebra. One vertebra (NMT RB116; Fig. 23J–L) is identified as belonging to the posterior region of the neck, because the parapophysis is placed on the centrum and the diapophysis is mainly ventrally oriented, but placed entirely on the neural arch, resembling the condition in the seventh to eighth cervical vertebrae of *Lewisuchus admixtus* (PULR 01). Additionally, there is a partially articulated series of posterior cervical vertebrae from the holotype locality (Fig. 24). NMT RB116

lacks the tips of the left and right postzygapophyses and the distal end of the neural spine. The neural arch is coossified to the centrum. The centrum is parallelogram-shaped in lateral view, with the anterior articular facet placed dorsally to the posterior one, contrasting with the sub-rectangular posterior cervical centra of the lagerpetid *Ixalerpeton polesinensis* (Cabreira et al., 2016). The ventral surface of the centrum lacks a median keel, as occurs in the posterior cervical vertebrae of *Ixalerpeton polesinensis* (ULBRA-PVT059) and at least in a sixth cervical vertebra of *Silesaurus opolensis* (ZPAL Ab III/1930, the absence of this keel cannot be determined in the more posterior cervical vertebrae of this specimen, because this area is covered with matrix). The centrum is approximately 1.6 times longer than its posterior height, being distinctly shorter than the more anterior cervical

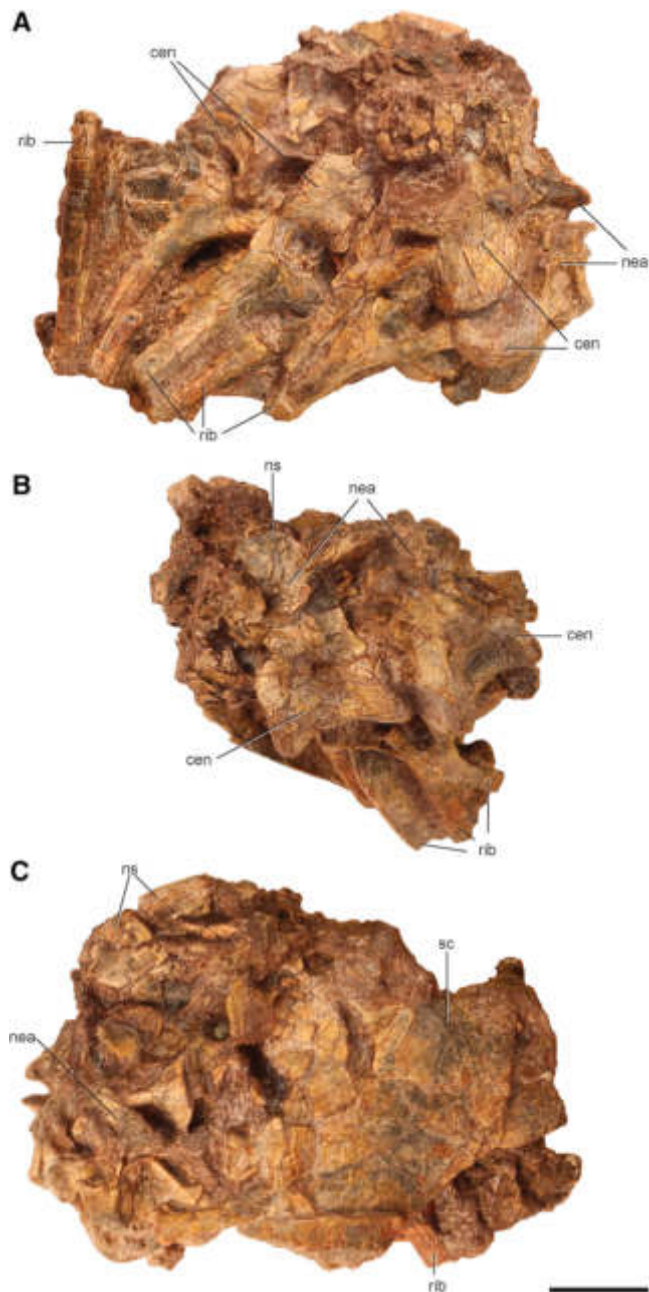


Fig. 24. Partially articulated posterior cervical vertebral series referred to *Asilisaurus kongwe* (NMT RB123) in three (A–C) views. Abbreviations: cen, centrum; nea, neural arch; nes, neural spine; rib, rib; sc, scapula. Scale bar equals 10 mm.

vertebrae of *Asilisaurus kongwe* and the posterior cervical vertebrae of *Lewisuchus admixtus* (PULR 01: ratio > 2.0 for the seventh to ninth postaxial centra) and *Silesaurus opolenensis* (Piechowski and Dzik, 2010: ratio > 2.0 for the seventh to ninth postaxial centra), but longer than in the posterior cervical centra of *Ixalerpeton polesinensis* (ULBRA-PVT059: ratio = 1.1–1.4). The length-posterior height ratio of the posterior cervical centrum of *Asilisaurus kongwe* resembles that of a posterior cervical vertebra of *Teleocrater rhadinus* (NMT RB514: ratio = 1.6). Both anterior and posterior articular surfaces of the

centrum are gently concave. Although the anterior articular surface is damaged, it seems to have been subcircular, whereas the better preserved posterior articular surface is suboval, being broader than tall. The lateral surface of the centrum possesses a shallow, not well-defined anteroposteriorly elongated fossa on its dorsal half.

The diapophysis is placed at the level of the neural canal and anteriorly displaced from the mid-length of the centrum (Fig. 23J–L). It is more ventrally than laterally oriented, thus contrasting with the more laterally projected diapophyses of the seventh to ninth postaxial cervical vertebrae of *Silesaurus opolenensis* (Piechowski and Dzik, 2010). The base of the diapophysis does not extend posteriorly as a ridge, contrasting with those of the more anterior cervical vertebrae. The neural arch lacks laminae, as occurs in *Ixalerpeton polesinensis* (ULBRA-PVT059), but contrasting with the short laminae present in at least the ninth postaxial (= 11) vertebra of *Lewisuchus admixtus* (PULR 01) and the well-developed laminae of the posterior cervical and anterior dorsal vertebrae of *Silesaurus opolenensis* (Piechowski and Dzik, 2010). There is a shallow, subcircular prespinal fossa between the bases of the prezygapophyses that does not extend dorsally onto the neural spine (Fig. 23K). The posterior portion of the base of the neural arch possesses an incipient postzygapophyseal centrodiapophyseal fossa (*sensu* Wilson et al., 2011). The prezygapophysis is anterodorsally projected and extends beyond the level of the anterior margin of the centrum. Its articular facet faces mainly dorsally. The postzygapophyses extend posterior to the posterior margin of the centrum and they are separated from one another by a deep and broad postspinal fossa that slightly invades the base of the neural spine (Fig. 23L). The postzygapophyses are connected to one another by a horizontal ridge above the neural canal, but it does not form a hyposphene. The neural spine is transversely narrow and extends anteroposteriorly along the entire median line of the neural arch. The height and shape of the neural spine cannot be determined because of damage, but it is distinctly higher than in *Ixalerpeton polesinensis* (ULBRA-PVT059).

Trunk Vertebrae—Anterior trunk vertebra. The only preserved anterior trunk vertebra (NMT RB118; Fig. 25D, G, J, M) lacks the ends of the prezygapophyses, diapophyses, and neural spine. The length of the centrum is 1.5 times its posterior height, resembling the condition in *Silesaurus opolenensis* (ZPAL Ab III/363: ratio = 1.5–1.6; ZPAL Ab III/1302: ratio = 1.4) and some anterior trunk vertebrae of aphanosaurs (e.g., *Teleocrater rhadinus*, NMT RB500: ratio = 1.4; *Yarasuchus deccanensis*, ISIR unnumbered: ratio = 1.5–1.6) and *Marasuchus lilloensis* (PVL 3872: ratio = 1.6). Nevertheless, *Marasuchus lilloensis* (PVL 3872: ratio = 1.7), *Lewisuchus admixtus* (PULR 01: ratio = 1.9), and aphanosaurs (e.g., *Yarasuchus deccanensis*, ISIR unnumbered: ratio = 1.8) also possess some anterior trunk vertebrae that are more elongated than the single available anterior trunk vertebra of *Asilisaurus kongwe*. The lagerpetid *Ixalerpeton polesinensis* has distinctly shorter anterior trunk centra (ULBRA-PVT059: ratio = 1.0–1.3 from the first to fifth trunk vertebrae). The centrum of the anterior trunk vertebra of *Asilisaurus kongwe* is incipiently parallelogram-shaped in lateral view, with the anterior articular surface situated more dorsal than the posterior, as occurs in other early avemetatarsalians, with the exception of *Ixalerpeton polesinensis* (ULBRA-PVT059). The anterior articular

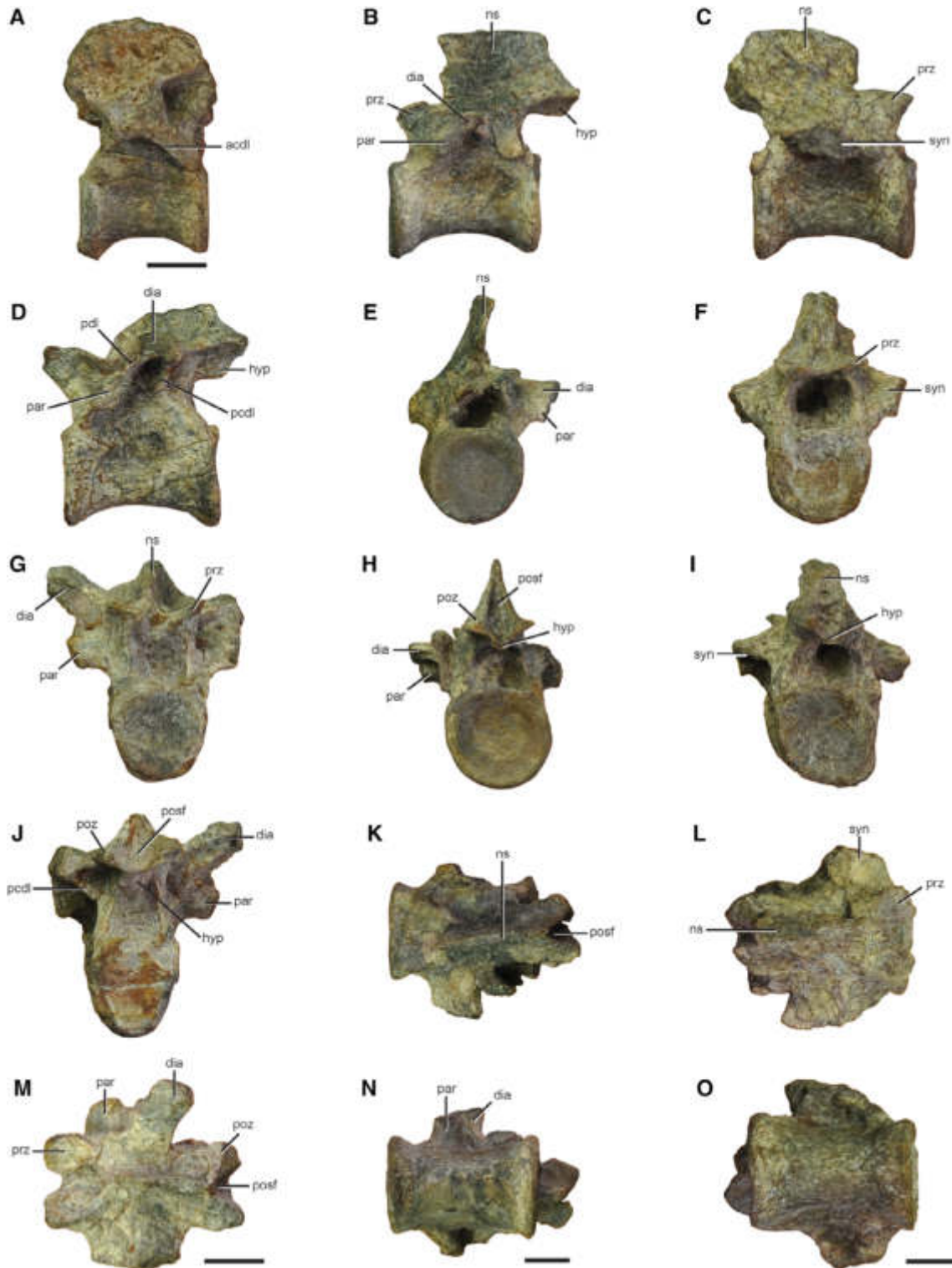


Fig. 25. Trunk vertebrae referred to *Asilisaurus kongwe*. Middle trunk vertebra (NMT RB117) in right lateral (A) view. Anterior trunk vertebra (NMT RB118) in left lateral (D), anterior (G), posterior (J), and dorsal (M) views. Posterior trunk vertebra (NMT RB120) in left lateral (B), anterior (E), posterior (H), dorsal (K), and ventral (N) views. Posterior trunk vertebra (NMT RB119) in right lateral (C), anterior (F), posterior (I), dorsal (L), and ventral (O) views. Abbreviations: acdl, anterior centrodiaepophyseal lamina; dia, diapophysis; hyp, hyposphene; ns, neural spine; par, parapophysis; pcdl, posterior centrodiaepophyseal lamina; posf, postspinal fossa; poz, postzygapophysis; prz, prezygapophyses; syn, synapophysis. Scale bars equal 5 mm.

surface of the centrum is subcircular and the posterior is slightly higher than broad. Both articular surfaces are shallowly concave. The centrum is slightly constricted transversely at mid-length, being spool-shaped in ventral view. The ventral surface of the centrum lacks a longitudinal keel, as occurs in *Teleocrater rhadinus* (Nesbitt et al., 2018), *Ixalerpeton polesinensis* (ULBRA-PVT059), *Lewisuchus admixtus* (PULR 01), and *Silesaurus opolensis* (ZPAL Ab III/1302). By contrast, a low median ventral keel is present in an anterior trunk vertebra of *Yarasuchus deccanensis* (ISIR unnumbered). The lateral surface of the centrum is shallowly depressed on its dorsal half. The neural canal is relatively large, subequal in size to the articular facets of the centrum.

The parapophyses are not preserved on the right side and not exposed on the left side, but they were not placed on the centrum (NMT RB118; Fig. 25D, G, J, M). The diapophysis is placed at the level of the roof of the neural canal and laterally projected. There are long anterior centrodiapophyseal and prezygodiapophyseal laminae, and shorter posterior centrodiapophyseal and postzygodiapophyseal laminae, resembling the condition in other early avemetatarsalians (e.g., *Teleocrater rhadinus*, Nesbitt et al., 2018; *Lewisuchus admixtus*, Bittencourt et al., 2015; *Herrerasaurus ischigualastensis*, Novas, 1994). As a result, the anterior trunk vertebra of *Asilisaurus kongwe* has broad and deep centrodiapophyseal and prezygapophyseal centrodiapophyseal fossae, and a smaller but also deep postzygapophyseal centrodiapophyseal fossa. The zygapophyses extend slightly beyond the level of the anterior and posterior rims of the centrum. There is a low, subrectangular hyposphene that forms an abrupt, obtuse angle with the articular facet of the postzygapophyses in posterior view. The neural spine extends anteroposteriorly along the entire median line of the neural arch and its anterior margin is slightly anteriorly oriented in lateral view, resembling the condition in the anterior trunk vertebrae of *Marasuchus lilloensis* (PVL 3872) and *Lewisuchus admixtus* (Bittencourt et al., 2015). A deep postspinal fossa is present between the postzygapophyses and dorsal to the hyposphene (Fig. 25J). In posterior view, it is drop-shaped, with a tapering dorsal end. This fossa extends slightly onto the base of the neural spine.

Middle and posterior trunk vertebrae. A middle trunk vertebra and two posterior trunk vertebrae are preserved (NMT RB117, Fig. 25A; NMT RB119, Fig. 25C, F, I, L, O; NMT RB120, Fig. 25B, E, H, K, N). The middle element possesses the parapophysis and diapophysis still well separated from one another, whereas in the posterior trunk vertebrae both structures are merged in the same process. The middle trunk vertebra lacks the end of the left diapophysis and most of the neural spine. One of the posterior trunk vertebrae lacks the ends of the right parapophysis and diapophysis, whereas the other lacks the ends of the transverse processes and the neural spine and the postzygapophyses are damaged. These three vertebrae have a similar morphology and are described together.

The neurocentral sutures are closed in the three middle-posterior trunk vertebrae. The length of the middle trunk centrum is 1.6 times its posterior height, and the same ratio is 1.5 and 1.7 for the two posterior trunk vertebrae, resembling the condition in the posterior trunk vertebrae of *Teleocrater rhadinus* (NMT RB516; ratio = 1.5). By contrast, the posterior trunk centra of

Yarasuchus deccanensis (ISIR unnumbered; ratio = 1.2), *Ixalerpeton polesinensis* (ULBRA-PVT059; ratio = 1.1–1.2 in the ninth to eleventh trunk), and *Silesaurus opolensis* (ZPAL Ab III/unnumbered; ratio = 1.2, ZPAL Ab III/1832/1; ratio = 1.1) are proportionally shorter, and those of *Marasuchus lilloensis* proportionally longer (PVL 3872; ratio = 1.9–2.0). The centra of the middle-posterior trunk vertebrae of *Asilisaurus kongwe* have the anterior and posterior articular surfaces situated at the same dorsoventral level. These articular surfaces are sub-circular to slightly higher than broad and shallowly concave. The centra are slightly constricted transversely at mid-length and the ventral surface lacks a longitudinal keel or groove. The lateral surface of the centra is shallowly depressed.

The parapophysis of the middle trunk vertebra is placed at the level of the floor of the neural canal, on the anterior third of the base of the neural arch, and is well differentiated from the base of the diapophysis. By contrast, in *Ixalerpeton polesinensis* (ULBRA-PVT059), the parapophysis occurs in the same process as the diapophysis from the third trunk vertebra onward and in the middle trunk vertebrae both structures are merged to one another. In *Asilisaurus kongwe*, the parapophysis is raised on a well laterally developed peduncle, resembling the condition in *Silesaurus opolensis* (Piechowski and Dzik, 2010). The articular facet of the parapophysis is sub-oval in outline, with an anteroventrally-to-posterodorsally oriented major axis, and mostly flat. This facet is proportionally larger in the middle trunk vertebra than in the two posterior trunk vertebrae. In the posterior trunk vertebrae, the articular facet of the diapophysis is subequal in size and shape to that of the parapophysis. The parapophysis is connected with the diapophysis by a well-developed paradiapophyseal lamina in the middle trunk vertebra. The diapophysis is dorsolaterally oriented in the middle trunk vertebra, whereas they are posteriorly oriented in the posterior trunk elements. The middle trunk vertebra possesses well developed posterior centrodiapophyseal and prezygodiapophyseal laminae. One of the posterior trunk vertebrae has only a short, posteroventrally oriented posterior centrodiapophyseal lamina, and the other vertebra, probably more posterior, lacks laminae in the neural arch.

The prezygapophyses of the middle trunk vertebra project anterodorsally and extend anteriorly beyond the level of the anterior margin of the centrum, whereas the prezygapophyses of the posterior trunk vertebrae project directly anteriorly and do not extend beyond the anterior rim of the centrum. A very similar pattern of change in the morphology of the prezygapophyses is present through the trunk series of *Marasuchus lilloensis* (PVL 3870). The articular facet of the prezygapophyses of the middle-posterior trunk vertebrae of *Asilisaurus kongwe* faces mainly dorsally, with a very slight medial orientation. These articular facets are sub-oval, anteroposteriorly longer than transversely broad, and proportionally longer in the middle trunk vertebra than in the posterior trunk vertebrae. The postzygapophyses extend posteriorly distinctly beyond the level of the posterior margin of the centra. These vertebrae lack epipophyses and have a hyposphene that is well differentiated from the postzygapophyseal facet by a distinctive change in slope in posterior view, as occurs in several other early avemetatarsalians (e.g., *Teleocrater rhadinus*, Nesbitt et al., 2017; *Silesaurus*

opolensis, Piechowski and Dzik, 2010). The postspinal fossa is deep and occurs immediately above the hyposphene. Contrasting with those of the more anterior presacral vertebrae, it extends dorsally along most of the posterior surface of the neural spine, as occurs in *Silesaurus opolensis* (Piechowski and Dzik, 2010). The complete neural spine of one of the posterior trunk vertebrae has 0.8 times the height of the posterior articular surface of the centrum and is proportionally lower than the middle-posterior trunk neural spines of *Yarasuchus deccanensis* (ISIR unnumbered; ratio = 2.1), *Marasuchus lilloensis* (PVL 3870; ratio = 1.15), and *Silesaurus opolensis* (Piechowski and Dzik, 2010). The neural spine of the posterior trunk vertebra of *Asilisaurus kongwe* is anteroposteriorly longer than tall and oriented strictly dorsally. By contrast, the neural spines of the posterior trunk vertebrae of the lagerpetid *Lagerpeton chanarensis* are anterodorsally oriented (Serenó and Arcucci, 1994a; PVL 4625). The anterodorsal corner of this neural spine of *Asilisaurus kongwe* is broken, but it is clear that its posterior margin is not posteriorly expanded, contrasting with the condition in *Marasuchus lilloensis* (Serenó and Arcucci, 1994b), *Lewisuchus admixtus* (Bittencourt et al., 2015), and *Silesaurus opolensis* (Piechowski and Dzik, 2010). The distal edge of the neural spine is not transversely thickened, contrasting with the faint transverse expansion present in *Marasuchus lilloensis* (PVL 3870), *Lewisuchus*

admixtus (PULR 01), and *Silesaurus opolensis* (Piechowski and Dzik, 2010).

Sacral Vertebrae and ribs—The sacral region of *Asilisaurus kongwe* is represented by a pair of primordial sacral vertebrae articulated to one another and the base of their ribs (NMT RB11; Fig. 26A, B) and an isolated second primordial sacral vertebra and its ribs (NMT RB159; Fig. 26C–F). The articular facets on the medial surface of preserved ilia indicate that the sacrum was composed of two sacral vertebrae, as occurs in most non-dinosaurian dinosauromorphs (Nesbitt, 2011; Nesbitt et al., 2017), but contrasting with the presence of three sacral vertebrae in *Silesaurus opolensis* (Dzik and Sulej, 2007). The preserved sacral vertebrae lack the distal end of the neural spines. The pair in NMT RB11 (Fig. 26A, B) bears no traces of the neurocentral suture, but this is still visible between the co-ossified centrum and neural arch of the isolated sacral vertebra.

In the articulated sacral vertebrae (NMT RB11; Fig. 26A, B), the first centrum is 1.6 times longer than tall and the second is proportionally shorter, with a 1.4 ratio, but they are subequal in length. By contrast, the second sacral centrum is longer than the first in *Ixalerpeton polsinensis* (ULBRA-PVT059). The sacral centra are transversely compressed at mid-length, being spool-shaped in ventral view. The ventral surface of the centra is transversely convex and lacks grooves or ridges, as occurs in

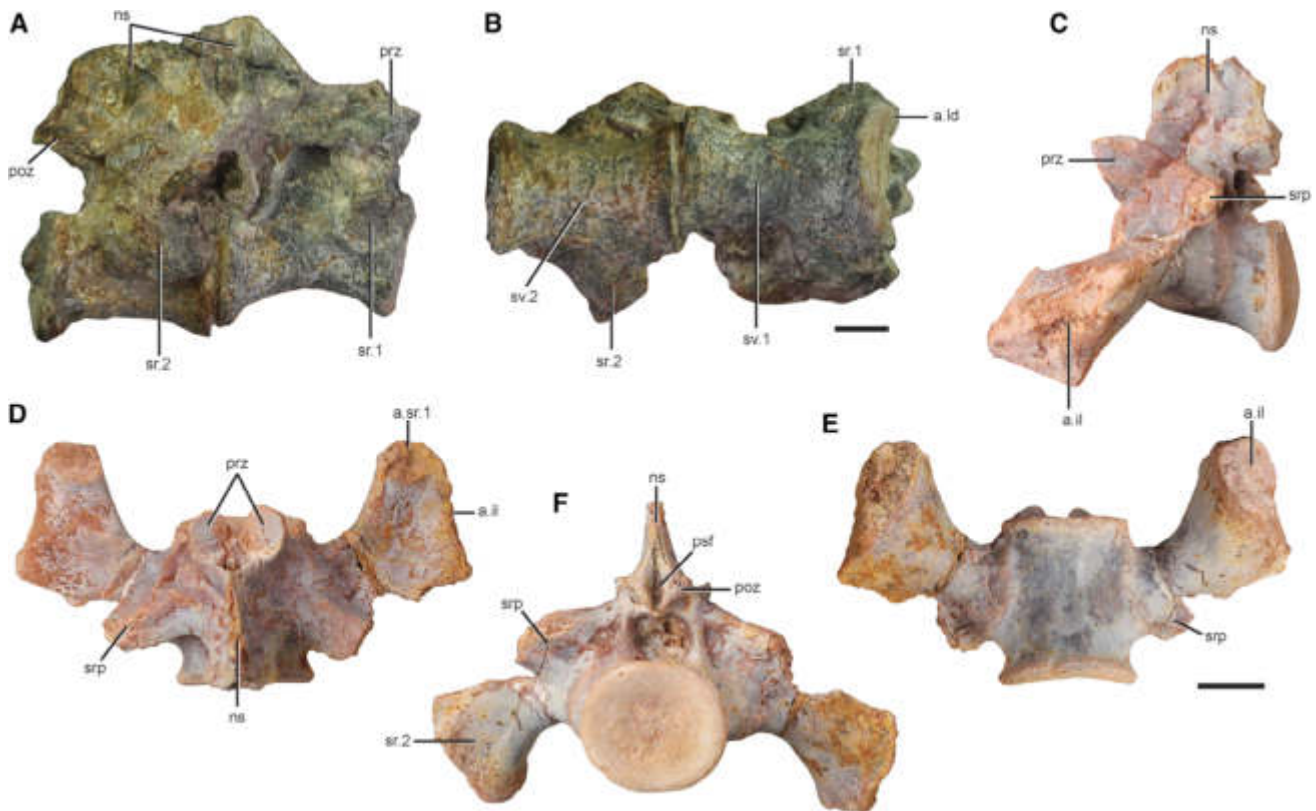


Fig. 26. Sacral vertebrae referred to *Asilisaurus kongwe*. Articulated sacrales one and two (NMT RB11) in right lateral (A) and ventral (B) views. Well preserved second sacral vertebra of an associated skeleton referred to *Asilisaurus kongwe* (NMT RB159) in left lateral (C), dorsal (D), ventral (E), and posterior (F) views. Abbreviations: a., articulation with; il, ilium; ns, neural spine; ld, last trunk vertebra; poz, postzygapophysis; prz, prezygapophyses; psf, postspinal fossa; srp, sacral rib process, sr.1, sacral rib 1; sr.2, sacral rib 2; sv.1, sacral vertebra 1; sv.2, sacral vertebra 2. Scale bars equal 5 mm.

aphanosaur (Nesbitt et al., 2017), *Ixalerpeton polesinensis* (ULBRA-PVT059), *Silesaurus opolensis* (ZPAL Ab III/362), and *Saturnalia tupiniquim* (MCP 3844-PV). The anterior and posterior articular surfaces of the centra are shallowly concave and transversely broader than tall. The transverse process of the first sacral is placed on the transition between the neural arch and the centrum, and adjacent to the anterior margin of the vertebra. The base of the corresponding sacral rib extends anteriorly slightly beyond the rim of the centrum and may have contacted the last trunk vertebra, as occurs in *Ixalerpeton polesinensis* (ULBRA-PVT059), *Silesaurus opolensis* (ZPAL Ab III/362), and at least some early dinosaurs (e.g., *Saturnalia tupiniquim*, MCP 3844-PV; *Panphagia protos*, PVSJ 874). The transverse process occupies the anterior two-thirds of the lateral surface of the second sacral vertebra, but it is not adjacent to the rim. Thus, the base of the second sacral rib is anteroposteriorly longer than that of the first sacral rib, a condition widespread among dinosauroforms (e.g., *Ixalerpeton polesinensis*, ULBRA-PVT059; *Saturnalia tupiniquim*, MCP 3844-PV). The prezygapophyses of the first sacral vertebra are short (Fig. 26A), well separated from one another and anteriorly projected, not exceeding the level of the anterior rim of the centrum. The prezygapophyses of the second sacral vertebra have a similar morphology, but they are proportionally longer, exceeding anteriorly the level of the anterior rim of the centrum. The postzygapophyses of both sacral vertebrae are relatively long, exceeding the level of the centrum, and the articular facets are ventromedially oriented, tilted in an angle of approximately 45° in posterior view. The neural spines of the sacral vertebrae are anteroposteriorly long, extending along the entire median line of the neural arch. The prespinal fossa is tear drop-shaped with a dorsal apex in anterior view, and invades the anterior base of the neural spine. The postspinal fossa is narrower and extends more dorsally onto the neural spine than the prespinal fossa. The floor of the postspinal fossa is formed by a horizontal ridge that connects the anterior portion of the ventromedial corner of both postzygapophyses between one another, but it does not form a hypophene.

The second sacral rib is restricted to its respective sacral vertebra, as occurs in *Teleocrater rhadinus* (Nesbitt et al., 2017), *Yarasuchus deccanensis* (ISIR 334), *Ixalerpeton polesinensis* (ULBRA-PVT059), and *Saturnalia tupiniquim* (MCP 3844-PV), but contrasting with the condition in *Silesaurus opolensis* (ZPAL Ab III/362), in which the sacral rib is shared between consecutive sacral vertebrae. The second sacral rib of *Asilisaurus kongwe* is divided at its base into two components, a distinctly larger and more laterally projected anterolateral process and a smaller, dorsally placed posterolateral process (Fig. 26D, E). The latter lacks an articular facet for the ilium, which is present in several other early avemetatarsalians, such as aphanosaurs (Nesbitt et al., 2017) and dinosaurs (e.g., *Saturnalia tupiniquim*: MCP 3844-PV), but is absent in *Ixalerpeton polesinensis* (ULBRA-PVT059). The distal end of the anterolateral process has a laterally facing, nearly vertical facet for the articulation with the iliac blade and an anteriorly facing, smaller facet for the articulation with the first sacral rib, as also occurs in other early avemetatarsalians (e.g., *Yarasuchus deccanensis*, ISIR 334; *Teleocrater rhadinus*, Nesbitt et al., 2017; *Ixalerpeton polesinensis*,

ULBRA-PVT059). The iliac facet is rhomboidal in lateral view, tapering posterodorsally and anteroventrally and with distinct dorsal and ventral apices. By contrast, this facet has a comma-shaped lateral profile in *Yarasuchus deccanensis* (ISIR 334) and *Ixalerpeton polesinensis* (ULBRA-PVT059). In particular, the sacral rib of *Ixalerpeton polesinensis* tapers posterodorsally into a long, ventrally curved process in lateral view (ULBRA-PVT059), which is absent in *Yarasuchus deccanensis* (ISIR 334), *Teleocrater rhadinus* (Nesbitt et al., 2017), and *Asilisaurus kongwe* (NMT RB159). The main axis of the iliac facet is oriented in an angle of approximately 30° to the horizontal plane, resembling the condition in *Ixalerpeton polesinensis* (ULBRA-PVT059), but contrasting with the more vertical main axis present in *Yarasuchus deccanensis* (ISIR 334: angle ca. 50°).

Caudal Vertebrae—Anterior caudal vertebrae. A series of anterior caudal vertebrae, belonging to different regions of this portion of the tail, are preserved (NMT RB159; Fig. 27A–D). All the anterior caudal vertebrae lack the distal portions of the transverse processes and the neural spine. The neurocentral suture is closed in all the available anterior caudal vertebrae. The centra are slightly parallelogram-shaped in lateral view, with a more dorsally placed anterior articular surface, and become proportionally longer toward the middle of the tail, a condition widespread among early dinosauriforms (e.g., *Marasuchus lilloensis*, Sereno and Arcucci, 1994b; *Silesaurus opolensis*, ZPAL Ab III/1975, Ab III/923). The centra of the anteriormost preserved caudal vertebrae are 1.0–1.2 times longer than tall, whereas this ratio increases in more posterior anterior caudal vertebrae to values of approximately 1.3 and 1.8. These ratios match those of *Yarasuchus deccanensis* (ISIR 334: ratio 1.1), *Silesaurus opolensis* (ZPAL Ab III/1289: ratio 1.2; ZPAL Ab III/923: ratio 1.8), and *Sacisaurus agudoensis* (MCN PV10028: ratio 1.0). The anteriormost caudal vertebrae (first and second) of *Marasuchus lilloensis* are proportionally longer (PVL 3871: ratio 1.9; PVL 3870: 1.8) than those of *Asilisaurus kongwe*. The centra in the latter taxon are spool-shaped in ventral view and their ventral surface lacks a keel or groove, being continuously transversely convex, as occurs in *Silesaurus opolensis* (ZPAL Ab III/1289) and *Herrerasaurus ischigualastensis* (MACN-Pv 18060, PVL 2566). By contrast, the ventral surface of an anterior caudal centrum of *Sacisaurus agudoensis* possesses a low longitudinal ridge (Langer and Ferigolo, 2013; MCN PV10028). The anteriormost caudal vertebrae lack facets for articulation with the hemal arches, but the more posterior anterior caudal vertebrae have a distinct beveling in the posteroventral corner of the centrum that houses a posteroventrally facing facet for the articulation with the hemal arch. This facet is partially subdivided anteriorly by a transversely broad concavity. The beveling on the anteroventral rim of the centrum is incipient. The anterior and posterior articular surfaces are subcircular in the anteriormost caudal vertebrae and suboval, taller than broad, in the more posterior anterior caudal vertebrae. These facets are slightly concave.

The transverse processes are placed entirely on the neural arch and approximately level with the mid-length of the centrum and the mid-height of the neural canal (Fig. 27A–D). The base of the transverse processes is oval in cross-section, being considerably anteroposteriorly

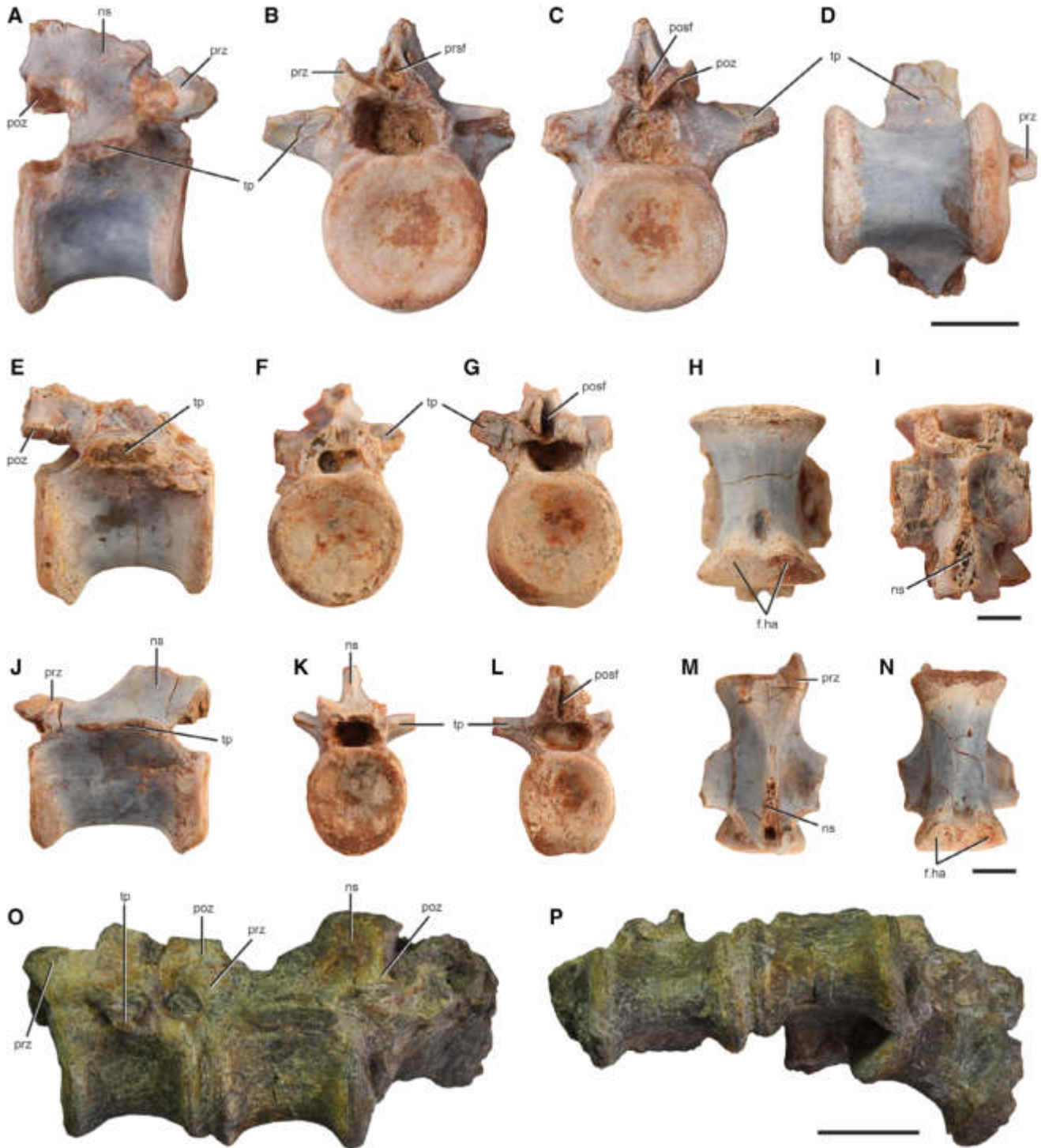


Fig. 27. Anterior to middle caudal vertebrae referred to *Asilisaurus kongwe*. Anterior caudal vertebra from an associated skeleton referred to *Asilisaurus kongwe* (NMT RB159) in right lateral (A), anterior (B), posterior (C), and ventral (D) views. Anterior to middle caudal vertebra (NMT RB159) in right lateral (E), anterior (F), posterior (G), ventral (H), and dorsal (I) views. Anterior to middle caudal vertebra (NMT RB159) in left lateral (J), anterior (K), posterior (L), dorsal (M), and ventral (N) views. Articulated middle caudal vertebrae (NMT RB125) in left lateral (O) and ventral (P) views. Abbreviations: a., articulation with; f., facet; ha, hemal arch; ns, neural spine; poz, postzygapophysis; prz, prezygapophyses; posf, postspinal fossa; prsf, prespinal fossa; tp, transverse process. Scale bars equal 10 mm.

longer than tall, and more laminar in the posteriormost preserved anterior caudal vertebra. The preserved portions of the transverse processes are horizontal and

laterally oriented. The transverse processes become dorsoventrally narrower toward their distal end. The zygapophyses project beyond the level of the rims of the

centrum and their articular facets are tilted in approximately 45° in all the anterior caudal vertebrae. The prezygapophyses are slightly divergent anteriorly from one another and anterodorsally oriented in lateral view, but in a lower angle in the posteriormost preserved anterior caudal vertebrae. The postzygapophyses are separated from one another by a deep median furrow that opens into the postspinal fossa (Fig. 27C). The floor of the postspinal fossa is formed by a V-shaped lamina, with a ventral apex, but it does not form a hyposphene, as occurs in other early dinosauriforms (e.g., *Silesaurus opolensis*, ZPAL Ab III/923). The postspinal fossa is present in one of the anteriormost preserved anterior caudal vertebrae and is deep, tear drop-shaped, and invades dorsally the base of the neural spine. The base of the neural spines is posteriorly displaced on the neural arch and, in those that preserve both anterior and posterior margins, it slants moderately posteriorly in lateral view, closely resembling the condition in other early dinosauriforms (e.g., *Lagerpeton chanarensis*, Sereno and Arcucci, 1994a, PVL 4625; *Marasuchus lilloensis*, PVL 4671; *Sacisaurus agudoensis*, Langer and Ferigolo, 2013; *Silesaurus opolensis*, ZPAL Ab III/923).

Middle caudal vertebrae. There are nine middle caudal vertebrae (NMT RB159; Fig. 27E–P), which retain a laminar, but well developed transverse process and posteriorly restricted, tall neural spine. The ends of the transverse processes and neural spine are broken off in all middle caudal vertebrae and there is no trace of the neurocentral suture in any of them. The centra have a length that ranges between 2.3 and 2.9 times their height, resembling the condition in *Marasuchus lilloensis* (PVL 3871: ratio 2.5–3.3) and a middle caudal vertebra of *Sacisaurus agudoensis* (MCN PV10097: ratio 2.3), and being slightly proportionally longer than the middle caudal vertebrae of *Silesaurus opolensis* (ZPAL Ab III/361/3: ratio 2.1; ZPAL Ab III/1975: ratio 2.0) and distinctly longer than those of *Yarasuchus deccanensis* (ISIR 334: ratio 1.7). The articular surfaces of the centrum are subcircular, shallowly concave, and placed at approximately the same dorsoventral level. The centra are slightly transversely compressed around mid-length and its ventral surface possesses a low, median ridge, as also occurs in *Sacisaurus agudoensis* (MCN PV10097). By contrast, the ventral surface of the middle caudal vertebrae of *Yarasuchus deccanensis* (ISIR 334) and *Silesaurus opolensis* (ZPAL Ab III/1975) is continuously transversely convex and in the early ornithischian *Heterodontosaurus tucki* (SAM-PK-K1332) and the sauropodomorph *Saturnalia tupiniquim* (MCP 3846-PV) there is a longitudinal groove. The facets for the hemal arch are well developed on the beveled ventral rims of the centra, being more distinct on the posterior than in the anterior margin. In the posterior end of the centra, these facets are partially separated from one another by a median shallow concavity. The lateral surface of the centra is dorsoventrally convex. The base of the transverse process is anteroposteriorly long and placed at level with the floor of the neural canal. The anterior margin of the transverse processes is more laminar than the posterior. The prezygapophyses are mainly anteriorly oriented and project distinctly beyond the level of the anterior rim of the centrum. One of these is incipiently bowed ventrally in lateral view, resembling the condition of a middle caudal vertebra of *Sacisaurus agudoensis* (MCN PV10097). The articular facet of the

prezygapophysis faces mainly medially. The postzygapophysis projects posteriorly slightly beyond the rim of the centrum and its articular facet is suboval, with an anteroposterior main axis, and faces mainly laterally. The neural spine is very thin transversely and is restricted to the posterior half of the neural arch, not reaching the level of the base of the prezygapophyses. The neural spine is very low anteriorly and increases abruptly in height posteriorly, resembling the condition in the middle caudal vertebrae of other dinosauriforms (e.g., *Pseudolagosuchus major*, MACN-Pv 18954; *Silesaurus opolensis*, ZPAL Ab III/1975; *Chromogisaurus novasi*, Ezcurra, 2010; *Heterodontosaurus tucki*, Santa, 1980). The anterodorsal margin of the spine is strongly concave in lateral view, but it cannot be determined if the anterior spur present in the middle caudal vertebrae of *Silesaurus opolensis* (ZPAL Ab III/1975) also occurred in *Asilisaurus kongwe*. The prespinal fossa is absent and the postspinal fossa is reduced to a pit between the postzygapophyses.

Posterior caudal vertebrae. Three posterior caudal vertebrae are preserved (NMT RB159; Fig. 28F–K), in which the transverse processes, neural spine, and facets for the hemal arch have been reduced or are lost completely. The centra are anteroposteriorly elongated, one of them 3.4 times longer than tall, being proportionally longer than those of the anterior and middle caudal vertebrae, as occurs in other avemetatarsalians (e.g., *Teleocrater rhadinus*, Nesbitt et al., 2017; *Marasuchus lilloensis*, Sereno and Arcucci, 1994b; *Sacisaurus agudoensis*, Langer and Ferigolo, 2013; *Silesaurus opolensis*, Dzik, 2003; *Herrerasaurus ischigualastensis*, Novas, 1994). The anterior and posterior

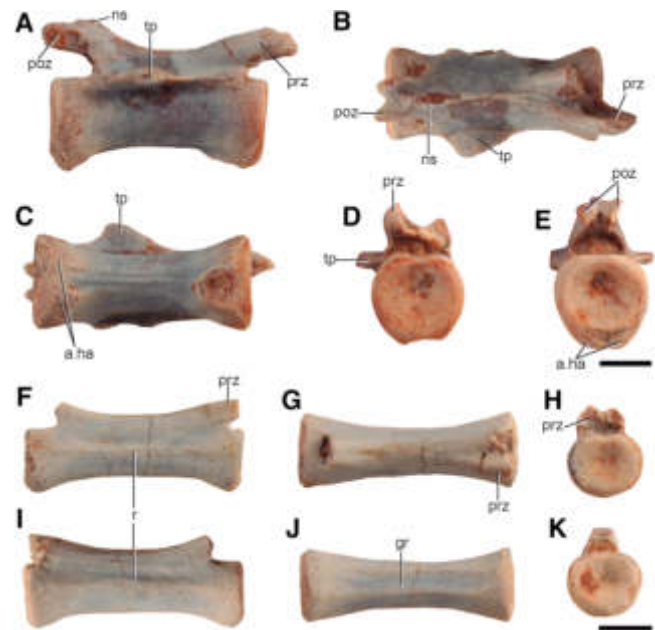


Fig. 28. Distal caudal vertebrae of an associated skeleton referred to *Asilisaurus kongwe* (NMT RB159). Distal caudal vertebra in right lateral (A), dorsal (B), ventral (C), anterior (D), and posterior (E) views. Distal caudal vertebra in right lateral (F), dorsal (G), anterior (H), left lateral (I), ventral (J), and posterior (K) views. Abbreviations: a., articulation with; gr, groove; ha, hemal arch; ns, neural spine; poz, postzygapophysis; prz, prezygapophyses; r, ridge; tp, transverse process. Scale bars equal 10 mm.

articular surfaces of the centra are shallowly concave, transversely broader than tall, and placed at the same dorsoventral level. The centra are slightly constricted transversely at mid-length. The ventral surface has a shallow and broad median groove, which contrasts with the incipient longitudinal ridge present in the posterior caudal vertebrae of *Silesaurus opolensis* (ZPAL Ab III/1975) and *Herrerasaurus ischigualastensis* (MACN-Pv 18060). The lateral surface possesses a low, longitudinal tuberosity that is dorsally displaced from the mid-height of the centrum, as usually occurs in the posterior caudal vertebrae of dinosauromorphs (e.g., *Sacisaurus agudoensis*, MCN PV10029; *Herrerasaurus ischigualastensis*, MACN-Pv 18060; *Saturnalia tupiniquim*, MCP 3846-PV). The neural arch is distinctly lower than the centrum and the neurocentral sutures are closed. Only the base of the zygapophyses is preserved, but the available portion of a prezygapophysis extends anteriorly beyond the level of the centrum. The base of the prezygapophyses is slightly anterodorsally oriented and placed closer to the rim of the centrum than that of the postzygapophyses.

Ribs—Very few ribs can be attributed to *Asilisaurus kongwe* because of disarticulation of much of the material recovered at the type locality (Z34). Fortunately, a few specimens have articulated ribs associated with posterior cervical and anterior trunk vertebrae (NMT RB123; Fig. 24) and rib fragments were recovered with the partial skeleton (NMT RB159; Fig. 29). The posterior cervical and anterior trunk ribs are proximally bifurcated, as predicted by the large separation between the diapophysis and the parapophysis in the respective vertebra (Fig. 24). The capitulum appears to be larger and extended further than the tuberculum in the posterior cervical ribs; there does not appear to be a thin web of bone connecting the capitulum and tuberculum (Figs. 24 and 29). Distal to the capitulum and tuberculum an anteriorly extending ridge is present in the isolated specimens (Fig. 29) collected with NMT RB159. A sharp ridge defines the lateral edge of the ribs in some examples (NMT RB15; Fig. 5) and distally, the ribs transform from an oval to a circular cross section.

Pectoral Girdle

Scapulocoracoid—Preserved elements of the pectoral girdle of *Asilisaurus kongwe* include the nearly complete left scapulocoracoid of NMT RB159 (Fig. 30) and a pair of right glenoid areas (NMT RB10, NMT RB848; Fig. 31), which match in most details. Based on NMT RB159, the whole scapulocoracoid bows laterally. The acromial area and most of the scapular blade are mediolaterally flattened, whereas the posteroventral portion of the blade, the glenoid area, and the posterior process of the coracoid are more robust mediolaterally. In lateral view, the blade expands gradually toward its convex dorsal margin (Fig. 30A). The anterior and posterior corners of the dorsal expansion are equally expanded from the anteroposterior center of the blade, but the former forms a slightly less acute angle and is somewhat more ventrally positioned. In total, the dorsal margin of the scapula expands anteroposteriorly for more than two times the narrowest portion of its blade. As mentioned above, the posteroventral portion of the scapular blade is mediolaterally broader, its posterior margin corresponding to a flat, subtriangular, and dorsoventrally concave surface. This is laterally bordered by the ventral continuation of the posterior margin



Fig. 29. Rib fragments from a partial skeleton referred to *Asilisaurus kongwe* (NMT RB159) in three views (A–C and D–F). Scale bar equals 10 mm.

of the scapular blade, as it extends ventrally to reach the dorsolateral corner of the glenoid. Right at that contact, there is a supraglenoid pit (Fig. 30) with a rugose surrounding (Langer et al., 2007) that, based on the musculature of living archosaurs (Romer, 1923), was the location of the attachment of the scapular head of the triceps. The medial margin of that subtriangular surface is formed by the medial scapular ridge (Langer et al., 2007), which extends dorsally from the dorsomedial corner of the glenoid, fading as it enters the medial surface of the scapular blade to reach its midlength. The acromion process of NMT RB159 is incomplete as in all examples. Its posterodorsal margin seems to form a near right angle to the anterior margin of the scapular blade. A preglenoid fossa, dorsally flanked by a preglenoid ridge, as seen in *Lewisuchus admixtus* (PULR 01), *Silesaurus opolensis* (Dzik, 2003), and *Sacisaurus agudoensis* (Langer and Ferigolo, 20013) seems to be absent, and no other details are available.

The scapula and coracoid of *Asilisaurus kongwe* are partially coossified in NMT RB159 (Fig. 30), but it is possible to follow the suture between the bones at both the medial and lateral surfaces. Other typically smaller specimens (e.g., NMT RB873) have no coossification. As seen in all available specimens, the suture extends anterodorsally from the glenoid, but its anteriormost



Fig. 30. Partial left scapulocoracoid of an associated skeleton referred to *Asilisaurus kongwe* (NMT RB159) in lateral (A), medial (B), and posterior (C) views. Abbreviations: act, acrocoracoid tubercle; cf, coracoid foramen; cor, coracoid; gl, glenoid; sc, scar; sca, scapula. Scale bar equals 10 mm.

part, along with the respective portions of the scapula and coracoid, is not preserved in any of them. The suture also separates the scapular and coracoidal portions of the glenoid. The former is subrectangular in outline, mediolaterally broader than dorsoventrally deep, with rounded dorsomedial and dorsolateral corners. Its articular surface is depressed medially and slightly mediolaterally convex laterally. The lateral margin of this convex portion wraps around the lateral surface of the scapula. The coracoidal portion of the glenoid expands more posteriorly and bears more strongly rimmed (lateral, medial, and posterior) margins than that of the scapula. Its medial portion is flat and strictly posterodorsally directed. Yet, as with the scapular portion of the glenoid, its lateral margin slightly expands to the lateral surface of the bone. The medial two-thirds of the glenoid is strongly concave, posteriorly directed, and seems to represent the main articular area for the humerus, whereas its lateral third is more subtly concave (Fig. 30C).

Only the posterior half of the coracoid is preserved in the available specimens (Figs. 30A, B and 31). The coracoid foramen is restricted to the eponymous bone, somewhat ventral to the oblique posterior portion of the scapula-coracoid suture. In NMT RB10, a groove expands posteroventrally from the coracoid foramen on the lateral surface of the bone, reaching the scapula contact. NMT RB159, with a coracoid broken right thought the coracoid foramen, reveals the channel that extends dorsomedially from it, as to probably perforate the inner surface of the bone right into the scapula articulation surface. The posterior process of the coracoid is a complex and well developed structure, projecting slightly posterior to the

posteriormost extent of the glenoid. It includes a laterally projecting tuber (= acrocoracoid tubercle of Langer et al., 2007; postglenoid process of Nesbitt, 2011) just ventral of the glenoid and connected to it, in some specimens (NMT RB10), by a broad vertical ridge (Fig. 31). As seen ventrally, the tuber increases in the lateromedial breadth of the ventral margin of the coracoid (Fig. 31D), forming a triangular lateral margin. Starting at the tuber, a rough ridge extends posteriorly along the lateroventral and posteroventral margins of the posterior process. Its posterior end is connected to the medial margin of the glenoid by a subvertical lamina. The lateral surface of that lamina is crossed by the “horizontal groove” of Langer et al. (2007), which separates the subglenoid buttress from the aforementioned lateroventral ridge.

Forelimb

Humerus—The humerus is known from a complete left element (NMT RB159; Fig. 32) and both distal (NMT RB136) and proximal halves (NMT RB16, NMT RB129) of other individuals. Based on the complete left bone of NMT RB159, the humerus of *Asilisaurus kongwe* is a remarkably straight bone, with only some posterior bending of its proximomedial corner. In fact, this may better result from the clockwise (c. 15°; seen from proximal view) rotation of its mediolaterally expanded proximal portion relative to the equally expanded distal articulation. The proximal facet is posteriorly arched, with its main posterior inflection point directed strictly posteriorly. From that point, the lateral segment of the facet expands anterolaterally, with its posteromedial corner

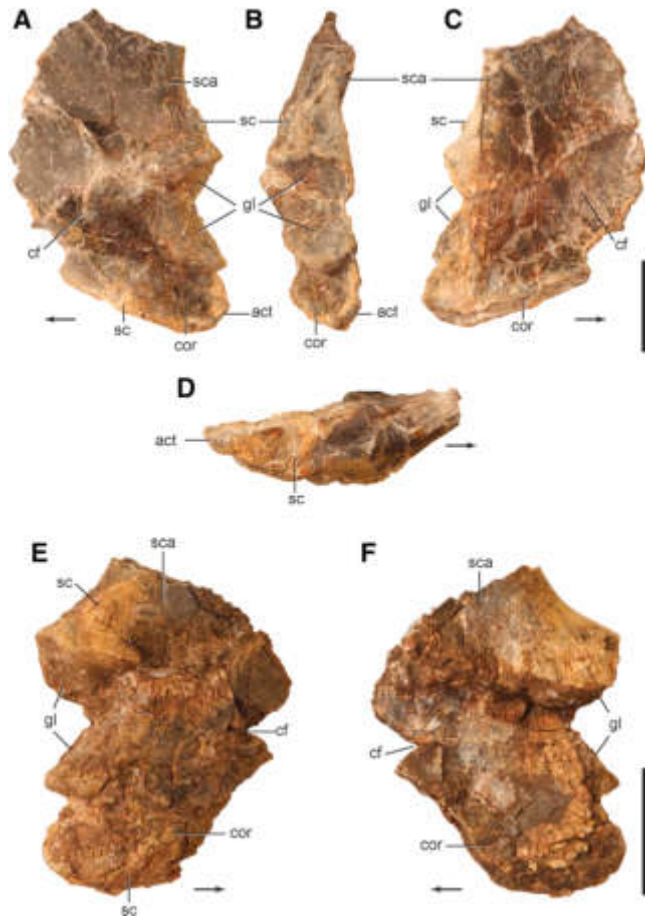


Fig. 31. Partial scapulocoracoids referred to *Asilisaurus kongwe* from the holotype locality. Glenoid area of a left scapulocoracoid (NMT RB10) in lateral (A), posterior (B), medial (C), and ventral (D) views. Glenoid area of a right scapulocoracoid (NMT RB848) in lateral (E) and medial (F) views. Abbreviations: act, acroracoid tubercle; cf, coracoid foramen; cor, coracoid; gl, glenoid; sc, scar; sca, scapula. Arrows indicate anterior direction. Scale bars equal 10 mm.

slightly posteriorly deflected. The medial segment expands anteromedially and is broader transversely, if compared to the lateral segment. The rims of the entire articular facet are more marked (“lip-like”) at its posterior and posteromedial margins. Just distal to the proximal articulation, a rugose tuber is present along the medial surface of the shaft, as seen in many Triassic dinosaurs (Serenó, 1994; Langer et al., 2007). In *Asilisaurus kongwe*, such a medial tuber is separated from the humeral head by an anteromedial to posterolateral directed (in proximal view) groove, also seen in *Herrerasaurus ischigualastensis* (Serenó, 1994). The tip of the tuber expands slightly proximally, but not as much as in *Herrerasaurus ischigualastensis* (Serenó, 1994), and its distal end continues as a sharp ridge extending distally along the medial margin of the shaft, for about one third the length of the bone. The lateral margin of the humeral head is formed by a robust, medially bowing and distally sloping ridge, which is continuous to the deltopectoral crest. This differs from the condition in many dinosaurs (Langer et al., 2007), in which a sharper ridge connects

the humeral head to the deltopectoral crest. The robust ridge of *Asilisaurus kongwe* narrows mediolaterally and expands anteriorly in the distal direction. Its distal summit represents the maximal anterior expansion of the deltopectoral crest. From that point, the crest extends distally in a slightly posteriorly sloping straight line (also getting mediolaterally narrower) to form a second, more distal inflection point, from which it carries on to smoothly merge into the humeral shaft. The latter inflection point of the deltopectoral crest is positioned slightly more than 20% down the total length of the humerus, but its more distal sloping portion can be traced along the proximal 35% of the bone. At its central part, the deltopectoral crest forms a nearly strict right angle to the distal intercondylar line. Medial to the crest, a longitudinally elongated biceps gutter (Langer et al., 2007) excavates the anterior surface of the proximal third of the humerus. On the lateral side, a distally pinched subtriangular muscle scar extends distally from the rugose ridge connecting the humeral head to the deltopectoral crest, along much of the lateral surface of the latter. Its distal tip gives rise to a faint intermuscular line that extends along the posterolateral corner of the humeral shaft, setting the posterolateral limits of the deltopectoral crest. The humerus has an ovoid mid-shaft cross-section, 50% broader mediolaterally than anteroposteriorly.

The distal end of the humerus is slightly less mediolaterally expanded than its proximal end, accounting for a bit more than 20% of the total length of the bone. Such expansion is more marked toward the lateral side, forming a better developed ectepicondyle. The epicondyles form the rugose outer margins of the pair of distal expansions of the humerus, the inner surfaces of which are formed by the smoother articular facets of the ulnar and radial condyles. These are separated by elevated borders from the laterally and medially expanded epicondyles. A subtle transverse groove separates the radial condyle from the ectepicondyle, the lateral surface of which is traversed by a deep, proximodistally elongated fossa. The rugose lateral surface of the ectepicondyle surrounds a distally positioned depression, laterally adjacent to the radial condyle. The entepicondyle is also separated from the medial margin of the ulnar condyle by a subtle transverse groove, and its striated surface is continuous with a ridge that extends proximally along the medial corner of the bone. One pit is seen on the medial surface of the entepicondyle. Proximal to the pit, the entepicondyle bears a smooth and slightly concave anterior surface. The central portion of both the anterior and posterior surfaces of the distal portion of the humerus are taphonomically compressed, but the radial (= cuboid; = brachial) fossa is still recognized in the latter surface immediately proximal to the intercondylar incisure, which separates the ulnar and radial condyles in distal view. Both condyles have rounded distal outlines, are equally projected distally, and face, respectively, distomedially and distolaterally. As a whole, the articulation occupies nearly 75% of the lateromedial width of the distal end of the bone. It is slightly anteriorly facing and is strongly concave in anterior/posterior views. The radial condyle is mediolaterally narrower, but anteroposteriorly broader than the ulnar condyle. The radial condyle is subtly anteroposteriorly convex, whereas the ulnar condyle is both more strongly concave and extensive into the anterior surface of the humerus. The entire distal outline of the

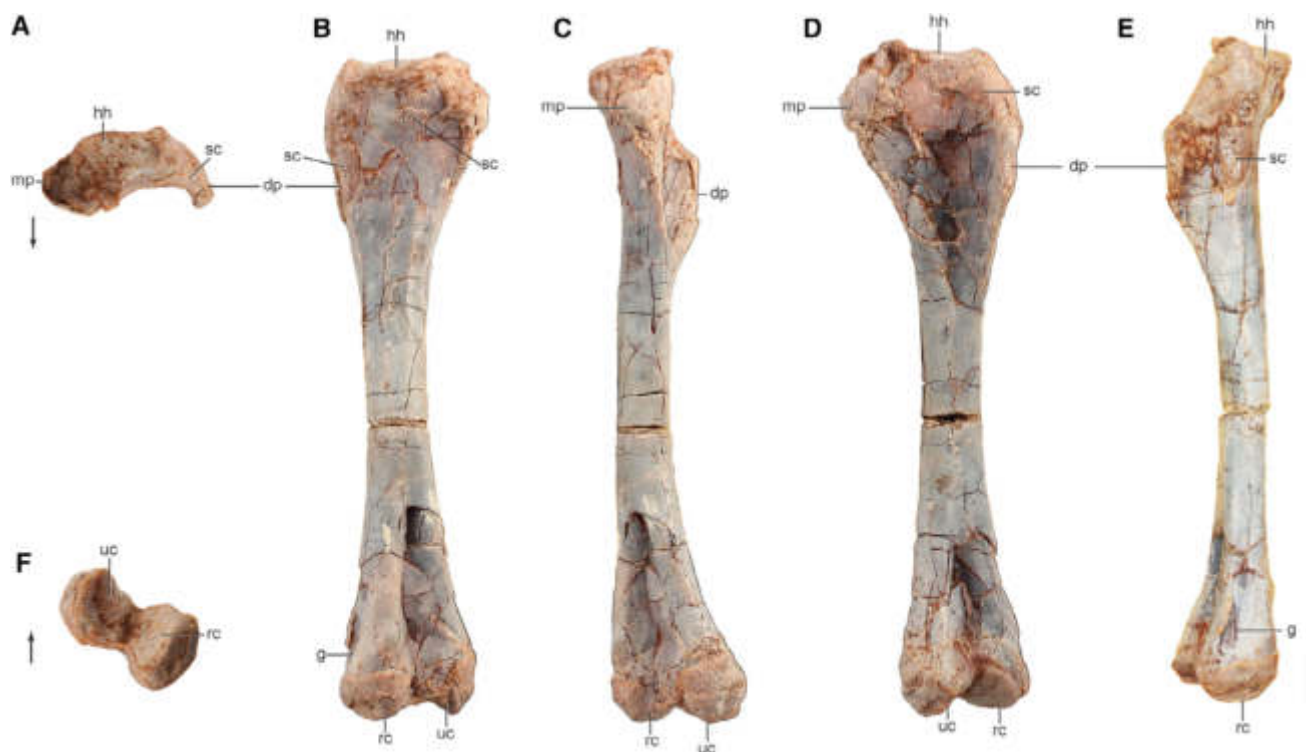


Fig. 32. Left humerus of an associated skeleton referred to *Asilisaurus kongwe* (NMT RB159) in proximal (A), posterior (B), medial (C), anterior (D), lateral (E), and distal (F) views. Abbreviations: dp, deltopectoral crest; g, groove; hh, humeral head; mp, medial process; rc, radial condyle; sc, scar; uc, ulnar condyle. Arrows indicate anterior direction. Scale bar equals 10 mm.

humerus is “8-shaped,” with a pair of rounded condyles/epicondyles constricted in the middle by well-developed olecranon fossa (posteriorly) and distal extension of the intercondylar incisure (anteriorly).

Radius—The radius is known from a complete right (Fig. 33), the distal portion of a left (NMT RB159; Fig. 33), and other fragments found at the holotype locality (NMT RB142; NMT RB143; NMT RB144). Based on the complete right bone of NMT RB159 (Fig. 33), the radius of *Asilisaurus kongwe* is a remarkably simple, straight and rod-like element, the length of which is about 85% that of the left humerus of NMT RB159 (Table 1). Its proximal end is anteroposteriorly expanded, twice broader in that direction than mediolaterally in proximal view, with rounded lateral and flattened medial margins. The articular surface is concave in lateral/medial views because of a proximal expansion of its posterior portion. The articulation surface is well marked by slightly everted margins all around. The medial surface of the proximal portion of the radius bears a subtriangular facet that articulates with the ulna, the distal summit of which approaches the anterior margin of the bone. In this area, the anterior margin of the radius is sharper and slightly projected, but there is no sign of a well-developed “biceps tubercle” (Serenó, 1994) distal to that. The radial shaft is straight in lateral and medial views, but slightly sigmoidal in anterior and posterior views, with medially and laterally bowed proximal and distal halves, respectively, so that its proximal portion is more closely fitted to the ulna. A similar, but much more distinct condition is present in *Herrerasaurus ischigualastensis* (Serenó, 1994). A faint longitudinal ridge marks the posterior edge of this surface. A

foramen pierces the medial surface of the radius at a distance corresponding to a third of its length from the proximal end. Longitudinal striations, related to the ulnar connection, occur along the medial surface of the entire radial shaft, which is generally rounded in cross section. The distal fifth of the radius expands gradually in all directions, so that the circular distal surface is about twice the minimal breadth of the shaft. The most conspicuous feature of the distal part of the radius is the rugose ovoid scar in its medial side, which represents the surface for articulation with the ulna. As observed in anterior and posterior views, the lateral margin of the distal end is kinked medially relative to that of the shaft. The radius has an abrupt distal ending, with a flat distal surface forming straight angles to the surrounding shaft.

Ulna—The ulna is known from complete left and right examples from NMT RB159 (Fig. 34) and partial extremities from the holotype locality (NMT RB145). Based on the complete left bone of NMT RB159, the ulna of *Asilisaurus kongwe* is a relatively simple element, with an expanded proximal end that is three times the anteroposterior breadth of the narrower portion of the shaft (Fig. 34). Its proximal outline is subtriangular, broader anteroposteriorly than mediolaterally, with concave medial, straight anterolateral, and rounded posterolateral margins. The latter two converge laterally to form the lateral process, whereas the anteromedially displaced medial process is set at the confluence of the medial and anterolateral margins. In lateral/medial views, the posterior portion of the ulna expands proximally, forming a well-developed olecranon process, the proximodistal length of which is half the

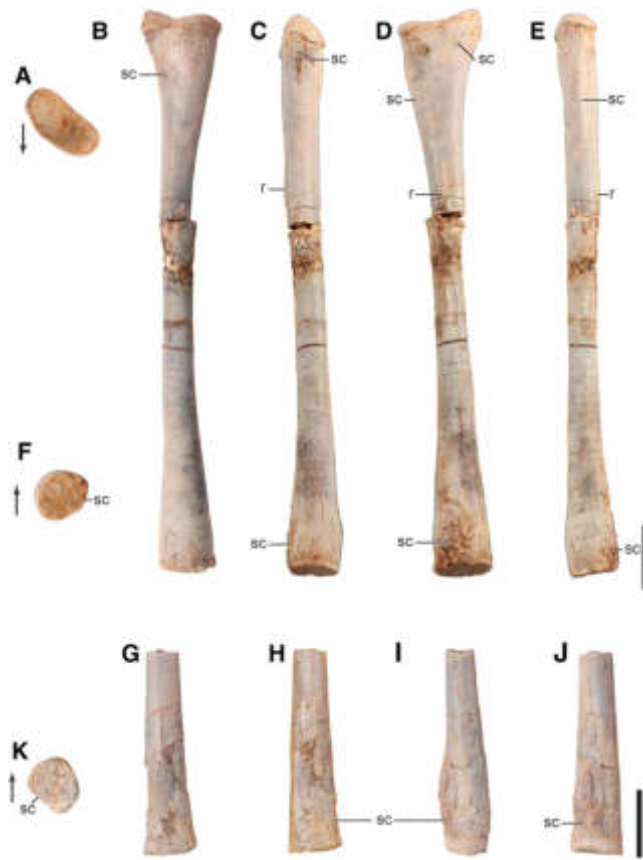


Fig. 33. Radii of an associated skeleton referred to *Asilisaurus kongwe* (NMT RB159). Right radius in proximal (A), lateral (B), posterior (C), medial (D), anterior (E), and distal (F) views. Distal end of the left radius in lateral (G), posterior (H), anterior (I), medial (J), and distal (K) views. Abbreviations: r, ridge; sc, scar. Arrows indicate anterior direction. Scale bar equals 10 mm.

anteroposterior breadth of the proximal margin of the bone. Its anterior surface takes part in the humeral articulation, whereas the others are heavily scarred for the insertion of the triceps tendon. The posterior margin of the bone is slightly expanded where the olecranon continues onto the ulnar shaft. Anterior to the olecranon, the humeral articulation expands in that same direction, forming a platform nearly perpendicular to the long axis of the ulna (but slightly sloped anterodistally). As a result, the anteroposterior expansion of the bone is more marked toward the anterior side, as seen in lateral/medial views. The smooth articulation facet is concave in lateral and medial views, but mostly flat in anterior view. This is separated from the olecranon by a shallow transverse depression and is also subtriangular in proximal view, with straight posterior (facing the olecranon) and anterolateral margins, and a rounded medial margin. The articulation of the radial head occupies a scarred and slightly depressed area on the anterolateral surface of the proximal end of the ulna, immediately distal to the humeral articulation. The scar is L-shaped in lateral view, with the proximal margin set between the lateral and medial processes and the anterior portion expanding more distally than the posterior. The ulnar shaft is oval in cross-section, and broader anteroposteriorly than mediolaterally. It bows anteriorly along

its entire length in lateral/medial views. In anterior and posterior views, the proximal three-fourths of the shaft is medially arched, a condition not clear in the distal fourth. This part of the bone seems medially bent, but this might be in part the result of fractures and deformation during fossilization. One anterior and two lateral longitudinal ridges extend along the shaft. The latter pair bounds a broad longitudinal groove and may represent the attachment sites of a radius/ulna interosseous membrane. The depth of this groove appears to be autapomorphic of *Asilisaurus kongwe* (Fig. 34). Along with the lateral groove, these are fainter in the distal fourth of the bone. The distal end of the ulna is slightly expanded and rotated relative to the rest of the bone. As a result, the distal outline is ovoid and its long axis anterolaterally to posteromedially oriented. Yet, its anteromedial margin is slightly flattened for the radial articulation. The distal articulation surface is slightly concave and, as with the radius, forms straight angles to the surrounding shaft surfaces.

Manus—The partial skeleton referred to *Asilisaurus kongwe* (NMT RB159) preserves one complete and one incomplete metacarpal (Fig. 35). Although the complete hand is not known, the length of the metacarpals is exceptionally short; the completely preserved metacarpal is ~30% the length of metatarsal III or ~12% the length of the femur (Table 1).

The complete element is tentatively identified as the second metacarpal of a right hand based on comparisons with dinosaurs (e.g., *Herrerasaurus ischigualastensis*, Sereno, 1994; *Heterodontosaurus tucki*, Santa, 1980). It is an elongated element with expanded proximal and distal portions. Their respective lateromedial breadths correspond to nearly 40 and 30% of the total length of the bone. The proximal articulation surface is flat, oblique to the distal intercondylar line, with its lateral portion reaching more proximally than the medial. The proximal outline is subelliptical, with the long axis more than twice the breadth of the short axis. The former is oriented posteromedially to anterolaterally, that is, rotated relative to the distal intercondylar line. The medial part of its anteromedial surface and the lateral part of its posterolateral surface are respectively flattened and concave to receive the adjacent metacarpals. These extend distally along the shaft as subtle depressions. The shaft is nearly straight in lateral or medial views, just slight ventrally curved in its distal fourth. The distal condyles are similar in size and equally extensive distally. The lateral condyle is, however, slightly more expanded toward the lateral side than the medial condyle is to the opposite side. There is a shallow extensor depression in the dorsal surface of the distal part of the bone, which is slightly better developed laterally. There are subtle collateral pits, the medial of which is larger. The distal articulation is subrectangular, nearly twice broader than deep.

Two other metacarpal fragments were found with NMT RB159, a proximal end and a distal end (Fig. 35); the position of the fragments within the manus is not known. Here, we interpret these as the same element missing a bit of the midshaft. The morphology of both the proximal and distal fragments is highly consistent with that of the more complete metacarpal described above.

Pelvic Girdle

Ilium—The ilium is well represented in the sample, but complete ilia have not been recovered. NMT RB159

TABLE 1. Measurements of an associated skeleton referred to *Asilisaurus kongwe* (NMT RB159)

Element	Measurement	Length (mm)
Scapula (left)	Length	93.2
	Anteroposterior minimum of shaft	13.2
	Anteroposterior width at dorsal end	36.9
Humerus (left)	Length	90.6
	Length of proximal end (long axis)	25.9
	Length of distal end (long axis)	19.4
	Midshaft width (max)	8.5
Ulna	Length	91.2 (l)/ 92 (r)
	Length of proximal end (long axis)	16.1 (l)/ 15.3 (r)
	Length of distal end (long axis)	8.8 (l)/ 8.1 (r)
	Midshaft width (max)	5.9 (l)/ 6 (r)
Radius (right)	Length	83.3
	Length of proximal end (long axis)	12.4
	Length of distal end (long axis)	8.6
	Midshaft width (max)	4.9
Metacarpal	Length	17.8
	Length of proximal end (long axis)	7.3
	Length of distal end (long axis)	5.1
	Midshaft width (max)	3.1
Pubis (right)	Length	121
	Distal width	15.9
Femur	Length	144.4 (l)/ 144.0 (r)
	Length of proximal end (long axis)	28.3 (l)/ 27.8 (r)
	Length of distal end (long axis)	28.6 (l)/ 28.8 (r)
	Midshaft width (max)	15.9 (l)/ 15.6 (r)
Tibia (left)	Length	124.2
	Length of proximal end (long axis)	30.9
	Length of distal end (long axis)	17.8
	Midshaft width (max)	10.9
Fibula (left)	Length	120
	Length of proximal end (long axis)	19.2
	Length of distal end (long axis)	16.2
	Midshaft width (max)	8.1
Metatarsal I	Length	27.6 (r)
	Length of proximal end (long axis)	8.4 (r)
	Length of distal end (long axis)	6.5 (l) / 6.1 (r)
	Midshaft width (max)	4.3 (l) / 4.3 (r)
Metatarsal II	Length	52.3 (l) / 50.4 (r)
	Length of proximal end (long axis)	15.5 (l) / 15.5 (r)
	Length of distal end (long axis)	9.9 (l) / 9.8 (r)
	Midshaft width (max)	6.2 (l) / 6.1 (r)
Metatarsal III	Length	60.0 (l) / 58.4 (r)
	Length of proximal end (long axis)	15.9 (l) / 16.0 (r)
	Length of distal end (long axis)	11.4 (l) / 11.3 (r)
	Midshaft width (max)	6.4 (l) / 6.6 (r)
Metatarsal IV	Length	54.0 (r)
	Length of proximal end (long axis)	16.8 (r)
	Length of distal end (long axis)	9.4 (l) / 9.0 (r)
	Midshaft width (max)	5.4 (r)
Metatarsal V	Length	34.4 (l) / 34.6 (r)
	Length of proximal end (long axis)	15.3 (l) / 14.8 (r)
	Length of distal end (long axis)	7.4 (l) / 7.5 (r)
	Midshaft width (max)	6.8 (l) / 6.9 (r)

Abbreviations: (l), left; (r), right; (max), maximum.

preserves both sides (Figs. 36 and 37) and many partial examples are known from the holotype locality (posterior half of a left ilium, NMT RB176; acetabular area, NMT RB13; NMT RB174; Fig. 37). The best preserved ilium of NMT RB159 (Fig. 36) is missing only a small portion of the iliac blade dorsal to the acetabulum and is the basis for the following description. The iliac blade corresponds to about half the total dorsoventral depth of the bone at the greatest depth of the acetabular area. In lateral view, the dorsal margin of the postacetabular process is slightly

convex, and probably concave anterior to that, although the missing piece of the bone hampers a confident estimate. In dorsal view, the lamina bows medially, but its anterior tip is more strongly bent laterally. This heavily scarred area represents the dorsal continuation of the preacetabular ridge (Fig. 36A), which extends from the lateral surface of the bone, just dorsal to the acetabulum, to form an anterolaterally to posteromedially oriented, subvertical wall, as in other dinosauriforms (e.g., *Silesaurus opolensis*, Dzik, 2003). This subvertical wall

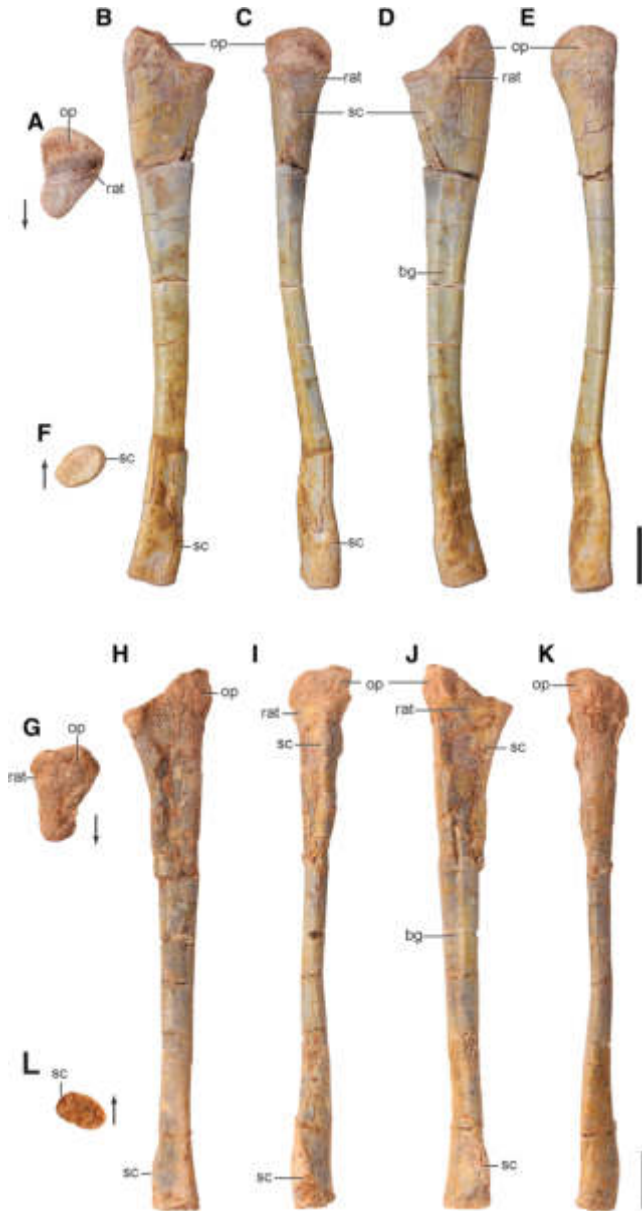


Fig. 34. Ulnae from a partial skeleton referred to *Asilisaurus kongwe* (NMT RB159). Left ulna in proximal (A), medial (B), anterior (C), lateral (D), posterior (E), and distal (F) views. Right ulna in proximal (G), medial (H), anterior (I), lateral (J), posterior (K), and distal (L) views. Abbreviations: bg, broad groove; op, olecranon process; rat, radial tuber; sc, scar. Arrows indicate anterior direction. Scale bars equal 10 mm.

forms most of the preacetabular process, which is short and does not extend anterior to the anterior extent of the pubic peduncle. In lateral view, the tip of the process forms an anteriorly directed right angle. A flat and anteriorly concave (in lateral/medial views) surface is present between the preacetabular ridge and another, more medial ridge that corresponds to the posterior continuation of the dorsal edge of the pubic peduncle. In other dinosauriform taxa, a groove (=preacetabular fossa of Langer et al., 2010; medial fossa of Sereno et al., 2013) is present instead of the flat surface. Posterior to that, the

lateral surface of the iliac blade dorsal to the acetabulum is smooth and depressed, but subtly striated near the dorsal margin of the postacetabular process (Fig. 36A).

The ventral margin of the anteriormost portion of the postacetabular process is formed by a sharp ridge extending posteriorly from the posterior edge of the ischial peduncle. This ridge extends for about half the length of the process, where it gives rise to an anteroposteriorly elongated subtriangular fossa. This corresponds to the brevis fossa (Novas, 1996; Langer and Benton, 2006), which occupies the ventral surface of the posterior half of the process, expands mediolaterally as it trends posteriorly, and is flanked by medial and lateral ridges. The former is sharper and closer to the horizontal plane, corresponding to the posterior continuation of a ridge extending along the medial surface of the ilium. The latter is more robust and ventrally bent, extending anteroposteriorly as a broad, but subtle ridge that dorsally parallels the ventral margin of the process. We consider this ridge homologous to the brevis shelf of various dinosaurs (Langer and Benton, 2006). An ovoid muscle scar is present at midlength dorsal to the lateral edge of the brevis shelf of *Asilisaurus kongwe* (Fig. 37A), as also seen in a specimen referred to *Lewisuchus admixtus* (CRILAR-Pv 552), in *Silesaurus opolensis* (ZPAL Ab III/404/1), and possibly in early dinosaurs (Baron and Williams, 2018). In dorsal/ventral views, both ridges project more posteriorly than the space between them, so that the posterior margin of the ilium is strongly concave. In various dinosauriforms, including a specimen referred to

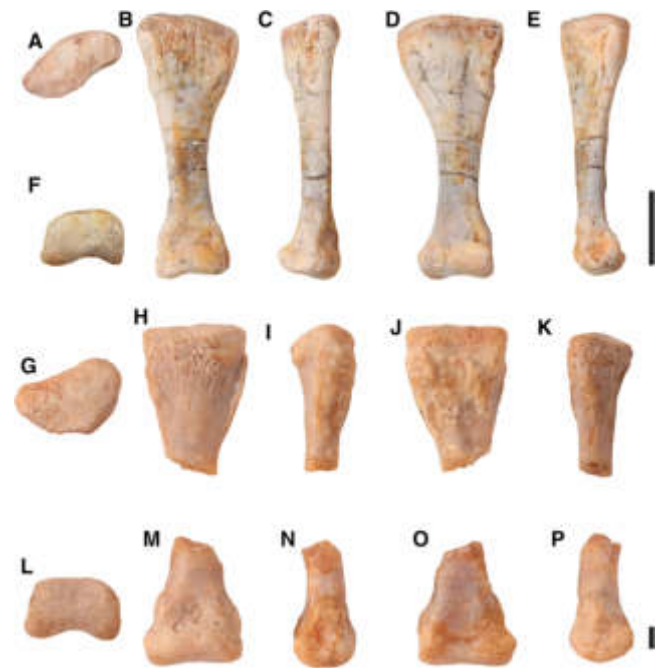


Fig. 35. Metacarpals of a partial skeleton referred to *Asilisaurus kongwe* (NMT RB159). Complete, right metacarpal II in proximal (A), anterior (B), lateral (C), ventral (D), medial (E), and distal (F) views. Proximal half of a positionally uncertain right metacarpal in proximal (G), anterior (H), lateral (I), ventral (J), and medial (K) views. Distal half of a positionally uncertain right metacarpal in distal (L), anterior (M), lateral (N), ventral (O), and medial (P) views. Scale bar equals 10 mm A-F and 1 mm in G-P.

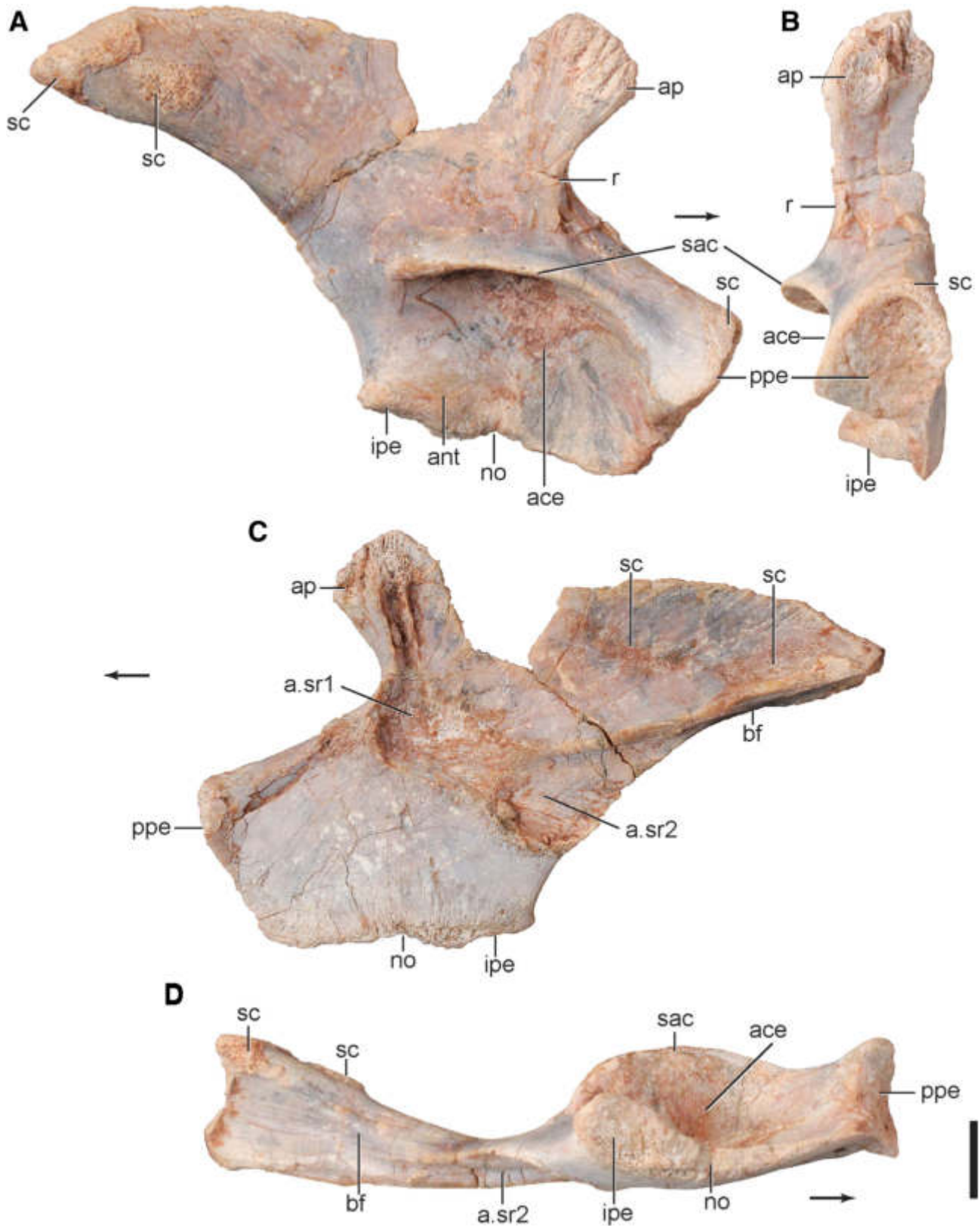


Fig. 36. Nearly complete right ilium of a partial skeleton referred to *Asilisaurus kongwe* (NMT RB159) in lateral (A), anterior (B), medial (C), and ventral (D) views. Abbreviations: a., articulates with; ace, acetabulum; ant, antitrochanter; ap, anterior process; bf, brevis fossa; ipe, ischial peduncle; no, notch; ppe, pubic peduncle; r, ridge; sac, supraacetabular crest; sc, scar; sr1, sacral rib 1; sr2, sacral rib 2. Arrows indicate anterior direction. Scale bar equals 10 mm.

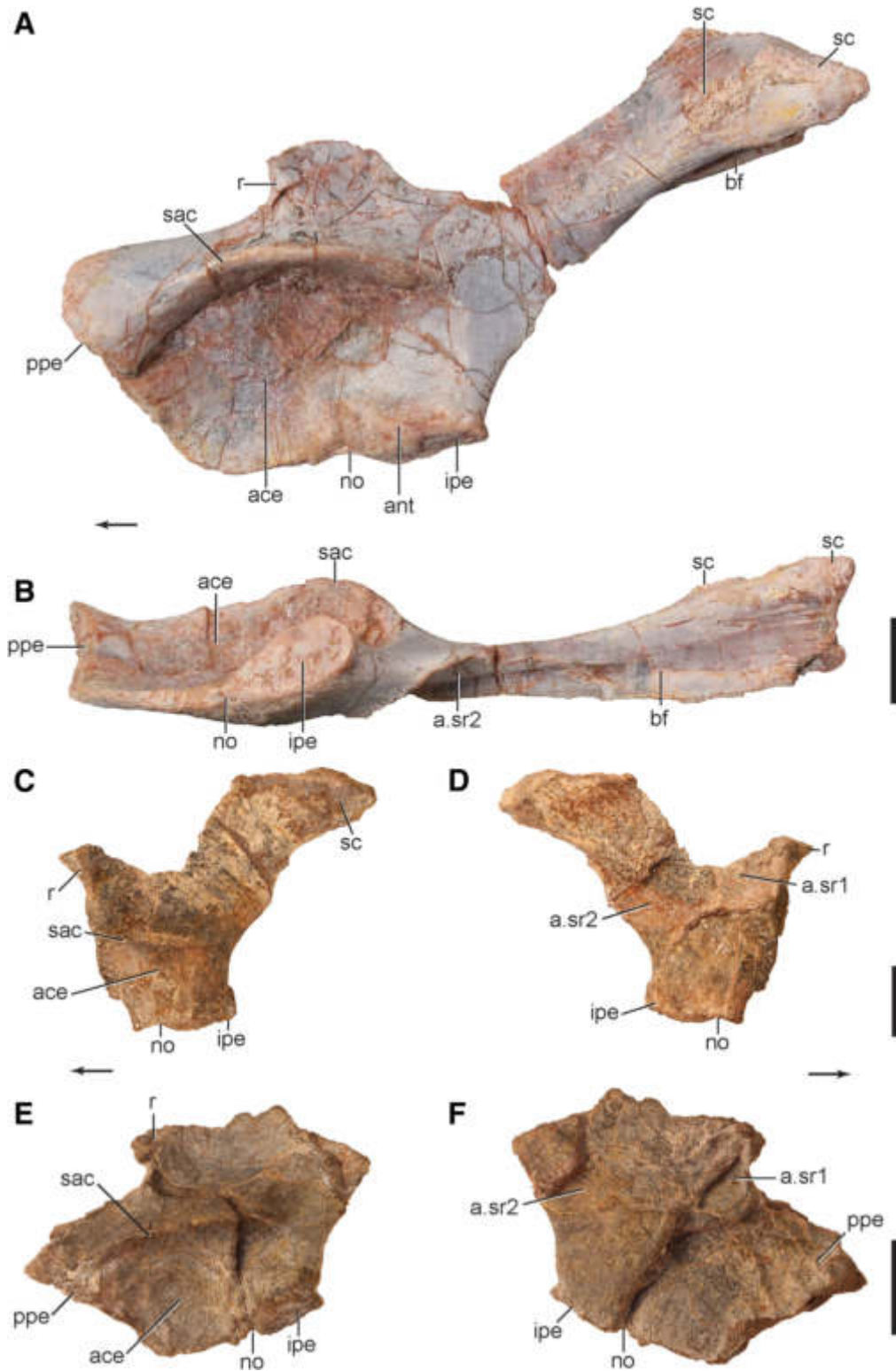


Fig. 37. Further ilia referred to *Asilisaurus kongwe*. Partial left ilium of a partial skeleton referred to *Asilisaurus kongwe* (NMT RB159) in lateral (A) and ventral (B) views. Partial left ilium (NMT RB176) from the holotype locality in lateral (C) and medial (D) views. Partial left ilium (NMT RB13) from the holotype locality in lateral (E) and medial (F) views. Abbreviations: a., articulates with; ace, acetabulum; ant, antitrochanter; bf, brevis fossa; ipe, ischial peduncle; no, notch; ppe, pubic peduncle; r, ridge; sac, supraacetabular crest; sc, scar; sr1, sacral rib 1; sr2, sacral rib 2. Arrows indicate anterior direction. Scale bar equals 10 mm.

Lewisuchus admixtus (CRILAR-Pv 552) and in *Silesaurus opolensis* (ZPAL Ab III/404/1), but not in *Asilisaurus kongwe*, the ridge that forms the ventral margin of the anterior portion of the process is more medially positioned, and continuous with the ridge that medially flanks the brevis fossa. Therefore, the brevis fossa of *Asilisaurus kongwe* is not visible in lateral view in any specimen, whereas the fossa is clearly visible in lateral view in *Lutungutali sitwensis* (Peacock et al., 2013), *Sacisaurus agudoensis* (Langer and Ferigolo, 2013), *Silesaurus opolensis* (Dzik, 2003), and a specimen referred to *Lewisuchus admixtus* (CRILAR-Pv 552).

The acetabulum of *Asilisaurus kongwe* is fully closed, as typical of most non-dinosaurian archosaurs (Gauthier, 1986; Langer and Benton, 2006; Nesbitt, 2011). The entire acetabular medial wall is, therefore, about as anteroposteriorly long as dorsoventrally deep. It is laterally concave and its convex ventral margin is formed of two nearly straight edges for the articulation with the pubis and ischium. The anterior articulation, for articulation with the pubis, is shorter, so that there is an obtuse inflection point with the posterior margin, positioned ventral of the anterior end of the acetabulum. A small gap is present between the inflection point and the posterior portion of the ischial peduncle articular surface, as in *Teleocrater rhadinus* (Nesbitt et al., 2017, 2018). At the posteroventral corner of the acetabulum, a rounded, smoother area corresponds to the antitrochanter (Figs. 36 and 37), which is slightly laterally raised from the rest of the surface of the acetabulum, especially near the ischium articulation surface, of which it is an anterodorsal continuation. From the anterior margin of that articular surface, a subtle ridge extends anterodorsally, dividing two rounded depressions apart on the lateral surface of the acetabular wall.

The pubic peduncle extends anteroventrally from the main body of the ilium. Its anterior end expands both laterally and anteroposteriorly. The resulting shape is subtriangular, with rounded anterior and posterolateral corners, and convex anterolateral, posterior, and medial margins. The latter is continuous with a posterior part of the pubic articulation, which corresponds to an extension of the acetabular wall projecting from the posteromedial corner of the main articulation surface with the pubis. The dorsal margin of the pubic peduncle, near the articulation surface with the pubis, is rugose. As with the supraacetabular crest, the posterior surface of the pubic peduncle slopes abruptly into the acetabular wall. On the contrary, the posterior margin of the acetabulum smoothly transitions onto the lateral surface of the ischial peduncle, between the posterior end of the supraacetabular crest and the iliac articulation to the ischium. The non-acetabular part of the ischial peduncle corresponds to a ventrally pointing, subtriangular surface anteroventral to the brevis shelf. It barely contacts the ischial articulation, which is mostly formed by the ventral margin of the acetabular wall. The posterior portion of that articulation, ventral to the antitrochanter, is mediolaterally expanded and ovoid in ventral outline. It expands only slight posteriorly, so that the postacetabular embayment of the ilium has almost no ventral component.

The supraacetabular crest expands over the dorsal margin of the acetabulum, also extending a bit ventrally along the anterior margin. The maximum lateral

projection of the crest is near its posterior end. Posterior to that point, in ventral and dorsal views, the crest terminates abruptly at the posterodorsal corner of the acetabulum. The supraacetabular crest reduces in breadth less abruptly in its anterior extension, reaching the midlength of the pubic peduncle, as occurs in a specimen referred to *Lewisuchus admixtus* (CRILAR-Pv 552). Dorsal to the acetabulum, the crest expands laterally and somewhat ventrally, so that the roof of the acetabulum is slightly dorsal to the lateral tip of the crest, as also seen in a specimen referred to *Lewisuchus admixtus* (CRILAR-Pv 552).

The medial surface of the ilium is smooth and convex in the acetabular area, but deeply excavated dorsal to that for the sacral vertebrae articulations (Fig. 36C). The slightly everted ventral margin of this articulation area has anterior and posterior convex portions, which received the ventral margins of the two primordial sacral ribs. An oblique ridge starts dorsal to the convexities setting the two articular areas apart and extends posterodorsally along the postacetabular process. This forms the dorsal limit for the articulation of the second sacral rib and this is confirmed based on the associated second sacral vertebra found with the same specimen (NMT RB159, see below). Anterior to that, the articulation area for the first sacral rib is more dorsoventrally extensive. It forms a depression, anterior to the oblique ridge, that extends anterodorsally along the preacetabular process, as a finger-like excavation. Dorsal to the anteroposterior trending ridge on the medial side of the postacetabular process, scars are present dorsal to the posterior extent of the second sacral rib and a further posterior scar contacts the medial ridge (Fig. 36).

Ischium—The ischium is not known from any complete elements; only partially from both sides of NMT RB159 (Fig. 38) and from fragments of the proximal portion (NMT RB12) and of the articulated distal end of the ischial pair (NMT RB135; NMT RB847; Fig. 39) from the holotype locality. The ischial body plus the proximal part

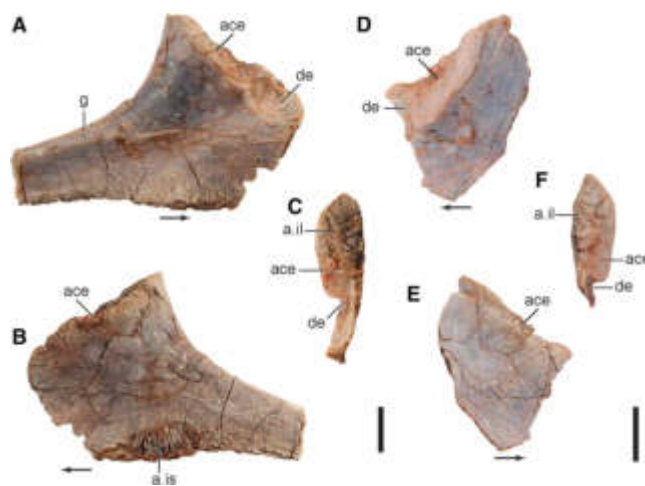


Fig. 38. Partial ischia of an associated skeleton referred to *Asilisaurus kongwe* (NMT RB159). Right ischium in lateral (A), medial (B), and proximal (C) views. Left ischium in lateral (D), medial (E), and proximal (F) views. Abbreviations: a., articulates with; ace, acetabulum; de, depression; g, groove; il, ilium; is, ischium. Arrows indicate anterior direction. Scale bar equals 10 mm.

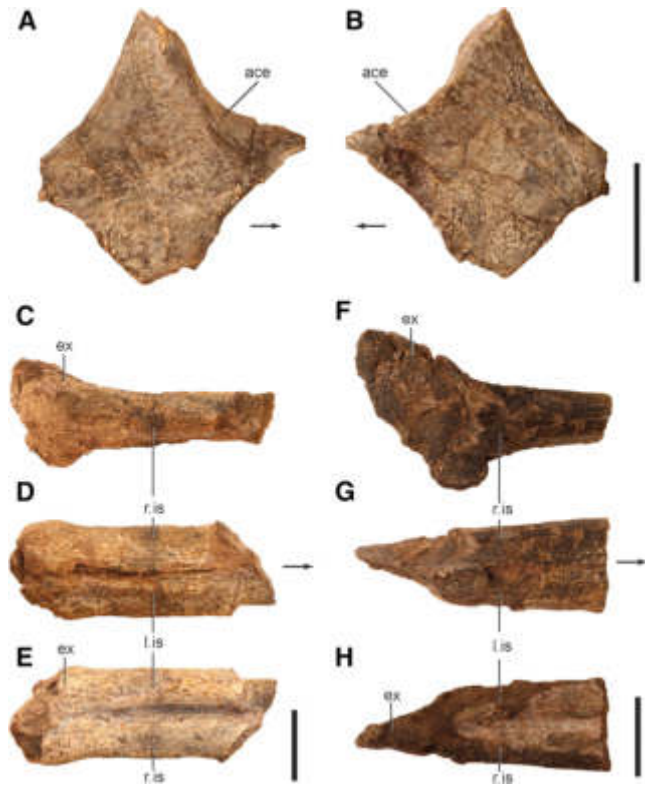


Fig. 39. Ischia fragments referred to *Asilisaurus kongwe* from the holotype locality. Proximal portion of the ischium (NMT RB12) in lateral (A) and medial (B) views. Left and right ischia (NMT RB135) joined at the midline in right lateral (C), ventral (D), and dorsal (E) views. Left and right ischia (NMT RB847) joined at the midline in right lateral (F), ventral (G), and dorsal (H) views. Abbreviations: ace, acetabulum; ex, expansion; is, ischium; l., left; r., right. Arrows indicate anterior direction. Scale bars equal 10 mm.

of the shaft is preserved in the right side of NMT RB159, whereas only part of the proximal articulation is preserved on its left side (Fig. 38), as well as in an isolated specimen (NMT RB12). The ischial body is composed of a mediolaterally broader dorsal portion and a ventrally expanding laminar obturator plate. The former has a slightly dorsoventrally convex medial surface and a more convex lateral surface. At its proximal summit, the broader dorsal portion of the body bears a flat, but rugose articulation surfaces with the ilium. The main surface of the ilium articulation faces strictly anterodorsally. It is subtriangular in proximal outline, with a short dorsolateral margin, and long ventrolateral and medial margins, the latter of which is slightly convex. A much mediolaterally narrower part of the ilium articulation surface extends anteroventral to that, along the straight proximal margin of the ventral edge. In lateral view, a fossa is present between the articulation surface with the ilium and with the pubis, a feature present in other silesaurids and other dinosauriforms (Nesbitt, 2011). The antitrochanter is adjacent to the broader part of the iliac articulation, sloping ventrolaterally relative to that. It also has a subtriangular outline, with its shorter margin facing anteromedially. The anterolateral corner and lateral margin of that articulation form lip-like rims that expand abruptly from the lateral surface of the proximal

portion of the ischium. The obturator plate is sigmoidal, with a laterally convex and medially concave anterodorsal portion, and a laterally concave and medially convex posteroventral portion. On the medial surface, the posterior edge of the concave portion matches the anteriormost extension of a rugose area that extends distally along the ventral margin of the ischium. This represents the contact surface with its counterpart and is more dorsoventrally expanded anteriorly. The lateral surface of the obturator plate bears a depression just posteroventral to the ilium articulation surface, in an area that represents the ischium contribution to the medial acetabular wall. The obturator plate is continuous to the dorsoventrally narrower and laminar ventral part of the ischium shaft. The blade-like ventral margin is present as distally as the shaft is preserved in NMT RB159, but fails to reach the distal part of the bone, as indicated by both preserved distal ends of the ischia (Fig. 39).

As preserved in NMT RB159, the proximal part of the ischial shaft is broader dorsally and thins ventrally (Fig. 38). It has a subtriangular cross section, with a narrow dorsolateral margin, a slightly concave ventrolateral margin, and a slightly convex medial margin. The dorsal surface of the shaft bears a proximodistally oriented groove, flanked medially by a raised medial margin, as also seen in *Sacisaurus agudoensis* (Langer and Ferigolo, 2013) and other archosauromorphs (Ezcurra, 2016). The groove subtly extends along the dorsolateral surface of the ischium. As present in NMT RB135 and NMT RB847, the distal portion of the ischial shaft is ovoid in cross section, with the long axis ventromedially to dorsolaterally oriented. This configuration produces a deep midline groove extending longitudinally along the dorsal surface of the articulated ischia. Yet, right at the distal end of the bone, the dorsolateral edge expands mediolaterally, so that its medial margin contacts that of the counterpart, preventing the dorsal groove of reaching the distal end of the ischium. The distal end of the ischium also expands dorsoventrally twice the depth of the shaft proximal to that. The dorsal expansion is more gradual, also extending more distally, so that the distal margin of the ischium is oblique to its long axis in lateral/medial views (Fig. 39). Finally, the distal outline of the ischium is subtriangular, with a long flat medial margin, equally long, but slightly convex lateroventral margin, and short/convex dorsolateral margin. These are separated by angled ventral and dorsomedial corners and a rounded dorsolateral corner.

Pubis—The pubis is known from a complete right element from NMT RB159 (Fig. 40), partial proximal ends (NMT RB14; Fig. 41), and distal ends from the holotype locality. The right pubis of NMT RB159 is nearly complete, missing only parts of the medial part of the apron and obturator plate. Two other preserved pubes are represented only by the proximal portion of the bones, which match NMT RB159 in most details. The proximal portion of the pubis is subtriangular in lateral view, with the proximal articulations occupying its posterodorsal surface. The articulation surface with the ilium is tear drop-shaped in proximal outline, with rounded anterior and lateral margins, and a flatter medial margin that extends posteriorly. This posterior extension corresponds to a continuation of the edge of the acetabular from the ilium, whereas the broader anterior portion of the facet articulates with the pubic peduncle of the ilium. That surface is

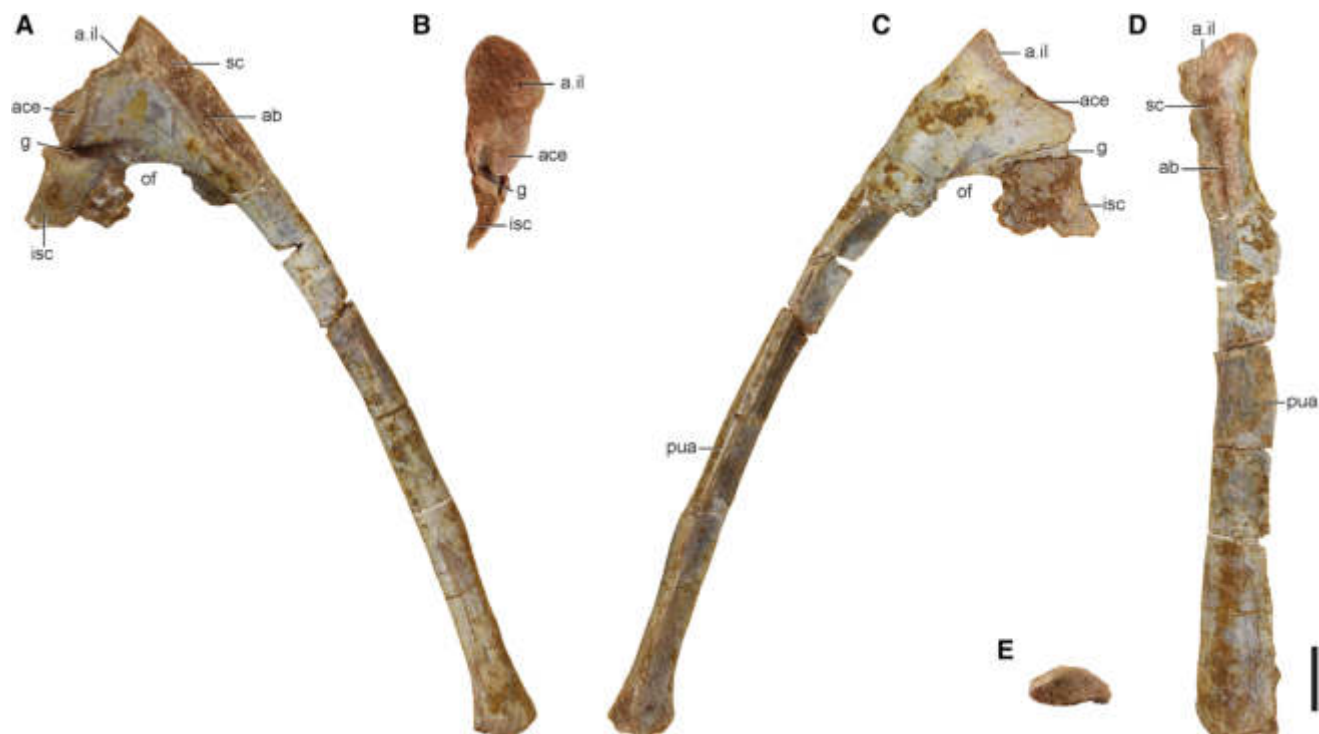


Fig. 40. Nearly complete right pubis of a partial skeleton referred to *Asilisaurus kongwe* (NMT RB159) in lateral (A), proximal (B), medial (C), anterior (D), and distal (E) views. Abbreviations: a., articulates with; ab, ambiens process/groove; ace, acetabulum; g, groove; il, ilium; isc, ischium; of, obturator foramen; pua, pubic apron; sc, scar. Arrow indicates anterior direction. Scale bar equals 10 mm.

transversally concave and separated by a subtle inflection from the acetabulum. This is flatter and slightly ventrally bent, expanding posterolaterally from the articulation with the pubic peduncle of the ilium. In lateral view, the pedicle that supports the femoral articulation is separated from the posterior process of the pubis by a groove as in other dinosauriforms (Nesbitt, 2011). Yet, the groove actually expands dorsomedially in *Asilisaurus kongwe*, as to separate the articulation surface with the femur laterally from the contribution of the pubis to the acetabular wall, medially. The latter corresponds to a bony lamina medially connecting the posterior pubic process ventrally and the articulation for pubic peduncle of the ilium dorsally.

The posterior process, which articulated with the ischium, is subtriangular in lateral view. Its ventral margin

extends anteriorly ventral to the ambiens process to form the lateroventral margin of the pubic shaft. The articulation surface with the ischium is dorsoventrally straight in lateral view and subtriangular in outline, subtly concave medially and more strongly convex laterally. The laminar obturator plate is not preserved, but it does not seem to be continuous to the equally laminar medial portion of the pubic shaft as in *Sacisaurus agudoensis* (Langer and Ferigolo, 2013). On the contrary, as preserved, the medial lamina of the pubic shaft turns from sub-horizontal along most of its length to a sub-vertical orientation at its posterior end, extending slightly along the medial surface of the pubic body separated from the more lateral putative anterior extension of the obturator plate. The medial surface of the pubis is smooth and slightly concave (dorsoventrally) at its ventral portion. More dorsally, the equally smooth but convex medial margin of the bone, mirrors a much more rugose dorsolateral surface. This bears a semicircular muscle scar, with raised distal borders, right anterolateral to the iliac pubic peduncle articulation. Distal to that, on the proximal end of the shaft, a proximodistally elongated pubic tubercle (=ambiens process of other dinosauriforms) is flanked dorsally by an equally elongated depression, as in a specimen referred to *Lewisuchus admixtus* (CRILAR-Pv 552) and in *Sacisaurus agudoensis* (Langer and Ferigolo, 2013). Dorsal to that, the dorsal margin of the pubis rises slightly forming a blunt crest.

The pubic shaft is formed by a rounded and thick lateral portion and a medial lamina, so that its cross section is medially narrow, expanding posteroventrally at its lateral margin. As a result, the ventral margin of the shaft is occupied by a persistent longitudinal groove. This

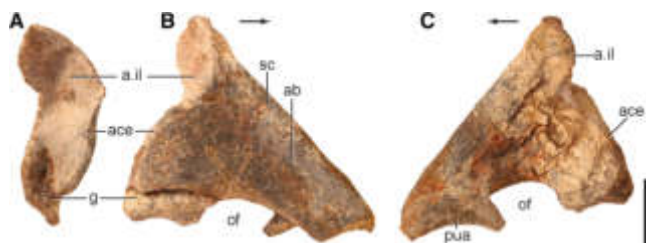


Fig. 41. Proximal portion of a right pubis (NMT RB14) referred to *Asilisaurus kongwe* from the holotype locality in proximal (A), lateral (B), and medial (C) views. Abbreviations: a., articulates with; ab, ambiens process/groove; ace, acetabulum; g, groove; il, ilium; of, obturator foramen; pua, pubic apron; sc, scar. Arrow indicates anterior direction. Scale bar equals 10 mm.

pattern extends for all, but the distal end of the bone, where its robust part expands medially and the laminar portion gets much narrower. The pubic shaft is somewhat bowed anteriorly along its length, but not as much as in *Silesaurus opolensis* (Dzik, 2003). The distal end of the bone slightly expands anteroposteriorly, so that its distal outline is ovoid, with a dorsomedially to ventrolaterally oriented long axis, and medially tapering, where it meets its counterpart. There is no indication of the distal bevel present in a specimen referred to *Lewisuchus admixtus* (CRILAR-Pv 552) and in *Silesaurus opolensis* (Dzik, 2003). In ventral and dorsal views, the outer margin of the pubic shaft is straight, but the reconstruction of the pelvis indicates that the pair was significantly narrower distally compared to its proximal width.

Hindlimb

Femur—Femora of *Asilisaurus kongwe* are well known from the type-locality (Z34) and other nearby localities (e.g., Z29). Both femora are extremely well preserved in NMT RB159 (Fig. 42) and a small specimen (NMT RB169; Fig. 43) referred to *Asilisaurus kongwe* helped understand the ontogenetic pathway the taxon takes (Griffin and Nesbitt, 2016a). A discussion of the muscle scars, their hypothesized muscle attachments, and their variation through ontogeny will not be repeated here given they are thoroughly described in Griffin and Nesbitt (2016a). Here, we provide a detailed description of the femoral anatomy, based on one of the larger and best preserved such elements of the sample, NMT RB159 (Fig. 42).

The proximal surface of the femur has an anteromedially-to-posterolaterally oriented long axis (~45° to the midline) with a deep groove trending in the same direction—a characteristic also present in *Eucoelophysis baldwini* (Ezcurra, 2006), *Sacisaurus agudoensis* (Langer and Ferigolo, 2013), and *Silesaurus opolensis* (Dzik, 2003). A facies articularis antitrochanterica is present on the posteromedial portion of the proximal surface as a rounded and sloped surface that extends distally between the lateral margin and the posteromedial condyle. This feature is also present in most early dinosaurs, *Marasuchus lilloensis*, lagerpetids, a specimen referred to *Lewisuchus admixtus* (CRILAR-PV 552), and pseudosuchians (Nesbitt, 2011), but is absent in the silesaurids *Silesaurus opolensis* (Dzik, 2003) and *Sacisaurus agudoensis* (Langer and Ferigolo, 2013). All three of the proximal tubera are present in *Asilisaurus kongwe* (Nesbitt, 2011). The posteromedial tuber is well developed as a straight ridge oriented proximodistally, situated halfway between the lateral edge and the anteromedial tuber. A concave surface, as observed in proximal view, separates the posteromedial and anteromedial tubera. The anteromedial tuber is equally developed as the posteromedial tuber. A shallow femoral head notch, which separates the anteromedial tuber from the rest of the medial surface, is present distal to the tuber. Proportionally, this notch is located more proximally than in *Silesaurus opolensis* (Dzik, 2003), *Eucoelophysis baldwini* (Ezcurra, 2006; Nesbitt et al., 2007), and *Sacisaurus agudoensis* (Langer and Ferigolo, 2013), but in a similar position as that of a specimen referred to *Lewisuchus admixtus* (CRILAR-PV 552). The medial surface of the head is rounded in proximal view, as in a specimen referred to *Lewisuchus admixtus* (CRILAR-Pv 552), but not straight as in *Silesaurus opolensis* (Dzik, 2003) and

Sacisaurus agudoensis (Langer and Ferigolo, 2013). Furthermore, the medial surface of the femoral head of *Asilisaurus kongwe* is nearly flat in anterolateral view, just like *Silesaurus opolensis* (Dzik, 2003). The anterolateral tuber, the distal extension of which corresponds to the femoral craniomedial crest of Langer and Ferigolo (2013), is continuous with the medial extent of the femoral head, as occurs in a specimen referred to *Lewisuchus admixtus* (CRILAR-Pv 552). This condition differs from the nearly flat condition in *Silesaurus opolensis* (Dzik, 2003), *Eucoelophysis baldwini* (Ezcurra, 2006; Nesbitt et al., 2007), and *Sacisaurus agudoensis* (Langer and Ferigolo, 2013). A small rim of bone marks the transition from the more spongy proximal surface of the bone to its more compact distal surroundings, a condition also found in extremely well preserved femora of *Silesaurus opolensis* (Piechowski et al., 2014) and in a specimen referred to *Lewisuchus admixtus* (CRILAR-Pv 552).

The anterolateral surface of the proximal portion of the femur preserves a number of scars in larger specimens that appear to be variable throughout ontogeny (Griffin and Nesbitt, 2016a). No femur of *Asilisaurus kongwe* preserves a ridge-like or distinct dorsolateral trochanter, a prominent feature in many dinosauriforms (Novas, 1996; Langer and Benton, 2006). Instead, *Asilisaurus kongwe* has a slightly rugose scar marking the homologous position. A large scar, identified as the anterolateral scar in Griffin and Nesbitt (2016a), occupies much of the area between the lateral edge and the anterolateral tuber (Fig. 42). Distal to this scar, a prominent anterior trochanter is present, as in other dinosauriforms (Novas, 1996; Langer and Benton, 2006). The proximodistally striated anterior trochanter has a proximal prominence that is completely attached to the shaft. Posterolaterally, the trochanter is connected to the trochanteric shelf; in some specimens these structures are well separated, whereas in other specimens they are combined (Griffin and Nesbitt, 2016a). Anteromedially, the proximal prominence of the anterior trochanter is connected to a prominent linea intermuscularis cranialis (= anterior intermuscular line). This is heavily striated on its anteromedial edge, defines that anteromedial margin of the femur, and extends distally to the midshaft. A small foramen located lateral to the linea intermuscularis cranialis proximal to the midshaft marks the origin of a second ridge that parallels the linea intermuscularis cranialis for its length, distally. Posterolateral, but connected to the trochanteric shelf, a linea intermuscularis caudalis is present and extends distally to define much of the posterolateral margin of the femur.

The posteromedial side of the proximal portion of the femur bears an anteromedially trending scar (posterior portion of the dorsolateral trochanter of Griffin and Nesbitt, 2016a; Fig. 42) and a prominent fourth trochanter (attachment of *M. caudofemoralis*; Hutchinson, 2001; Griffin and Nesbitt, 2016a). The medial edge of the trochanter varies from crest-like in smaller specimens (NMT RB169; Fig. 43) to rounded and much more massive in larger specimens (NMT RB159; Fig. 42). A large pit with a rugose surface and surrounded by proximodistally oriented bone fibers is present medial to the fourth trochanter. Proximoposteriorly of the fourth trochanter, a scar marks the attachment location for *M. caudofemoralis brevis* and a small scar at the distal portion of the trochanter marks its distolateral protrusion.

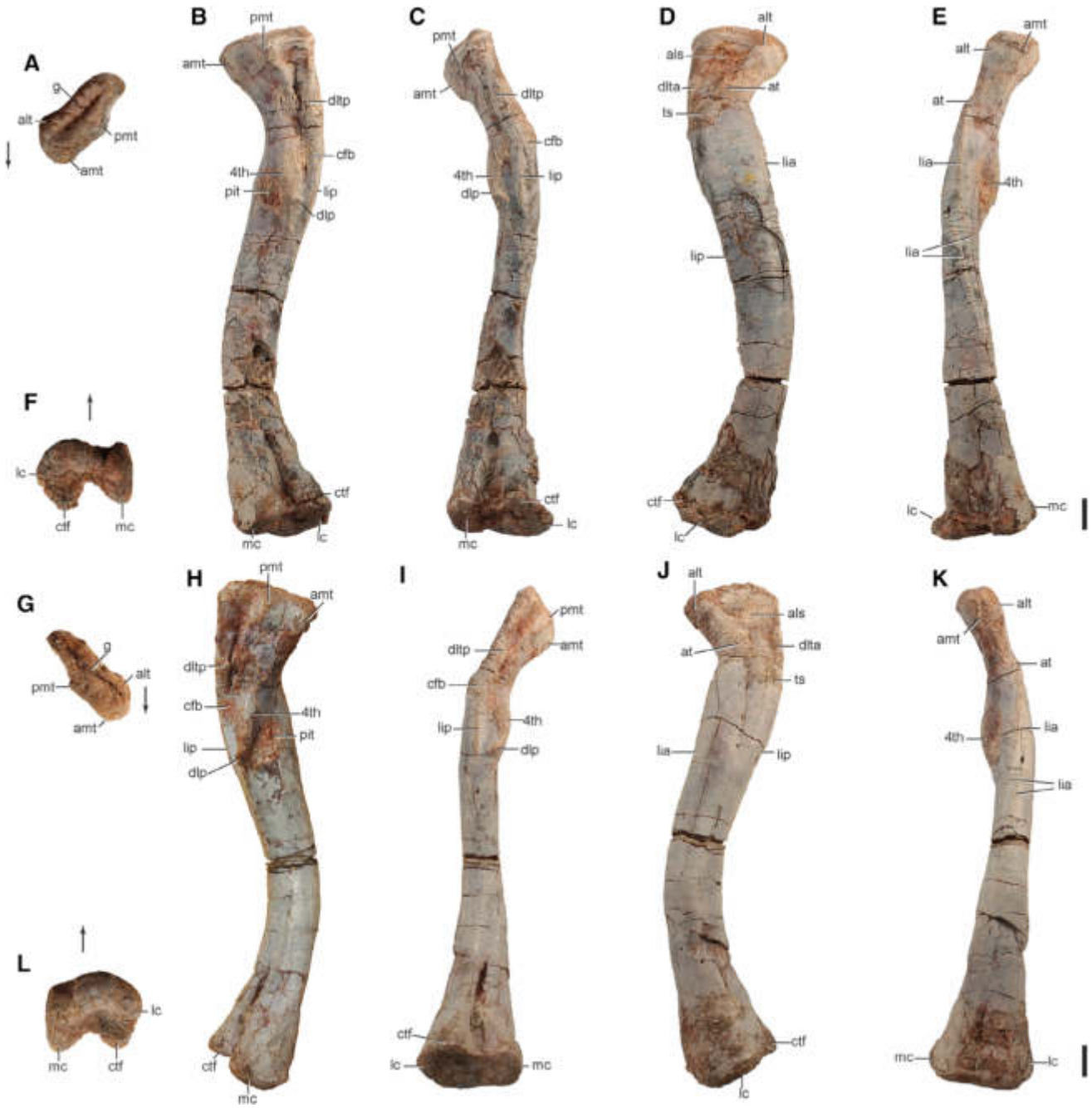


Fig. 42. Femora of an associated skeleton referred to *Asilisaurus kongwe* (NMT RB159). Left femur in proximal (A), posteromedial (B), posterior (C), anterolateral (D), anteromedial (E), and distal (F) views. Right femur in proximal (G), posteromedial (H), posterior (I), anterolateral (J), anteromedial (K), and distal (L) views. Abbreviations: 4th, fourth trochanter; als, anterolateral scar; alt, anterolateral tuber; amt, anteromedial tuber; at, anterior trochanter; cfb, *M. caudofemoralis brevis* insertion scar; ctf, crista tibiofibularis; dlp, distolateral protrusion on the fourth trochanter; dlta, anterior portion of the dorsolateral trochanter; dltp, posterior portion of the dorsolateral trochanter; g, groove; lc, lateral condyle; lia, linea intermuscularis cranialis; lip, linea intermuscularis caudalis; mc, medial condyle; pit, pit; pmt, posteromedial tuber; ts, trochanteric shelf. Arrows indicate anterior direction. Scale bars equal 10 mm.

The distal end of the femur bears weakly expanded distal condyles relative to the shaft. Posteriorly, the crista tibiofibularis and the medial condyle are separated by a well-defined popliteal fossa that is deepest distally and shallows proximally. The slight division between the condyles extends nearly to midshaft in NMT RB159 (Fig. 42),

but tracing this feature proximally requires excellent surface preservation. Near the distal end of the popliteal fossa, a muscle scar slightly constricts the subparallel sides of the fossa. The medial side of the medial condyle possesses a distinct proximodistally oriented scar similar to that of other avemetatarsalians (Nesbitt et al., 2017,

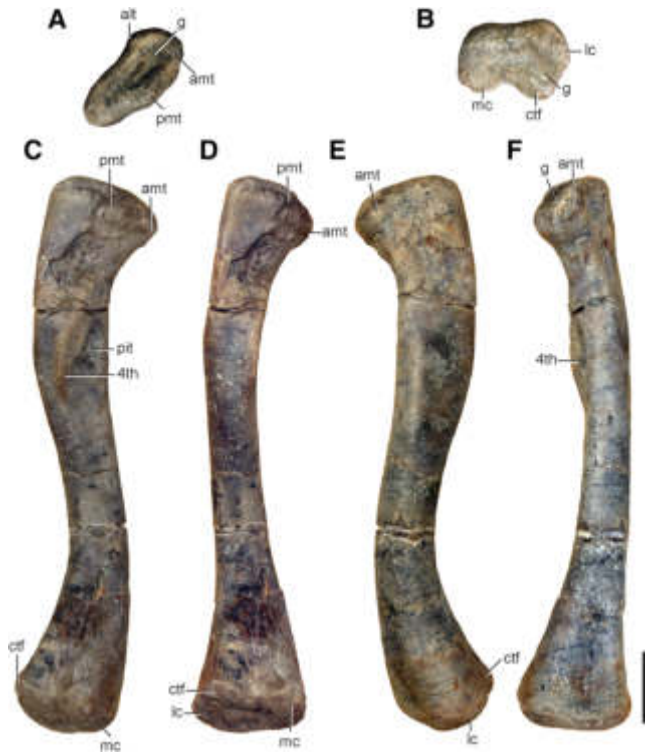


Fig. 43. Small left femur referred to *Asilisaurus kongwe* (NMT RB169) in proximal (A), distal (B), posteromedial (C), posterior (D), anterolateral (E), and anteromedial (F) views. Abbreviations: 4th, fourth trochanter; alt, anterolateral tuber; amt, anteromedial tuber; ctf, crista tibiofibularis; g, groove; lc, lateral condyle; mc, medial condyle; pit, pit; pmt, posteromedial tuber. Scale bar equals 10 mm.

2018). However, the distinction between the medial surface and the scar is not marked by a rim of bone in some of the larger specimens assigned to *Asilisaurus kongwe* (NMT RB159, Fig. 42). The anterior surface of the distal end bears a prominent scar located on the anterolateral side similar to that of other dinosauriforms. In lateral view, there is nearly no distinction between the lateral condyle and the poorly expanded crista tibiofibularis. Similarly, in distal view, the crista tibiofibularis is poorly separated from the lateral condyle of the femur and only a slight depression or broad groove set the two apart. A large depression is present on the distal surface of the femur that, like the proximal surface, is composed of spongy bone. In distal view, the crista tibiofibularis tapers posteriorly, whereas the medial condyle tapers posteromedially.

Tibia—The tibia of *Asilisaurus kongwe* is well represented in the sample from the holotype locality (NMT RB20, NMT RB132; NMT RB50; Fig. 44) and in the well preserved individual (NMT RB159; Figs. 45 and 46), which includes the complete left element and the proximal and distal ends of the right element. The proximal surface is triangular with a clear anteriorly directed cnemial crest separated from the posterior condyles by a small gap on the lateral edge. The cnemial crest, like that of all non-saurischian dinosauriforms (Irmis et al., 2007a; Nesbitt et al., 2010; Nesbitt, 2011; Baron et al., 2017), is straight anteriorly in proximal view. The proximal surface is irregular and none of the specimens have identical

morphologies; small grooves forms an anastomosing pattern across the surface. The cnemial crest lies on the same transverse plane as the rest of the proximal surface. The posterior half of the proximal surface is subdivided into two condyles, one lateral and one more posterior and medial. The proximal surface of the medial condyle slopes anterodorsally, whereas the lateral condyle is more convex and its proximal surface is depressed further distally than that of the medial condyle in posterior view. Both condyles are equal in size and a small gap divides them at the posterolateral edge of the proximal end. The lateral condyle is located more anteriorly than the medial, as in other non-dinosaur dinosauriforms (*Marasuchus lilloensis*, Sereno and Arcucci, 1994b; a specimen referred to *Lewisuchus admixtus*, CRILAR-Pv 552), sauropodomorphs (*Saturnalia tupiniquim* MCP 3845-PV), ornithischians (e.g., *Lesothosaurus diagnosticus*, NHMUK PV RU B17; Baron et al., 2016). This is contrast to the condition in neotheropods where the two condyles are located at the posterior margin (Langer and Benton, 2006).

In medial view, the proximal edge is slightly convex and a slight, medially expanded rim marks this surface. The proximal portion bears a number of scars on its medial surface. In NMT RB159, a scar formed by proximodistally oriented grooves extends from the anterior extent of the cnemial crest posteriorly to its maximum posterior expansion 13 mm distal to the proximal surface, in the anteroposterior middle of the medial surface (Fig. 45). This scar, which extends 23 mm distally from the proximal surface of the cnemial crest also occurs in *Silesaurus opolensis* (ZPAL Ab III/361/22), some sauropodomorphs (e.g., *Saturnalia tupiniquim* MCP 3845-PV), neotheropods (e.g., *Megapnosaurus rhodesiensis*; Griffin, 2018), and a specimen referred to *Lewisuchus admixtus* (CRILAR-Pv 552), and have been attributed to the insertion of the

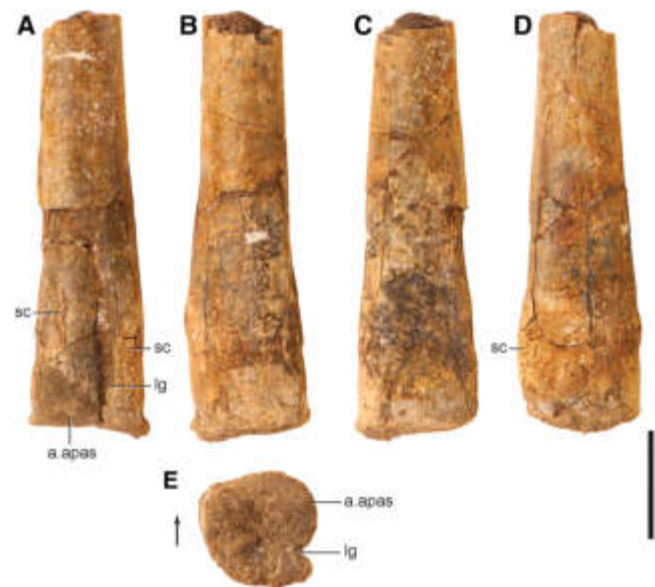


Fig. 44. Distal end of a left tibia (NMT RB850) referred to *Asilisaurus kongwe* from the holotype locality in lateral (A), anterior (B), medial (C), posterior (D), and distal (E) views. Abbreviations: a, articulates with; apas, ascending process of the astragalus; lg, lateral groove; sc, scar. Arrow indicates anterior direction. Scale bar equals 10 mm.



Fig. 45. Left tibia of an associated skeleton referred to *Asilisaurus kongwe* (NMT RB159) in proximal (A), lateral (B), anterior (C), medial (D), posterior (E), and distal (F) views. Abbreviations: a., articulates with; apas, ascending process of the astragalus; cc, cnemial crest; lc, lateral condyle; lg, lateral groove; mc, medial condyle; sc, scar. Arrows indicate anterior directions. Scale bar equals 10 mm.

triceps femoris muscle group (Carrano and Hutchinson, 2002; Griffin, 2018). A second scar extends anterodistally from the posteroproximal corner of the medial side for 16 mm as a striated ridge until it nearly touches the previous scar. This scar has also been reported in *Coelophysis bauri* and *Megapnosaurus rhodesiensis* (Griffin, 2018) and was hypothesized to be the insertion of *M. flexor tibialis*

internus 3, (FTI3; = avian *M. flexor cruris medialis*) and *M. flexor tibialis externus* (FTE; = avian *M. flexor cruris lateralis pars pelvica*) in neotheropods (Carrano and Hutchinson, 2002; Griffin, 2018). Both scars of the medial surface of the tibia appear to be absent in smaller specimens of *Asilisaurus kongwe* (e.g., NMT RB50; Fig. 44) and the absence/presence of these scars has been correlated with ontogeny in neotheropod dinosaurs (Griffin and Nesbitt, 2016b; Griffin, 2018). Just distal to the two scars, a faint proximodistally elongated rugose ridge is present in the medial surface of the tibia. A similar ridge is also present in *Sacisaurus agudoensis* (MCN PV10020; Langer and Ferigolo, 2013) and has been hypothesized to be the origin of *M. tibialis* anterior in theropods (Carrano and Hutchinson, 2002).

In posterolateral view, the condyles slightly overhang the shaft. Just distal to this overhang, the surface is concave with a few proximodistally oriented grooves. The lateral surface of the proximal end bears a large scar ventral to the cnemial crest and extending posteriorly to the anterior margin of the lateral condyle. The scar consists of proximodistally oriented ridges that lie in the lateral gap between the cnemial crest and the lateral condyle, extending distally for 17 mm to terminate in a rounded, more distinct tuberosity. This scar is in the same position as the proximodistally oriented scar of a specimen referred to *Lewisuchus admixtus* (CRILAR-Pv 552), *Silesaurus opolensis* (ZPAL Ab III/361/22), and *Sacisaurus agudoensis* (MCN PV10020; Langer and Ferigolo, 2013), but is far less distally expanded and more rounded. Distal to this scar, there is a proximally opening foramen that measures

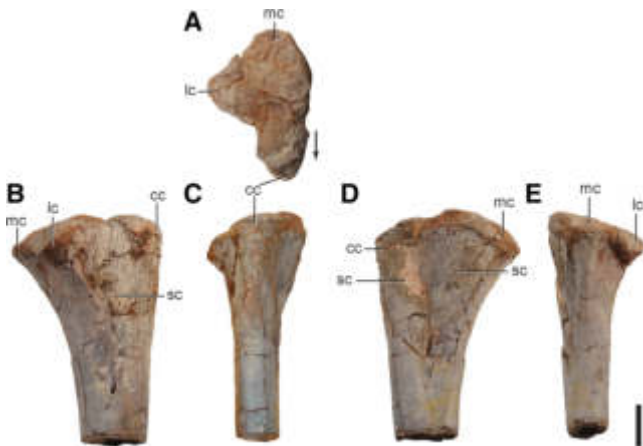


Fig. 46. Partial right tibia of an associated skeleton referred to *Asilisaurus kongwe* (NMT RB159) in proximal (A), lateral (B), anterior (C), medial (D), and posterior (E), views. Abbreviations: cc, cnemial crest; lc, lateral condyle; mc, medial condyle; sc, scar. Arrow indicates anterior direction. Scale bar equals 10 mm.

2 mm wide, a common feature of dinosauriforms (e.g., *Sacisaurus agudoensis*, MCN PV10020; Fig. 18d, Langer and Ferigolo, 2013; *Saturnalia tupiniquim*, MCP 3845-PV). However, in *Asilisaurus kongwe*, this foramen appears to be proportionally larger.

The tibial shaft is smooth, nearly straight, and ovoid in cross section (longer anteroposteriorly than mediolaterally) throughout its length. The distal surface is exceptionally well preserved in NMT RB159. In posterior view, the lateral process has a straight and slightly rugose lateral margin and the proximal part of the process terminates in a small point where it integrates with the rest of the shaft. The lateral process does not expand more laterally than the lateral surface that articulates with the ascending process of the astragalus. This short process of *Asilisaurus kongwe* differs from the much more laterally expanded process of sauropodomorphs (*Saturnalia tupiniquim* MCP 3845-PV), neotheropods (*Coelophysis bauri*, Colbert, 1989), ornithischians (*Lesothosaurus diagnosticus*, NHMUK PV RU B17), and most silesaurids (*Silesaurus opolensis*, Dzik, 2003; *Sacisaurus agudoensis*, Langer and Ferigolo, 2013). It is, instead, more similar to the short process of *Marasuchus lilloensis* (Serenó and Arcucci, 1994b) and a specimen referred to *Pseudolagosuchus major* (PULR 53). The posteromedial margin of the tibia bears a faint proximodistally trending and rounded ridge that also occurs in *Silesaurus opolensis* (Ab III 361/22) and as a more distinct ridge in saurischians (the sauropodomorph *Saturnalia tupiniquim* MCP 3845-PV and neotheropod *Coelophysis bauri*, Colbert, 1989). The ridge in *Asilisaurus kongwe* and *Silesaurus opolensis* is faint, but can be observed in distal view (Figs. 45 and 46).

The medial and anteromedial portion of the distal end bears a slightly rugose scar and, at the anterior surface of the bone, the scar turns proximally to form a thin proximodistally oriented ridge. In lateral view, a proximodistally oriented groove, a common feature of dinosauriforms (Novas, 1996; Nesbitt, 2011), divides the lateral process (posteriorly) from the facet that articulates with the ascending process of the astragalus. The proximodistally oriented lateral groove is better defined distally, but continues proximally as a broad depression. A small rim defines the lateral margin of the facet that articulates with the ascending process of the astragalus. Proximal to this rim, a rugose surface narrows to a series of small tubercles.

In distal view, the tibial surface is generally rounded with a notch on the lateral side that corresponds to the distal expression of the lateral groove. Overall, the surface is flat with small anastomoses of ridges and its anterolateral portion is proximally deflected for the articulation with the ascending process of the astragalus. The lack of differentiation of the distal surface of the tibia in *Asilisaurus kongwe* is similar to the condition seen in a specimen referred to *Lewisuchus admixtus* (CRILAR-PV 552) and in *Teleocrater rhadinus* (Nesbitt et al., 2017, 2018), and contrasts to the much more complex distal surface of the tibia of dinosaurs (Langer and Benton, 2006), *Silesaurus opolensis* (Ab III/361/22), *Sacisaurus agudoensis* (Langer and Ferigolo, 2013), and lagerpetids (Irmis et al., 2007a; Nesbitt et al., 2009a).

Fibula—Both proximal (NMT RB851; Fig. 47) and distal fibular ends are known from the holotype locality, whereas a complete left and nearly complete right element is preserved in NMT RB159 (Fig. 48). The fibula is



Fig. 47. Proximal end of a left fibula (NMT RB851) referred to *Asilisaurus kongwe* from the holotype locality in proximal (A), lateral (B), anterior (C), medial (D) and posterior (E) views. Abbreviations: sc, scar. Arrow indicates anterior direction. Scale bar equals 10 mm.

less robust than the tibia and bears anteroposteriorly expanded proximal and distal ends. In lateral view, the shaft is sigmoidal, but not to the extent apparent in Fig. 48; the kink near the distal third appears to be the result of preservation. The long axis of the proximal surface is anteroposteriorly oriented and is set at $\sim 30^\circ$ to the anteromedially to posterolaterally oriented long axis of the distal surface.

The proximal end of the fibula is exceptionally preserved in both sides of NMT RB159. In proximal view, the posterior edge is rounded and broader than the anterior edge, like that in *Silesaurus opolensis* (ZPAL Ab III/361/24) and *Saturnalia tupiniquim* (MCP 3845-PV). The anterior edge tapers and curls medially, as in other dinosauriforms (Nesbitt, 2011). In lateral view, the proximal surface reaches its greatest height near the anterior edge and is slightly concave between its anterior and posterior edges, as in the aphanosaur *Teleocrater rhadinus* (Nesbitt et al., 2018), the silesaurid *Silesaurus opolensis* (ZPAL Ab III/361/24), and the sauropodomorph *Saturnalia tupiniquim* (MCP 3845-PV). In lateral view, the proximal portion of the bone is distinctly asymmetrical, with the anterior edge bowing anteriorly at a rugose scar (Figs. 47 and 48) and the posterior edge gently concave in profile. The scar on the anterior edge nearly touches the proximal surface, whereas the same scar is more distally positioned in the sauropodomorph *Saturnalia tupiniquim* (MCP 3845-PV). The lateral surface of the fibula of *Asilisaurus kongwe* is gently concave anteroposteriorly and smooth in all known specimens, whereas a distinct, circular scar is present in *Silesaurus opolensis* (ZPAL Ab III 361/24). Medially, a rugose anterodistally trending scar connects the posteroproximal corner of the fibula with the distal end of the scar present on the anterior edge (Fig. 48). This robust scar, measuring 11 mm in length, is also present in *Silesaurus opolensis* (ZPAL Ab III 361/24) and may be homologous to the proximal portion of the much more distally expanded scar of *Saturnalia tupiniquim* (MCP 3845-PV).

The lateral surface of the fibular shaft bears a long, strap-like iliofibularis crest that originates near the anterior edge of the bone and extends posterodistally to near

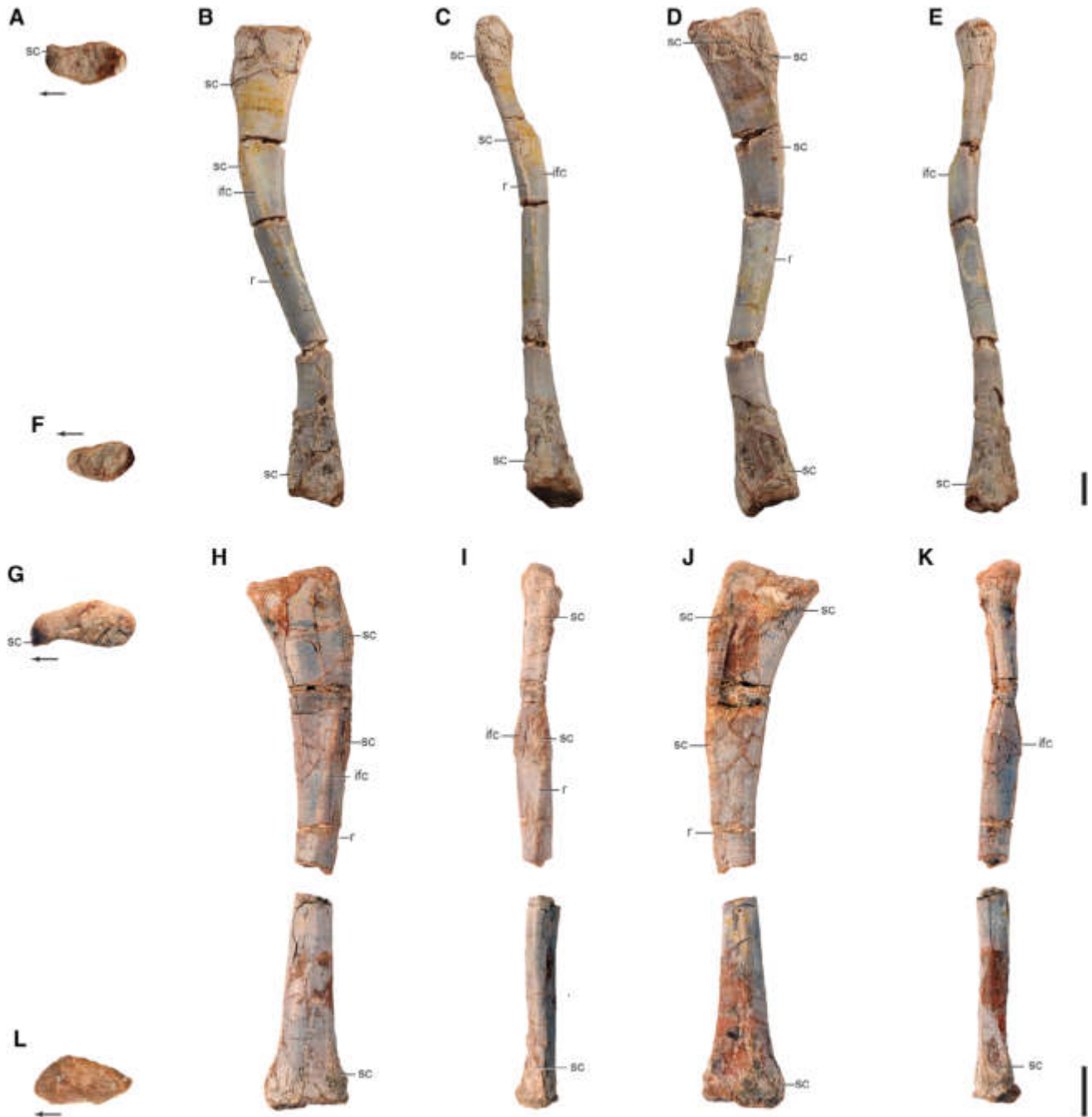


Fig. 48. Fibulae of a partial skeleton referred to *Asilisaurus kongwe* (NMT RB159). Left fibula in proximal (A), lateral (B), anterior (C), medial (D), posterior (E), and distal (F) views. Right fibula in proximal (G), lateral (H), anterior (I), medial (J), posterior (K), and distal (L) views. Abbreviations: ifc, iliofibularis crest; r, ridge; sc, scar. Arrows indicate anterior direction. Scale bars equal 10 mm.

its midshaft. Its length and overall morphology is similar to that of *Teleocrater rhadinus* (Nesbitt et al., 2018), a specimen referred to *Lewisuchus admixtus* (CRILAR-Pv 552), *Silesaurus opolensis* (Dzik, 2003), and the sauropodomorph *Saturnalia tupiniquim* (MCP 3845-PV). However, the more proximal portion of the crest of *Asilisaurus kongwe* (NMT RB 159) is more rugose and sharp than that of the aforementioned taxa. Anterior to the proximal end of the iliofibularis crest, a rugose area

wraps around the anterior edge and extends onto the medial surface. This extension of the iliofibularis crest is also present in *Teleocrater rhadinus* (Nesbitt et al., 2018) and the sauropodomorph *Saturnalia tupiniquim* (MCP 3845-PV). Most of the anterior edge of the fibula is sharp, as in *Teleocrater rhadinus* (Nesbitt et al., 2017, 2018), whereas the posterior margin is rounded. Therefore, the midshaft is oval in cross section, with a slightly longer anteroposterior axis.

The distal end of the fibula expands anteromedially and posterolaterally. In anterolateral view, the posterolateral portion extends further distally, resulting in a distinctly asymmetric profile as in most archosaurs, including pseudosuchians (Nesbitt, 2011), *Teleocrater rhadinus* (Nesbitt et al., 2018), the dinosauriform *Marasuchus lilloensis* (Sereno and Arcucci, 1994b), and dinosaurs (*Saturnalia tupiniquim*, MCP 3846-PV). The anteromedial edge has a proximodistally aligned depression framed by parallel ridges. A similar scar is seen in *Saturnalia tupiniquim* (MCP 3846-PV), but it is positioned more medially than that of *Asilisaurus kongwe*. In distal view, the fibula is oval with a longer anteromedial-posterolateral axis.

Calcaneum—The calcaneum is represented by a left element from NMT RB159 (Fig. 49A–F), an isolated right element from the holotype locality (NMT RB18; Fig. 49G–L), and from many disarticulated examples from Z90 (see Sidor and Nesbitt, 2018). The triangular bone articulates with the fibula proximally, the astragalus medially (Fig. 50), and the 4th tarsal distally. The articulation with the fibula is also triangular with an anteroposteriorly straight medial edge. This proximally elevated surface is largely convex, with a small concave portion at the posterior edge. Such a largely convex articulation is also present in stem archosaurs, pseudosuchians, the aphanosaur *Teleocrater rhadinus* (Nesbitt et al., 2017, 2018), and possibly in *Marasuchus lilloensis* (PVL 3870; Sereno and Arcucci, 1994b). In *Silesaurus opolensis* (ZPAL Ab III 361/20) and dinosaurs (*Saturnalia tupiniquim*, MCP PV 3845; *Herrerasaurus ischigualastensis*, PVSJ 373), on the contrary, the surface for articulation with the fibula is concave (Sereno, 1991; Nesbitt, 2011). The articulation surface with the fibula is well separated from the rest of the calcaneum, including the calcaneum tuber at the posterolateral margin, by a steep margin (Fig. 49A, G). A similar separation is present in *Teleocrater rhadinus* (Nesbitt et al., 2017, 2018), but in *Saturnalia tupiniquim* (MCP PV 3845) and *Herrerasaurus ischigualastensis*, PVSJ 373, this articulation surface is separated from the tuber by a rim of bone. There is no separation between the fibular articulation and the posterolateral tuber in *Silesaurus opolensis* (ZPAL Ab III 361/20) and neotheropods (e.g., *Liliensternus liliensterni*, MB R. 2175). The posterolateral portion of the calcaneum tapers to a proximally expanded tuber that is connected to the articular surface with the fibula by means of a ridge on the lateral side. A similar tuber is present in stem archosaurs (e.g., *Euparkeria capensis*, Sereno, 1991), pseudosuchians (Sereno, 1991; Parrish, 1993; Juul, 1994; Benton, 1999; Brusatte et al., 2010a, 2010b; Nesbitt, 2011; Ezcurra, 2016), *Saturnalia tupiniquim* (MCP PV 3845), and *Herrerasaurus ischigualastensis* (PVSJ 373), but almost completely lost in *Silesaurus opolensis* (ZPAL Ab III/361/20) and completely lost in neotheropods (e.g., *Liliensternus liliensterni*, MB R. 2175). As in *Saturnalia tupiniquim* (MCP PV 3845), the tapering medial process of the calcaneum of *Asilisaurus kongwe* lies ventral to the posterolateral process of the astragalus.

The anterolateral surface bears a non-articular, large, and oval fossa (Fig. 49D, J). Anterior to this, the non-articular surface wraps around the anterior end of the calcaneum. This surface aligns with the shelf on the lateral surface of the proximal part of the astragalus when the two elements are articulated (Fig. 50). In contrast, the anteriormost extension of the calcaneum tapers without a non-articular surface in dinosaurs (e.g., *Saturnalia tupiniquim*, MCP PV 3845). The lateral side of the tuber is slightly rugose and this wraps

around the tuber posteriorly and medially. The medial surface of the calcaneum precisely articulates with the distolateral surface of the astragalus. A concave surface, longer anterolaterally-posteromedially than proximodistally, stretches from the anteriormost edge of the calcaneum to the medialmost edge of the medial process. A similar concave facet is present in *Teleocrater rhadinus* and hypothesized to be homologous to the concave surface of pseudosuchians (Nesbitt et al., 2017, 2018).

Distally, the triangular calcaneum bears a large, well define articular surface for the 4th distal tarsal (Fig. 49B, H). This surface, which is concave in the center of the bone with a convex rim defining the rest of the articulation, extends on the medial process, but not onto the posterolateral tuber. The posterior portion of the calcaneum is rounded and gradually tapers toward the tuber.

Astragalus—The astragalus is well represented in *Asilisaurus kongwe*; left and right examples are preserved in NMT RB159 (Fig. 51A–F)), well preserved examples are known from the holotype locality (NMT RB17, NMT RB138; Fig. 51G–L) and from Z90. The astragalus is the largest of the tarsals and was instrumental in identifying *Asilisaurus kongwe* as a dinosauriform (Nesbitt et al., 2010).

In proximal view, the astragalus has two articulation facets, a tibial facet that occupies the medial $\frac{3}{4}$ of the mediolateral length and a fibular facet that occupies the lateral $\frac{1}{4}$. The oval tibial articulation surface is simply concave with a rounded rim that surrounds much of the surface. This simple morphology contrasts with that of most dinosauriforms (e.g., *Saturnalia tupiniquim*, MCP PV 3845; *Coelophysis bauri*, Nesbitt et al., 2007), in which the facet is much wider mediolaterally than anteroposteriorly long. Laterally, this concave articular surface with the tibia expands proximally to form a short anterior ascending process, similar to that of a specimen referred to *Pseudolagosuchus major* (PVL 3454). The anterior ascending process tapers laterally to a thin anterodorsally straight margin that would have contacted the fibula. The ascending process defines the lateral rim of the tibial facet and lies between an anterior foramen and a larger posterior foramen. The ascending process is anteroposteriorly longer than that of all other comparative dinosauriforms, in which it occupies only the anterior half of the facet (e.g., *Silesaurus opolensis*, ZPAL Ab III/361/20; *Saturnalia tupiniquim*, MCP PV 3845). The proximal surface of the ascending process is nearly flat with a slight anterodistal slant, contrasting with the much more anterodistally slanted proximal surfaces present in *Silesaurus opolensis* (ZPAL Ab III/361/20), *Marasuchus lilloensis* (PVL 3870), and dinosaurs (*Saturnalia tupiniquim*, MCP PV 3845; *Herrerasaurus ischigualastensis*, PVSJ 373). A fossa with an anterodistally directed foramen excavates the posterior portion of the ascending process of *Asilisaurus kongwe*. This fossa/foramen is much deeper in the larger (NMT RB138) than in the smaller specimens (e.g., NMT RB 159). The area of this fossa is typically occupied by the articular surface for the posterolateral process of the tibia, as in *Silesaurus opolensis* (ZPAL Ab III 361/20) and dinosaurs (*Saturnalia tupiniquim*, MCP PV 3845; *Herrerasaurus ischigualastensis*, Novas, 1994; *Scutellosaurus lawleri*, MNA V175; *Tawa hallae*, GR 242). The lack of this articulation surface in *Asilisaurus kongwe* matches the lack of a laterally projected posterolateral process. An overall similar condition, with a non-articular area and a foramen, may be present in *Marasuchus lilloensis* (PVL 3870), but

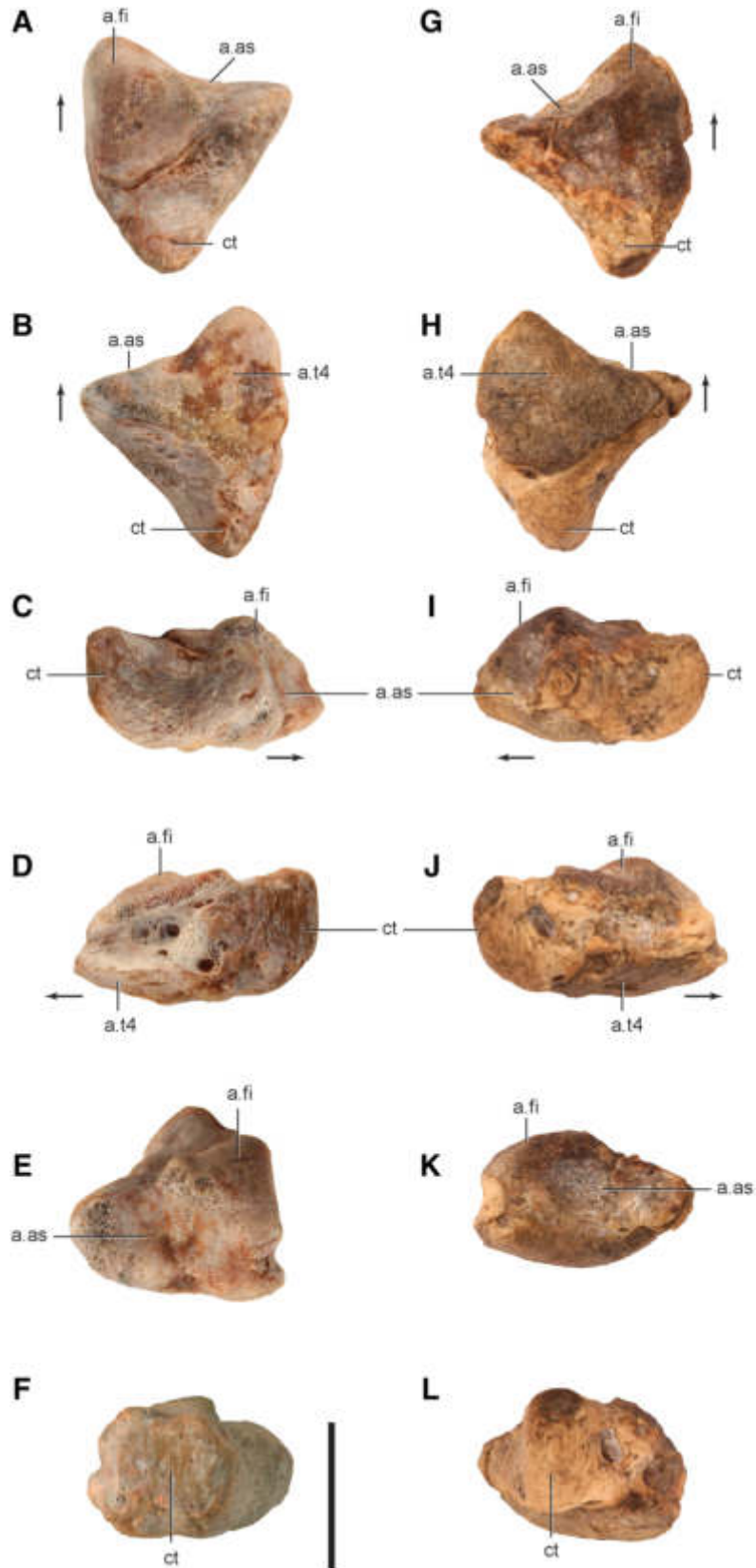


Fig. 49. Calcanea referred to *Asilisaurus kongwe*. Left calcaneum of an associated skeleton referred to *Asilisaurus kongwe* (NMT RB159) in proximal (A), distal (B), medial (C), lateral (D), anterior (E), and posterior (F) views. Right calcaneum (NMT RB18) from the holotype locality in proximal (G), distal (H), medial (I), lateral (J), anterior (K), and posterior (L) views. Abbreviations: a., articulates with; as, astragalus; ct, calcaneum tuber; fi, fibula; t4, tarsal 4. Arrows indicate anterior direction. Scale bar equals 10 mm in A–F and 5 mm in G–L.



Fig. 50. Rearticulated left proximal tarsals of a partial skeleton referred to *Asilisaurus kongwe* (NMT RB159). Abbreviations: as, astragalus; cal, calcaneum. Arrow indicates anterior direction. Scale bar equals 10 mm.

the corresponding surface is incompletely preserved (Sereno, 1991; Sereno and Arcucci, 1994b). The fibular articulation surface is concave, its medial border contacting the ascending process. A small rim of bone separates that articular surface from the posterior foramen. The posterolateral portion of that surface is blunt in some specimens (NMT RB159), but pointed in others (NMT RB138) as in the sauropodomorph *Saturnalia tupiniquim* (MCP PV 3845). The anterolateral corner of the astragalus is rounded and not laterally projected, with a small process, as in *Marasuchus lilloensis* (PVL 3870). A small gap, which corresponds to part of the articulation surface for the calcaneum, lies between the anterior and posterior parts of the lateral edge, as typical of dinosaurs such as *Saturnalia tupiniquim* (MCP PV 3845). However, the gap is located more posteriorly in *Asilisaurus kongwe*, and not at the anteroposterior middle as in dinosaurs (*Saturnalia tupiniquim*, MCP PV 3845; *Herrerasaurus ischigualastensis*, PVSJ 373). This gap is absent in the astragalus of *Silesaurus opolensis* (ZPAL Ab III/361/20), the lateral margin of which is straight.

In proximal view, the anterior margin of the astragalus is nearly straight in *Asilisaurus kongwe* (Fig. 51B, H), as in *Silesaurus opolensis* (ZPAL Ab III/361/20), whereas this margin is more sigmoidal in dinosaurs such as *Saturnalia tupiniquim* (MCP PV 3845). The posterior margin is sigmoidal and bears a gap that represented the proximal expression of the posterior groove. The posteromedial corner is gently rounded in proximal view. The anteromedial corner of the tibial articular surface forms an angle of $\sim 90^\circ$, whereas the more distal portion of this corner changes to an acute angle like that of other dinosauromorphs (Sereno, 1991).

A small shelf is present on the anterolateral margin of the astragalus, extending from the anterior foramen to the lateral margin of the element (Fig. 51A, G). This shelf also appears to be present in *Marasuchus lilloensis* (PVL 3870), but is absent in *Silesaurus opolensis* (ZPAL Ab III/361/20) and dinosaurs (*Herrerasaurus ischigualastensis*, PVSJ 373; *Saturnalia tupiniquim* MCP PV 3845). The margin proximal to the shelf, which defines the anterior edge of articulation surface with the calcaneum, is sharp.

In anterior view, the astragalus is much wider mediolaterally than proximodistally high (Fig. 51A, G). A mediolaterally oriented, weakly developed groove transects much of the anterior surface as in lagerpetids

(*Dromomeron romeri*, Nesbitt et al., 2009a), *Marasuchus lilloensis* (PVL 3870), and dinosaurs (e.g., *Coelophysis bauri*, Colbert, 1989). The distal portion of the antero-medial corner tapers to a rounded prominence as in other dinosauromorphs (Sereno, 1991). The medial margin of the bone is rounded in proximal view and this rounded surface continues on the posterior surface, as in *Silesaurus opolensis* (ZPAL Ab III/361/20). In contrast, the medial margin of the astragalus is relatively flat in dinosaurs (*Herrerasaurus ischigualastensis*, PVSJ 373; *Saturnalia tupiniquim* MCP PV 3845; *Liliensternus liliensterni*, MB R. 2175). Small parallel ridges decorate the medial surface of the astragalus in *Asilisaurus kongwe*. In posterior view, the posterior surface is rounded and curls distally to the ventral surface (Fig. 51C, I). The lateral side bears a well defined, but shallow groove that is tentatively homologized with the “posterior groove” (*sensu* Sereno, 1991) of some dinosauromorphs, pseudosuchians, and stem-archosaurs (Nesbitt, 2011). The groove in *Asilisaurus kongwe* wraps around a posterolateral process and continues proximally to the posterior foramen/fossa. The proximal half of the lateral surface bears the articulation for the fibula, whereas its distal half bears the articulation surface for the calcaneum. The latter surface is rounded, creating a convex-concave articulation between the astragalus and the calcaneum, as suggested for *Teleocrater rhadinus* (Nesbitt et al., 2017, 2018), a specimen referred to *Pseudolagosuchus majori* (PVL 3454), and pseudosuchians (Sereno, 1991; Brusatte et al., 2010a, 2010b; Nesbitt, 2011). This convex-concave articulation is, however, lost in *Silesaurus opolensis* (ZPAL Ab III 361/20) and dinosaurs (*Herrerasaurus ischigualastensis*, PVSJ 373; *Saturnalia tupiniquim* MCP PV 3845; *Liliensternus liliensterni*, MB R. 2175).

The distal surface of the astragalus is generally rounded with a low transverse ridge that originates at the articulation with the calcaneum laterally and trends posteromedially (Fig. 51D, J). A parallel groove is present posterior to this low ridge.

Distal Tarsal 4—The fourth distal tarsal is preserved in both sides of NMT RB159 (Fig. 52) and from isolated examples from locality Z90. Its proximal surface is wider anteriorly than posteriorly and much of the anterior half of the surface is flat (Fig. 52A). Posteriorly, the surface slightly expands proximally to form a rounded peak, which is equivalent to the “heel” (*sensu* Sereno and Arcucci, 1994a, 1994b) present in *Lagerpeton chanarensis* (PVL 4619), *Marasuchus lilloensis* (PVL 3870), and possibly in dinosaurs (*Saturnalia tupiniquim*, MCP 3845-PV). In proximal view, the medial surface is nearly flat and lacks the medial projection present in dinosaurs (*Saturnalia tupiniquim*, MCP 3845-PV). The flat medial surface would have likely articulated with the third distal tarsal (Fig. 52D), but this element was not preserved in any specimen. The medial and lateral surfaces of the fourth distal tarsal project distally to form a rounded expansion. Posteriorly, the medial surface expands distally as in *Lagerpeton chanarensis* (PVL 4619). The posterior surface is rounded and taller proximodistally than mediolaterally wide, whereas the anterior surface is wider mediolaterally than proximodistally. The lateral surface bears a large articular facet for metatarsal V, which covers most of the anterior half and ventral portion of that surface (Fig. 52C). Such large facet is more similar to that of pseudosuchians (Nesbitt, 2011) and contrasts with the

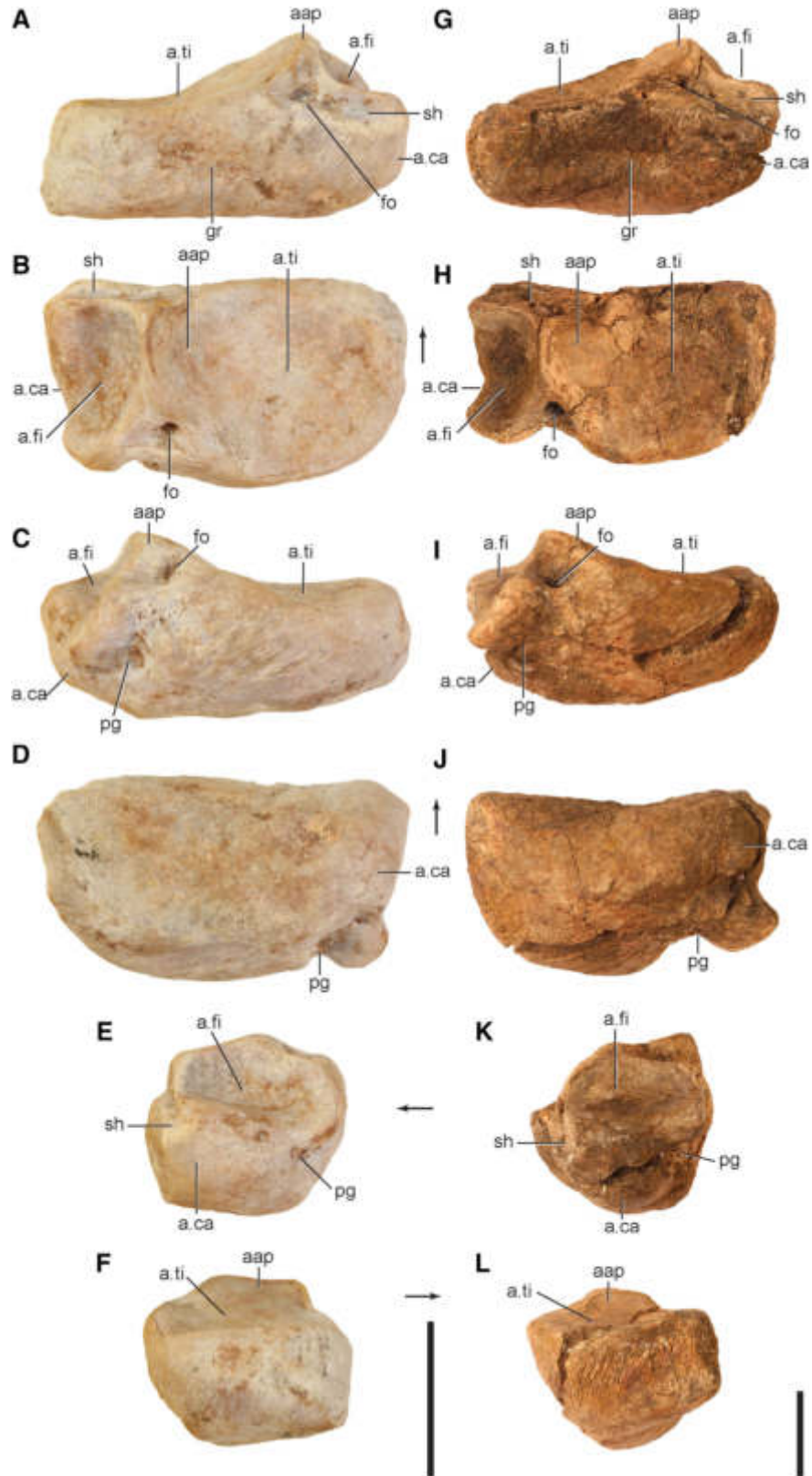


Fig. 51. Astragali referred to *Asilisaurus kongwe*. Left astragalus of an associated skeleton referred to *Asilisaurus kongwe* (NMT RB159) in anterior (A), proximal (B), posterior (C), ventral (D), lateral (E), and medial (F) views. Left astragalus (NMT RB138) from the holotype locality in anterior (G), proximal (H), posterior (I), ventral (J), lateral (K), and medial (L) views. Abbreviations: a., articulates with; aap, anterior ascending process; ca, calcaneum; fi, fibula; fo, foramen; gr, groove; pg, posterior groove; sh, shelf; ti, tibia. Arrows indicate anterior direction. Scale bars equal 10 mm.

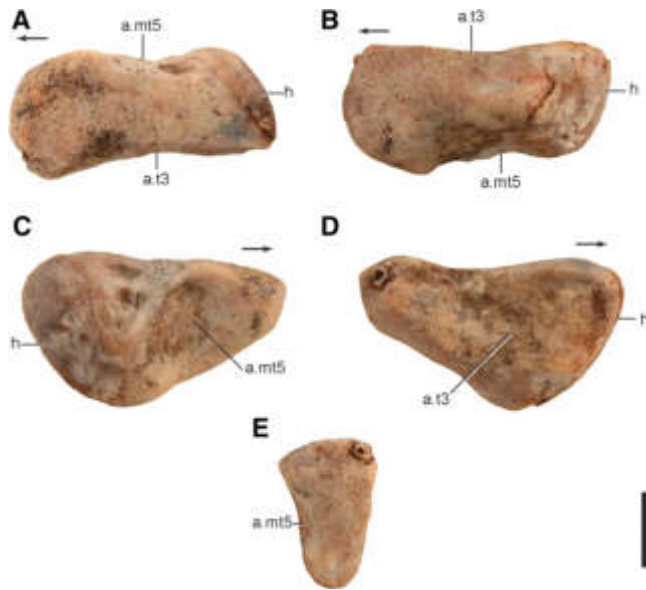


Fig. 52. Right tarsal 4 of an associated skeleton referred to *Asilisaurus kongwe* (NMT RB159) in proximal (A), distal (B), lateral (C), medial (D), and anterior (E) views. Abbreviations: a., articulates with; h, heel; mt5, metatarsal 5; t3, tarsal 3. Arrows indicate anterior direction. Scale bar equals 10 mm.

much smaller facet typical for dinosauromorphs (*Lagerpeton chanarensis*, PVL 4619; *Saturnalia tupiniquim*, MCP 3845-PV; Sereno, 1991). In addition, the articular facet is concave laterally and a small rim sets it apart from the rest of the lateral surface. Proximoposterior of the facet, a few small foramina are present in a non-articular surface.

Metatarsals—The metatarsals of *Asilisaurus kongwe* are largely represented by the complete right series (Fig. 53) and the partial left pes of NMT RB159 and the following description is supplemented by isolated elements from the holotype locality (Fig. 54). The length of the metatarsals increases toward metatarsal III from I to III and from V to III; metatarsal III is the longest (Table 1). Proximally, the surfaces are imbricated, where the long axes of metatarsals I-IV are directed posteromedially as in the sauropodomorph *Saturnalia tupiniquim* (Langer, 2003; MCP 3845-PV). Metatarsal III is ~48% the length of the tibia. Overall, the length of metatarsals II-IV versus the proximal and distal widths is less than that observed in *Silesaurus opolensis* (ZPAL Ab III/361/19); thus, *Asilisaurus kongwe* has proportionally shorter metatarsals (Table 1) than other silesaurids.

Metatarsal I—Complete metatarsals I are known from the right and left pes of NMT RB159 (Fig. 53E). It is the shortest and least robust of all of the metatarsals of *Asilisaurus kongwe*. This is not the case in *Saturnalia tupiniquim* (MCP 3845-PV), where metatarsal V is shorter, neither in *Marasuchus lilloensis* (Sereno and Arcucci, 1994b) and *Lagerpeton chanarensis* (Sereno and Arcucci, 1994a), in which the element is splint-like. In *Asilisaurus kongwe*, the proximal surface is slightly more expanded relative to the shaft immediately distal to it. It has a proximal oval outline, with a much longer anterolateral/posteromedial axis than anteromedial/posterolateral axis. The anterolateral edge curls more

laterally than the rest of the proximal portion and the resulting concave lateral surface (in proximal view) articulates with the anteromedial surface of the proximal end of metatarsal II, as in *Saturnalia tupiniquim* (MCP 3845-PV). The lateral side of the proximal end is gently convex and the medial surface bears a number of scars on a flatter surface. The shaft of metatarsal I is straight with an oval cross section at midshaft.

The distal end of metatarsal I expands asymmetrically, where the anterolateral portion expands laterally and is much more expanded distally than the medial portion. This is nearly identical to that of *Saturnalia tupiniquim* (MCP 3846-PV). This asymmetry is most apparent in distal view and comparing the large lateral pit with the much smaller medial pit. The distal articular surface is distinctly convex and wraps around the anterior edge to meet a shallow extensor depression. Posteriorly, two expansions from the distal surface frame a shallow depression. In distal view, the surface tapers posteromedially.

Metatarsal II—Metatarsal II is represented by the complete right bone and the distal end of the left bone in NMT RB159 (Fig. 53D). The long axis of the proximal surface is twisted 45° from the long axis (mediolateral) of the distal end. The proximal surface is nearly flat. The straight anterior edge extends laterally to a tapered corner that forms an angle of ~45°, where it meets the anteromedial corner of metatarsal III; this angle is more acute in *Asilisaurus kongwe* compared to that of *Silesaurus opolensis* (ZPAL Ab III/361/19). In proximal view, the posterolateral surface of metatarsal II is weakly sigmoidal and terminates posteriorly in a lateral projection that wraps around the posteromedial corner of metatarsal III. The posterior edge is rounded and the anteromedial surface is weakly concave. This anteromedial edge closely matches the posterolateral surface of metatarsal I, the articulation of which is demarked by a small scar on the anterior portion of the anteromedial edge (Fig. 53). Overall, the proximal outline is strikingly similar to that of *Saturnalia tupiniquim* (MCP 3845-PV) even when compared to that of the other silesaurid *Silesaurus opolensis* (ZPAL Ab III/361/19). Scars are present on the posterior and posteromedial surfaces of the proximal portion, where metatarsal II meets metatarsal III, as a series of near proximodistally oriented ridges.

The bone tapers distally to a minimum width just distal to midshaft. A small, rugose tubercle is present on the anterolateral edge, ~16 mm from the proximal surface and a similar tubercle is also present in the same place on metatarsal II of *Silesaurus opolensis* (ZPAL Ab III/361/19). The midshaft cross section is subtriangular. The distal end expands laterally, medially, and posteriorly. In anterior view, the distal end is asymmetric as in *Silesaurus opolensis* (ZPAL Ab III/361/19), with the pit just proximal to the distal articular surface deeper laterally, with a distinct ridge bounding it laterally, and a medial edge more flared than the lateral edge. No pit is present on the medial surface, whereas the lateral pit is circular and deep. The distal surface is subdivided by a shallow groove that wraps on the posterior surface, terminating in a pair of diverging medial and lateral peaks. The surface is concave between these peaks, directly proximal to the articulation surface.

Metatarsal III—Metatarsal III is complete in both sides of NMT RB159 (Fig. 53C) and the distal end is articulated with that of metatarsal IV in NMT RB133



Fig. 53. Right metatarsals (A–E) of a partial skeleton referred to *Asilisaurus kongwe* (NMT RB159) including metatarsal 5 (A), metatarsal 4 (B), metatarsal 3 (C), metatarsal 2 (D) and metatarsal 1 (E). From the top of each column: proximal, dorsal, lateral or medial, ventral, lateral or medial, distal. Abbreviations: a., articulates with; mt#, metatarsal #; t4, tarsal 4. Scale bar equals 10 mm.

(Fig. 54) from the holotype locality. As with metatarsal II, the long axis of the proximal surface is twisted 45° from the long axis (mediolateral) of the distal end. The

proximal outline is trapezoidal and the proximal surface is flat, with a small rounded peak in the center. The anterior edge is nearly straight and meets the posterolateral

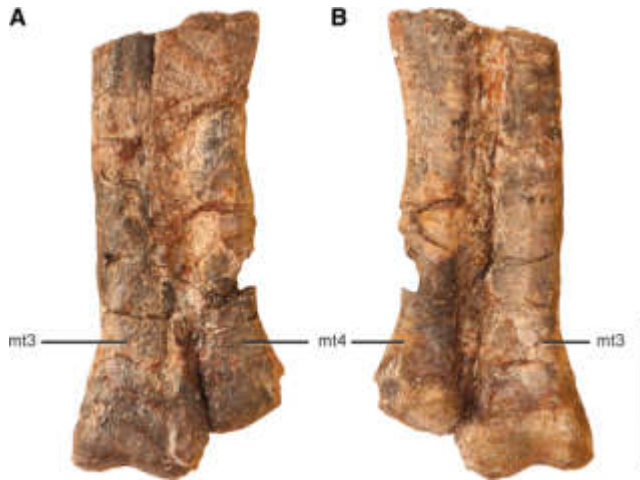


Fig. 54. Articulated distal halves of the metatarsals III and IV (NMT RB133) referred to *Asilisaurus kongwe* from the holotype locality in anterior (A) and posterior (B) views. Abbreviation: mt#, metatarsal #. Scale bar equals 10 mm.

margin at a $\sim 45^\circ$ angle; this angle is more rounded in metatarsal III of *Silesaurus opolensis* (ZPAL Ab III/361/19). The posterolateral margin is straight in proximal view and the anteromedial edge is sigmoidal, matching the corresponding margin of metatarsal II. A rounded ridge, with a rugose proximal portion, originates near the proximal part of the anteromedial surface and extends distally passed the midshaft. The lateral side of this ridge is further defined by a parallel low depression. On the medial portion of the ridge, another proximodistally oriented depression is present. The base of the depression is slightly rugose. A proximodistally oriented scar defines the anterolateral edge of metatarsal III. This ridge is straight in anterior view and terminates at a clear change in angle 12.3 mm from the proximal edge of the bone. Just distal to this ridge, a smaller ridge is present (Fig. 53). Further rugose areas are present on the proximal part of the posterior and posterolateral surfaces. The posterolateral surface also bears a number of proximodistally oriented ridges. The longest of these originates on the posterolateral edge and stretches distally to the lateral edge of the distal articular surface. A number of proximodistally oriented thin and short ridges converge with the sigmoidal ridge throughout its length.

The shaft of metatarsal III tapers distally to a maximum just distal to midshaft. Here, its cross section is comma-shaped, as the result of the ridge present on the lateral surface and the depression on the lateral side of the anterior surface. The distal end is asymmetric in anterior view, where the pit immediately proximal to the articulation surface is deeper laterally, with a better defined bounding ridge on the medial side. The distal articulation surface expands across the anterior surface and there is a small gap in the distal surface between the medial and lateral edges. The medial surface of the distal end is nearly flat with a small rugose scar in a slight depression, whereas the lateral surface has a much deeper central depression. However, this depression is not nearly as deep as the lateral depression. In posterior view, the distal articular surface tapers proximally toward the medial and lateral edges and these two surfaces are separated by a broad concave surface.

Metatarsal IV—Metatarsal VI is represented by a complete right element and the distal half of the left bone of NMT RB159 (Fig. 53B), and the distal half a few other specimens from the holotype locality (e.g., NMT RB133; Fig. 54). The long axis of the proximal articulation forms an angle of $\sim 45^\circ$ degrees with that of the distal end. The proximal surface is concave between the anterolateral and posteromedial edges, as in *Saturnalia tupiniquim* (MCP PV3846). The proximal portion of the bone is mediolaterally narrower than those of metatarsals II and III. The anterolateral portion is the broadest and the proximal surface tapers posteriorly to an acute point. This tapering is also present in sauropodomorphs (*Saturnalia tupiniquim*, MCP PV3846) and *Silesaurus opolensis* (ZPAL Ab III/361/19). The anteromedial surface of the proximal portion is flat where it meets metatarsal III; that surface also has low rugosities near the anterolateral portion. The anterolateral extent of the articulation surface with metatarsal III is marked only by a subtle change in slope, whereas this area is typically marked by a proximodistally oriented ridge in dinosaurs (*Saturnalia tupiniquim*, MCP PV3846). Posteromedially, the edge of metatarsal IV is straight and marked by a rugose scar which is also present in *Silesaurus opolensis* (ZPAL Ab III/361/19). The ventral termination of this scar is marked by a notch with a steep angle to the rest of the posteromedial edge of the bone, as with *Saturnalia tupiniquim* (MCP PV3846). The posterolateral surface is slightly concave and a weakly rimmed depression is located on the anterior part of the surface (Fig. 53). The proximal portion of the anterior surface is rugose and the lateral edge of this surface forms a thin ridge. This ridge slightly broadens distally and forms the lateral margin of the element. The shaft is D-shaped in cross section throughout its length, with the flat portion oriented posterolaterally. This flat surface bears two poorly defined, proximodistally oriented ridges, and the anteromedial surface bears a rounded ridge with a proximal peak 15 mm distal from the proximal end. A similar ridge and peak is present in at least some dinosaurs (*Saturnalia tupiniquim*, MCP PV3846) and *Silesaurus opolensis* (ZPAL Ab III/361/19).

The distal end of metatarsal IV is highly asymmetrical in distal and anterior views as in other dinosauriforms (Novas, 1996; Langer and Benton, 2006). It has a triangular outline, with an expanded lateral process relative to the medial edge. A very shallow depression is present immediately proximal to the distal articular surface on the anterior surface. Its medial bounding ridge is rugose and extends medially beyond the rest of the distal end. The pit on the medial surface is shallow and larger in diameter than the circular pit on the lateral surface. A small gap is present between the divided articular surfaces in posterior view.

Metatarsal V—Metatarsal V is represented by both bones of NMT RB 159 (Fig. 53E) and many examples from locality Z90. Overall, metatarsal V is robust (the shaft is similar in diameter to that of metatarsal IV) and not reduced relative to that as in *Lagerpeton chanarensis* (Sereno and Arcucci, 1994a), *Marasuchus lilloensis* (Sereno and Arcucci, 1994b), *Silesaurus opolensis* (ZPAL Ab III/364), *Herrerasaurus ischigualastensis* (Novas, 1994), and other dinosaurs (e.g., *Saturnalia tupiniquim*, MCP 3845-PV). Particularly, the proximal portion of metatarsal V of *Asilisaurus kongwe* is greatly expanded relative to that of other dinosauriforms. However, metatarsal V

retains much of the overall morphology seen in the aforementioned taxa. Proximally, metatarsal V bears a distinct convex surface on its anteromedial portion that articulated with a concave surface of distal tarsal 4 (see above). This head occupies much of the proximal surface, but it is flanked by a distally descended medial flange and a proximally expanded lateral process. This morphology appears to be autapomorphic, but comparisons with other closely related taxa are limited because metatarsal V is rarely preserved or buried in matrix in articulated specimens (e.g., *Silesaurus opolensis*, ZPAL Ab III/364). The medial flange has a medially bounded ridge that trends laterally and is connected through a series of small bone spurs to a ridge that defines the anterior edge of the shaft. A rugose scar is present on the posterolateral surface of the medial process. The lateral process is directly connected to the articulation surface for distal tarsal 4. It expands well proximal to it, and tapers proximally to a sharp point. In lateral view, the proximal part of the bone is highly rugose, the anterior edge of the lateral process forms a ridge visible in anterior view, and the posterior margin defines a straight margin that thins posteriorly to become a ridge that continues distally. This ridge expands distally to form much of the shaft of metatarsal V in posterior view. The distal end expands anteriorly into a small boot, as in *Saturnalia tupiniquim* (MCP 3845-PV) and *Silesaurus*

opolensis (ZPAL Ab III/364), but also expands a bit medially, a condition not present in *Saturnalia tupiniquim* (MCP 3845-PV). The distal end is oval in outline, with a longer anteroposterior than a mediolateral axis.

Pedal Phalanges—Many phalanges have been found at the type-locality (Z34), at other localities in its proximity (Z90), and were also unambiguously associated with the skeleton of the single individual of *Asilisaurus kongwe* (NMT RB159). Unfortunately, none of the pedal phalanges can be clearly assigned to certain digits because the specimen was found on the surface and not in articulation and both feet are present; so, differentiating the left and right sides is difficult. However, we provide here a description of the general morphology and of some of the more distinct specimens (Fig. 55). The largest phalanx (Fig. 55A) recovered measures 20.0 mm long whereas the smallest (Fig. 55D) measures 8.3 mm long.

Most of the phalanges bear the same general characteristics. The proximal outline is weakly triangular, with a dorsal peak, and the proximal surface is distinctly concave in lateral view, with a ventral portion that extends more proximally than the dorsal portion. Ventrally, most of the phalanges bear parallel ridges that flank the sides, but do not extend to the distal articular surface; the development of these ridges varies among the preserved phalanges. In both dorsal/ventral and lateral/medial

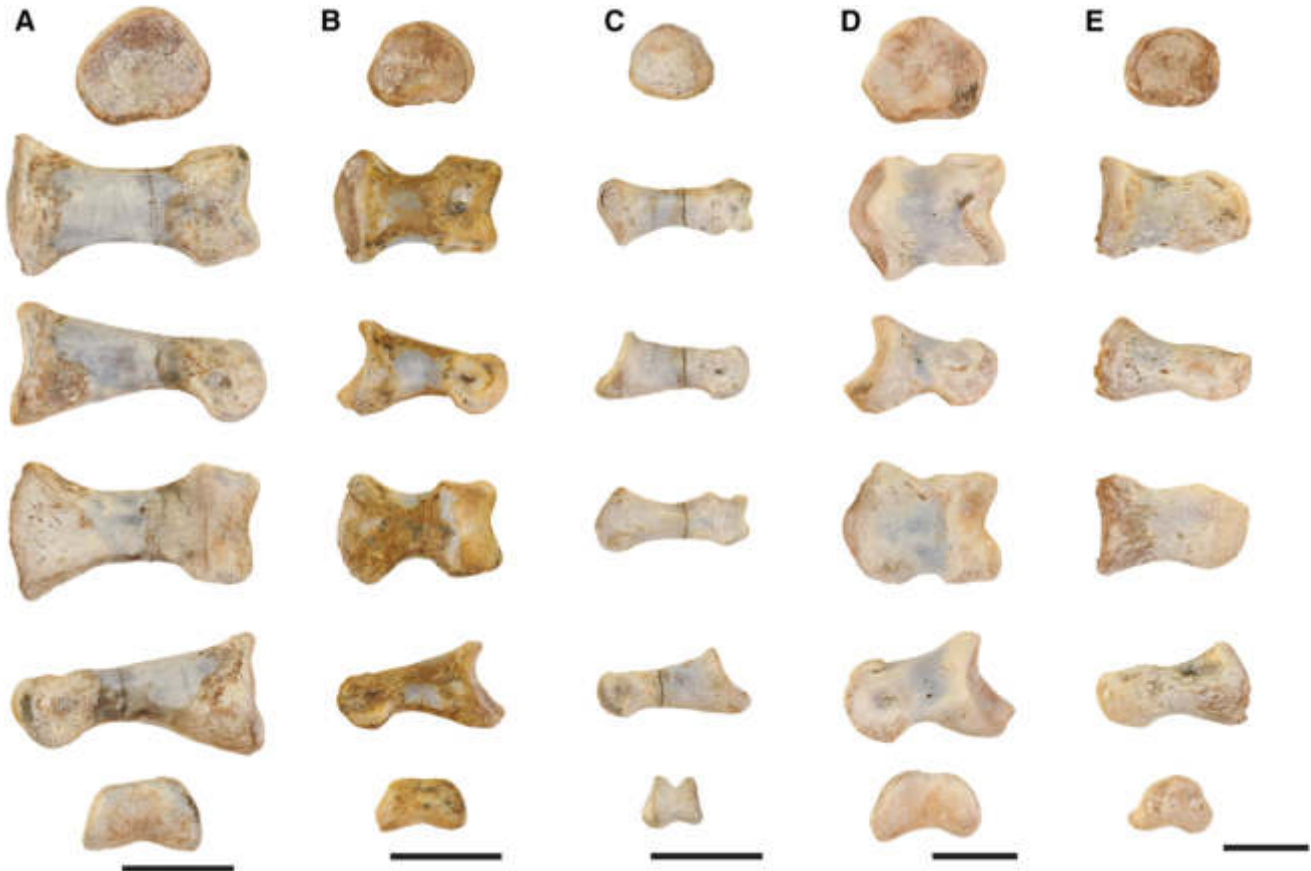


Fig. 55. Pedal phalanges (A–E) of an associated skeleton referred to *Asilisaurus kongwe* (NMT RB159). The digit identity and the position of each phalanx within the digit is not known. From the top of each column: proximal, dorsal, lateral or medial, ventral, lateral or medial, distal. Scale bar equals 10 mm in A–C and 5 mm in D, E.

views, the shaft between the articular surfaces is waisted. The distal articular end expands laterally, medially, and ventrally relative to the shaft. The distal surface is indented at the midline of the element, so that there is a small gap between the lateral and medial portions of the articular surface. Both the lateral and medial sides bear deep pits that are only visible in lateral or medial view, but not dorsally or ventrally. The dorsal surface of the distal end bears a prominent pit in all specimens and, with a few exceptions, most of the phalanges are symmetrical across an anteroposterior axes. In distal view (bottom row of Fig. 55), the width of the articular surfaces is greater than the height in all cases.

Among the preserved phalanges, two morphologies are strikingly different (Fig. 55C, E). A pair of phalanges (Fig. 55C) may represent the first phalanx of digit one given that the proximal articular surface is cup-shaped and does not bear the midline, vertical ridge present in non-first phalanges. The proximal articulation surface matches the distal articular surface of metatarsal I, and the overall narrow proportions (i.e., length > width) is similar to that of the 1st phalanx of digit one of some dinosaurs (e.g., neotheropods). The presence of a large distal articular surface in this phalanx suggests that digit one had at least two phalanges. A second peculiar morphology is represented by a single phalanx (Fig. 55E). This small phalanx has a cup-like proximal articular facet without a midline, vertical ridge, suggesting that it is the first in the digit. Moreover, the size matches well with the distal articular surface of metatarsal V. The distal end tapers, but still appears that it could articulate with a tiny phalanx.

The unguals are well represented as isolated examples from the type-locality (Z34) and a locality with dozens of examples (Z90), and pristine examples from NMT RB159. Of the NMT RB159 examples (seven elements), four morphotypes are present (Figs. 56 and 57): one much larger (two partial specimens preserved) that is mediolaterally compressed (Fig. 57G–I); one that is medially or laterally deflected anteriorly (two complete examples; Fig. 57A–F); one that is laterally or medially deflected in the anterior direction (one complete, one partial example; Fig. 56); and one that is much smaller than all of the others. The smallest and the specimens that are deflected laterally or medially (the actual direction is unknown because the side

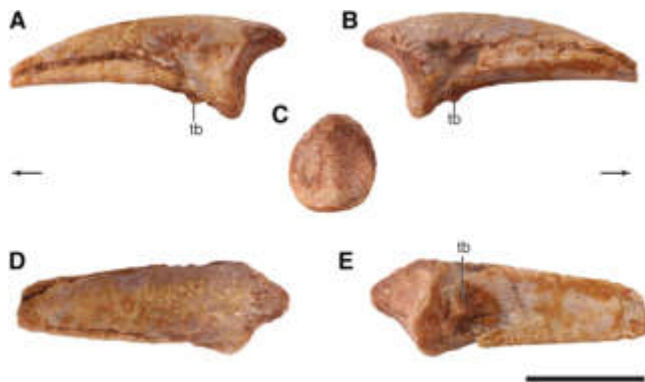


Fig. 56. Complete pedal ungual from an unknown digit of a partial skeleton referred to *Asilisaurus kongwe* (NMT RB159) in lateral or medial (A, B), proximal (C), dorsal (D), and ventral (E) views. Abbreviations: tb, tubercle. Arrows indicate anterior direction. Scale bar equals 5 mm.



Fig. 57. Pedal unguals of unknown position of an associated skeleton referred to *Asilisaurus kongwe* (NMT RB159). Ungual in lateral or medial (A), proximal (B), and dorsal (C) views. Ungual in lateral or medial (D), ventral (E), and dorsal (F) views. Ungual in lateral or medial (G), proximal (H), and dorsal (I) views. Scale bars equal 10 mm.

of the pes could not be determined) all share a number of basic features, namely (Figs. 56 and 57): proximal articular surfaces that have a vertical ridge in a cup-like articulation surface; grooves that parallel the lateral and medial margins and converge distally; a transversally rounded dorsal surface and a nearly flat and mediolaterally expanded ventral surface that lacks a tubercle at the proximal portion; a tapering distal tip; and a weakly dorsally arching main body in lateral/medial views. The smallest ungual matches the size of the distal end of what we interpret as the first phalanx of the first digit. Therefore, we hypothesize that two phalanges were present on first digit. The largest of the unguals is much taller than the other unguals at the proximal articular surface. Grooves near the ventral surface are present, but are hidden in dorsal view and the ventral margin is not medially and laterally expanded as in the other unguals. A large tubercle on the ventral surface is present in one of the large unguals, but not in the other one. The anterior tips of the large unguals are both broken, but it is clear that they are much more mediolaterally compressed than those of the other unguals.

Hoof-like pedal unguals are shared between *Asilisaurus kongwe* and the only other silesaurid with unambiguous pedal unguals, *Silesaurus opolensis* (Dzik, 2003; ZPAL Ab/III/363). Unfortunately, no complete feet are known for *Silesaurus opolensis*, thus making comparisons difficult. This form of ventrally flat unguals are also present in the pseudosuchian clade Shuvosauridae (Nesbitt, 2007) and currently, they are difficult or impossible to tell apart between the two clades.

Phylogenetic Relationships

We updated the scores of *Asilisaurus kongwe* into the large dinosauromorph phylogenetic dataset of Baron et al. (2017), as modified by Langer et al. (2017). We chose this phylogenetic dataset because: 1) it contains the broadest taxonomic sampling; 2) it incorporates newly constructed characters with characters from early and recent phylogenies incorporating early dinosaurs (e.g., Gauthier, 1986; Sereno, 1991; Langer and Benton, 2006; Yates, 2007; Irmis et al., 2007a; Butler et al., 2008;

Ezcurra, 2010; Nesbitt, 2011; Pol et al., 2011; Ezcurra, 2016 and references therein), and 3) the dataset will likely be used often because of reasons stated above. Character states of *Asilisaurus kongwe* in Baron et al. (2017) and Langer et al. (2017) were originally scored based on the holotype and the other specimens referred to the taxon from the holotype locality either from the literature (e.g., Baron et al., 2017) or in person (e.g., MCL in Langer et al., 2017). Here, we score all of the available material of *Asilisaurus kongwe* (Table 2) including the holotype, the referred specimens from the holotype locality, and the largely complete and well preserved example from the eastern portion of the Manda Beds (NMT RB159). No characters, character states, or scores from any other taxa were changed.

The final matrix has 83 taxa and 457 characters. Characters 24, 35, 39, 60, 68, 71, 117, 145, 167, 169, 174, 180, 197, 199, 206, 214, 215, 222, 251, 269, 272, 286, 289, 303, 305, 307, 313, 322, 333, 334, 338, 353, 360, 376, 378, 387, 393, 442, and 446 were ordered. We ran the phylogeny using the same procedure as presented in Langer et al. (2017): the matrix was run under maximum parsimony in TNT 1.5 (Goloboff et al., 2008; Goloboff and Catalano, 2016); a new technology search was conducted until 100 hits to the same minimum length were achieved; the saved most parsimonious trees (MPTs) were subjected to a final round of TBR branch swapping; zero length branches in any of the recovered MPTs were collapsed. This procedure resulted in 218,922 MPTs of 1957 steps (CI: 0.2698, RI: 0.6212).

With the new scores added from *Asilisaurus kongwe*, the relationships of most silesaurids result in a polytomy where *Lewisuchus admixtus*-*Pseudolagosuchus major* is the sister taxon of *Asilisaurus kongwe* and other silesaurids (Fig. 58). This position of *Asilisaurus kongwe* near the base of a silesaurid clade was found by the phylogenetic assessment of the taxon in its original description (Nesbitt et al., 2010). *Asilisaurus kongwe* was found among other non-dinosaur dinosauromorphs in a polytomy with Saurischia and Ornithischia (Langer and Ferigolo, 2013) and, at least in some optimal topologies, not within a silesaurid clade (Bittencourt et al., 2015). Later, Cabreira et al. (2016) found *Asilisaurus kongwe* as the earliest diverging taxon within Ornithischia and just outside a clade composed of “core” silesaurids (including *Silesaurus opolensis*) plus “traditional” ornithischians. Clearly, *Asilisaurus kongwe* is important given its potential phylogenetic position as an early diverging silesaurid, with Silesauridae as the sister taxon to Dinosauria (found here using the Baron et al., 2017 dataset), or as one of the earliest diverging Ornithischia—a clade that has an extremely poor to non-existent Triassic fossil record (Irmis et al., 2007b; Langer et al., 2010; Brusatte et al., 2010a, 2010b; Olsen et al., 2011; Agnolín and Rozadilla, 2018).

Our goal in this contribution is to describe the anatomy of the well preserved specimens of *Asilisaurus kongwe*, but not to detail the phylogenetic position of the taxon given the tidal wave of new data on dinosaur precursors, new early dinosaur species and better specimens of poorly known taxa, and phylogenies with new characters that need further vetting. Therefore, we recognize that the relationships of *Asilisaurus kongwe* are far from being well understood, but also recognize that our knowledge of dinosaur character evolution and relationships is at a critical juncture that needs careful assessment. In another

contribution, our team will critically assess the relationships of newly named silesaurids, potential silesaurids, their interrelationships, and the relationship of Silesauridae to other dinosauromorphs through careful anatomical descriptions, character construction, and consistent scoring across a wide variety of archosaur morphologies.

DISCUSSION

Asilisaurus Bears a Number of Character States Once Thought to Diagnose Dinosauria

The skeleton of *Asilisaurus kongwe* helps to understand character distribution among avemetatarsalians, dinosauriforms, and dinosaurs, and is particularly important for helping constrain the diagnosis of Dinosauria. Specifically, the skeleton of *Asilisaurus kongwe* is ideal for this task because: (1) it is well preserved and features can be easily assessed because almost all bones are completely prepared from the matrix; (2) the comparatively larger size of the specimens relative to other non-dinosaurian avemetatarsalians allows features to be examined more easily without the problem of taphonomic distortion or loss; this is a typical problem in the much smaller dinosauromorphs previously studied (e.g., *Lagerpeton chanarensis*; *Marasuchus lilloensis*), (3) we have a broad understanding of skeletal maturity patterns in *Asilisaurus kongwe* (Griffin and Nesbitt, 2016a) and the associated skeleton of a well preserved individual (NMT RB159) is one of the most skeletally mature, (4) the Middle Triassic age of the species, in general, suggests that it retained more plesiomorphies (see phylogenetic section above) and; (5) it preserves parts of the skeleton, like the skull and parts of the forelimb, that are typically not preserved in the immediate outgroups of Dinosauria. *Asilisaurus kongwe* and other recently described avemetatarsalians (Cabreira et al., 2016; Nesbitt et al., 2017) have been very useful for identifying anatomical traits that once were thought as diagnostic of Dinosauria, but now are understood to be present in more inclusive clades. Here, the following list documents some of the features present in *Asilisaurus kongwe* that were thought to previously diagnose Dinosauria (see Brusatte et al., 2010a, 2010b for summary):

1. Articulated head of quadrate laterally exposed in the squamosal (Fig. 11)
2. Supratemporal fossa on dorsal part of the skull (Fig. 10)
3. Epipophyses in the cervical vertebrae (Fig. 23)
4. Ectopterygoid recess (Fig. 13)
5. Hyposphene-hypantra (Fig. 25)
6. C-shaped (in lateral view) sacral rib 1 (Fig. 26)

Overall, this growing trend has weakened the overall support for Dinosauria and, as a consequence, has led to a lack of a consensus on early dinosaur relationships (see Baron et al., 2017; Langer et al., 2017).

Unexpected Combination of Morphologies in *Asilisaurus kongwe* and Implications for Morphological Trends in Avemetatarsalia

The morphology of *Asilisaurus kongwe* is a mix of unexpected autapomorphic features in the skull, plesiomorphic

TABLE 2. Changes to the phylogenetic scores of *Asilisaurus kongwe* from those of Langer et al. (2017) in the Baron et al., 2017 dataset

1. ?→0	111. ?→1	243. ?→0	336. ?→2	449. ?→0
3. ?→1	112. ?→0	244. ?→1	338. ?→1	450. ?→0
4. ?→0	113. ?→1	245. ?→1	339. ?→0	451. ?→0
5. ?→0	119. ?→0	251. ?→1	340. ?→2	
6. ?→1	127. 1→0	252. ?→0	341. ?→0	
8. ?→0	128. 0→1	253. ?→0	343. ?→-	
9. ?→0	130. 0→1	254. ?→1	344. ?→-	
11. ?→0	131. ?→0	256. ?→0	345. ?→-	
12. ?→1	139. ?→0	257. 0&1→	346. ?→0	
13. ?→0	141. ?→1	258. 1→0 1	348. ?→0	
14. ?→1	142. ?→0	260. ?→0	349. ?→1	
15. ?→0	144. 0→1	261. ?→0	350. ?→-	
16. ?→0	145. 0→1	262. ?→1	351. 0→1	
17. ?→-	148. ?→0	263. ?→1	352. ?→0	
18. ?→1	150. ?→0	264. ?→1	360. 1→0	
19. ?→1	151. ?→5	265. ?→0	361. 1→0	
22. ?→0	158. 0→?	266. ?→-	378. 0→1	
23. ?→0	162. 0→?	267. ?→0	381. ?→0	
25. ?→0	167. 0→?	280. ?→0	398. ?→0	
26. ?→0	168. 0→?	293. ?→0	399. ?→0	
27. ?→0	169. 0→1	294. ?→0	400. ?→0	
29. ?→0	170. 0→?	295. ?→0	404. ?→1	
31. ?→0	174. 2→1	296. ?→0	405. ?→0	
32. ?→-	178. 0→?	297. ?→0	407. ?→0	
33. ?→1	180. 1→?	299. ?→1	408. ?→0	
35. ?→0	183. 0→?	300. ?→1	413. 1→0	
36. ?→0	184. 0→?	301. ?→1	425. ?→1	
39. ?→2	185. 0→?	302. ?→0	426. ?→0	
41. ?→1	189. 0→1	303. ?→0	427. ?→0	
42. 1→?	191. ?→0	307. ?→0	428. ?→0	
43. ?→1	202. ?→0	317. ?→0	429. ?→1	
54. ?→1	203. 0→1	318. ?→1	432. ?→0	
55. ?→0	204. 0→?	319. ?→0	433. ?→0	
56. ?→0	208. ?→0	321. ?→0	434. ?→0	
58. ?→2	211. ?→0	322. ?→2	435. ?→0	
60. ?→0	219. ?→0	323. ?→0	436. ?→1	
66. ?→0	221. ?→0	324. ?→0	437. ?→0	
72. ?→0	222. ?→0	325. ?→1	438. ?→0	
73. ?→0	223. 0→1	326. ?→1	439. ?→1	
74. ?→1	225. ?→0	327. ?→1	440. ?→1	
75. ?→0	230. 1→0	328. ?→-	441. ?→0	
76. ?→0	233. 0→?	331. ?→0	442. ?→0	
80. ?→0	234. 1→?	332. ?→0	443. ?→1	
81. ?→1	240. ?→0	333. ?→0	444. ?→1	
83. ?→1	241. ?→0	334. ?→0	445. ?→0	
84. ?→0	242. ?→0	335. 0→1	447. ?→0	

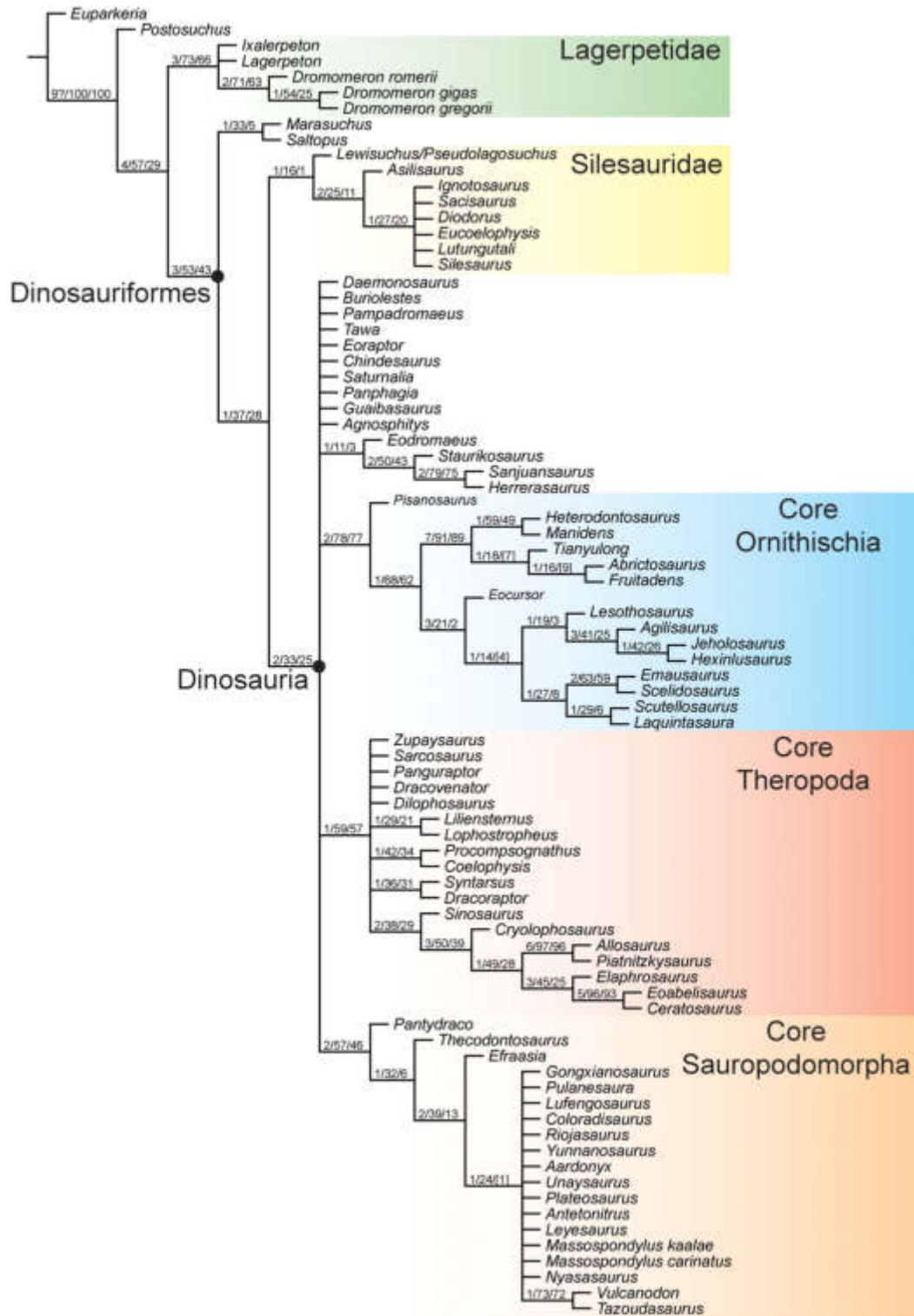


Fig. 58. The phylogenetic position of *Asilisaurus kongwe* in the dataset of Baron et al., 2017, followed by modifications of Langer et al., 2017. Bremer support values (left) and bootstrap values (absolute (middle) and “group present/contradicted” (right)) are shown for each clade.

traits as expected for an early diverging dinosauriform, and unusual character states in the hindlimb that were not predicted based on phylogenies incorporating dinosaurs and their closest relatives. Here, we highlight some

of the apparent patterns emerging from the well preserved remains of *Asilisaurus kongwe*.

Cranial morphology—The morphology of skull elements of *Asilisaurus kongwe* is particularly unexpected,

comparatively to that of the other relatively well known silesaurid, *Silesaurus opolensis*. Particularly, the relatively large premaxilla of *Asilisaurus kongwe* is modified into a beak for most of its length, with a single alveolus present at the posterior portion of the ventral margin. This is in complete contrast to the morphology of *Silesaurus opolensis*, which bears five teeth throughout the premaxillary length, and to that of all other dinosauriforms, including early dinosaurs. A beak-like upper jaw does occur in a number of dinosaur clades (e.g., Zanno and Makovicky, 2011) and in shuvosaurid pseudosuchians (Nesbitt and Norell, 2006; Nesbitt, 2007; Nesbitt et al., 2007), groups that have no close relation to *Asilisaurus kongwe*. The morphology of the maxilla of *Asilisaurus kongwe* is also unexpected for an early dinosauriform. It is short, possibly tall, and contains only ~10 teeth, far fewer than most dinosauriforms.

The edentulous anterior portion of the mandible of *Asilisaurus kongwe* is generally similar to that of other silesaurids (e.g., *Silesaurus opolensis*, *Sacisaurus agudoensis*). However, *Asilisaurus kongwe* is the only early dinosauriform that has a ventrally deflected mandible, whereas the lower jaw of other members of the group are either dorsally or anteriorly directed. Whether the edentulous anterior portion of the mandible of *Asilisaurus kongwe* and other silesaurids represents a homologous predeulatory “precursor” (Ferigolo and Langer, 2006; Langer and Ferigolo, 2013) or not (Nesbitt et al., 2010; Nesbitt, 2011), silesaurids and ornithischians do share morphology in the anterior end of the mandible, and this shared morphology may indicate a similar ecology (Ferigolo and Langer, 2006).

Taken together, the jaw morphology of *Asilisaurus kongwe* radically differs from that of other Triassic archosaurs in that has (1) a short preorbital portion of the skull, (2) a premaxilla that is proportionally large relative to the length of the maxilla, (3) poorly occluding (at least for the dental portion) anterior ends of the upper and lower jaws, and (4) few teeth. On a broader evolutionary scale, the pattern seen in *Asilisaurus kongwe* appears unique compared to archosaurs currently known, but similar morphologies may be present within the transitions to beaks in ornithomimid, therizinosaurid, and avian theropods (Zanno and Makovicky, 2011). Therefore, cranial changes more common in later dinosaurs were possibly present prior to the origin of Dinosauria.

Brevis fossa of the ilium—The homology of the *M. caudofemoralis brevis* origin on the posterior portion of the ilium of dinosaurs and their closest relatives has been widely debated (Gauthier and Padian, 1985; Novas, 1996; Langer and Benton, 2006; Nesbitt, 2011; Baron et al., 2017). The discovery of a deep *brevis fossa* in *Silesaurus opolensis* (Dzik, 2003) added to the confusion given that some dinosaurs (e.g., herrerasaurids) lack the fossa. The well preserved ilia of *Asilisaurus kongwe* clearly lack a *brevis fossa* as developed as that of *Silesaurus opolensis*. Therefore, the condition in *Lewisuchus admixtus*, *Silesaurus opolensis*, and other silesaurids (e.g., *Lutungutali sitwensis*, *Sacisaurus agudoensis*) is either convergent with that of dinosaurs with a large *brevis fossa*, or the feature is synapomorphic of the Silesauridae + Dinosauria and was lost in the lineage leading to *Asilisaurus kongwe*, or *Asilisaurus kongwe* lacks some of the synapomorphies of the Silesauridae + Dinosauria clade and is outside of the clade (regardless

of its internal relations). Nevertheless, the presence and absence of the *brevis fossa* has a complex distribution in dinosauriforms.

Pelvis with two sacral vertebrae—The sacrum of *Asilisaurus kongwe* bears only the two primordial sacral vertebrae of Archosauria (see Nesbitt, 2011). The presence of two sacral vertebrae can be confirmed based on a number of specimens (Fig. 26) from the holotype locality and from the morphology of the sacral rib scars on the medial side of the ilium (Figs. 36 and 37). In contrast, *Silesaurus opolensis* has a sacrum composed of three (Dzik, 2003) or four (Dzik and Sulej, 2007) sacral vertebrae, all contacting the ilium. Additionally, the number of sacral vertebrae increases independently within Theropoda, Ornithischia, and Sauropodomorpha (Langer and Benton, 2006; Nesbitt, 2011). The presence of only two sacral vertebrae in *Asilisaurus kongwe* suggests that the trend of increasing sacral vertebrae may also be occurring independently within Silesauridae, if *Asilisaurus kongwe* and *Silesaurus opolensis* are found to be more closely to one another than to any dinosaur.

Proximal tarsals—The astragalus and calcaneum of *Asilisaurus kongwe* have been key to understand the origin of the mesotarsal ankle of avemetatarsalians (Nesbitt et al., 2010, 2017). Previously, it was hypothesized that the “advanced mesotarsal” ankle evolved from an archosaur common ancestor that had neither a “crocodile-normal” ankle configuration nor an avemetatarsalian “advanced mesotarsal” ankle (Nesbitt et al., 2017). Nevertheless, a recent pattern has emerged suggesting that the common ancestor of Archosauria had a “crocodile-normal” ankle configuration, which was retained in avemetatarsalian taxa like *Asilisaurus kongwe*, and that the “advanced mesotarsal” ankle in pterosaurs and dinosaurs may have evolved independently (Nesbitt et al., 2017). Furthermore, the ankle of *Silesaurus opolensis* (Dzik, 2003) is more similar to the “advanced mesotarsal” ankle of dinosaurs (small, block-like calcaneum with a concave surface, tall ascending process of the astragalus) than it is to that of *Asilisaurus kongwe*. Therefore, if *Asilisaurus kongwe* and *Silesaurus opolensis* are found to be more closely related to one another than to any dinosaur, the “crocodile-normal” ankle configuration in *Asilisaurus kongwe* may have, convergently with dinosaurs, given rise to a more “advanced mesotarsal” ankle in *Silesaurus opolensis* within Silesauridae.

Pes—The pes of *Asilisaurus kongwe* bears unexpectedly short metatarsals (relative to the epipodium) compared to those of other avemetatarsalian clades, where there appears to be a number of independent trends that lengthen the metatarsals relative to other hindlimb elements (Nesbitt et al., 2017). The pes of *Asilisaurus kongwe* does have the hallmarks of Dinosauriformes, including metatarsal III being the longest, metatarsals II and IV about equal in length, and metatarsals I and V shorter than the rest of the series. However, the lengths and morphology of metatarsals I and V are seemingly unique of *Asilisaurus kongwe* within ornithodirans given the typical trend of 1) a relative decrease in length of metatarsal I, 2) a reduction in size of the proximal portion of metatarsal V, and 3) a relative decrease in length of metatarsal V to a splint of bone. Furthermore, metatarsal V of *Asilisaurus kongwe* appears to retain phalanges whereas these are lost in nearly all dinosauriforms. This common dinosauriform pattern of metatarsals I and V reduction also occurs in Silesauridae, given that

Silesaurus opolensis reduces these bones in a similar way as dinosaurs.

CONCLUSION

The skeleton of *Asilisaurus kongwe* is one of the most completely known for a non-dinosaurian dinosauriform and it is also known from a wealth of individuals from different ontogenetic ages. The specimens of *Asilisaurus kongwe* demonstrate that there were a number of changes throughout ontogeny, many of them also present in other silesaurids and some early dinosaurs. The morphology of this early silesaurid is a mix of features expected from other dinosauriforms, but also includes a number of character states, like the presence of a premaxillary beak, that were not predictable based on previous discoveries. The more plesiomorphic morphology of *Asilisaurus kongwe* also shows that there were parallel trends within Silesauridae and in dinosaur lineages and that convergences make single bones or even partial skeletons difficult to place phylogenetically. Finally, the likely Middle Triassic age and the combination of characters-states of *Asilisaurus kongwe* illustrates the importance of sampling the early part of avemetatarsalian lineages to elucidate dinosaurian character acquisition, given the abundance of convergence and parallel evolution among dinosaur relatives.

ACKNOWLEDGMENTS

We thank Robert Gaston for a physical model of the skull reconstruction and Scott Hartman for the skeletal reconstruction of *Asilisaurus*. Discussions with R. B. Irmis and M. R. Stocker have been useful. C. A. Sidor, K. D. Angielczyk, R. M. H. Smith, J. S. Steyer, M. R. Stocker, L. Tsuji, N. Tabor, A. Tibajuka, and L. Nampunju helped discover and collect *Asilisaurus kongwe* fossils. We thank the careful reviews conducted by A. D. Marsh, B. R. Peacock, and W. G. Parker. We thank Christina Nelson for the charcoal illustration of the skull bones. This work was funded by a National Geographic Society grant 7787-05, National Science Foundation grants 0306158EAR-1337291, and EAR-1337569 (to SJN), and FAPESP grant 2014-03825-3 (to MCL).

LITERATURE CITED

- Agnolín FL, Rozadilla S. 2018. Phylogenetic reassessment of *Pisanosaurus mertii* Casamiquela, 1967, a basal dinosauriform from the Late Triassic of Argentina. *J Syst Palaeontol* 16:853–879.
- Arcucci A. 1987. Un nuevo lagsuchidae (theodontia-pseudosuchia) de la fauna de Los Chañares (edad reptil Chañarense, Triasico Medio), La Rioja, Argentina. *Ameghiniana* 24:89–94.
- Bakker RT. 1968. The superiority of dinosaurs. *Discovery* 3:11–22.
- Bakker RT. 1971. Dinosaur physiology and the origin of mammals. *Evolution* 25:636–658.
- Baron MG, Williams ME. 2018. A re-evaluation of the enigmatic dinosauriform *Caseosaurus crosbyensis* from the Late Triassic of Texas, USA and its implications for early dinosaur evolution. *Acta Palaeontol Pol* 63:129–145.
- Baron MG, Norman DB, Barrett PM. 2016. Postcranial anatomy of *Lesothosaurus diagnosticus* (Dinosauria: Ornithischia) from the Lower Jurassic of southern Africa: implications for basal ornithischian taxonomy and systematics. *Zool J Linnean Soc* 179:125–168.
- Baron MG, Norman DB, Barrett PM. 2017. A novel hypothesis of dinosaur relationships and early dinosaur evolution. *Nature* 543: 501–506.
- Barrett PM, Nesbitt SJ, Peacock BR. 2015. A large-bodied silesaurid from the Lifua Member of the Manda beds (Middle Triassic) of Tanzania and its implications for body-size evolution in Dinosauromorphs. *Gondwana Res* 27:925–931.
- Benton MJ. 1983. Dinosaur success in the Triassic; a noncompetitive ecological model. *Q Rev Biol* 58:29–55.
- Benton MJ. 1999. *Scleromochlus taylori* and the origin of dinosaurs and pterosaurs. *Philos Trans R Soc Lond B* 354:1423–1446.
- Bittencourt JS, Arcucci AB, Marsicano CA, Langer MC. 2015. Osteology of the Middle Triassic archosaur *Lewisuchus admixtus* Romer (Chañares Formation, Argentina), its inclusivity, and relationships amongst early dinosauromorphs. *Journal of Systematic Palaeontology* 13:189–219.
- Bonaparte JF. 1984. Locomotion in raucosuchid thecodonts. *J Vertebr Paleontol* 3:210–218.
- Brusatte SL, Benton MJ, Ruta M, Lloyd GT. 2008. Superiority, competition, and opportunism in the evolutionary radiation of dinosaurs. *Science* 321:1485–1488.
- Brusatte S, Nesbitt SJ, Irmis RB, Butler R, Benton MJ, Norell MA. 2010a. The origin and early radiation of dinosaurs. *Earth Sci Rev* 101:68–100.
- Brusatte SL, Benton MJ, Desojo JB, Langer MC. 2010b. The higher-level phylogeny of Archosauria (Tetrapoda: Diapsida). *J Syst Palaeontol* 8:3–47.
- Brusatte SL, Lloyd GT, Wang SC, Norell MA. 2014. Gradual assembly of avian body plan culminated in rapid rates of evolution across the dinosaur-bird transition. *Curr Biol* 24:2386–2392.
- Butler RJ. 2005. The “fabrosaurid” ornithischian dinosaurs of the upper Elliot Formation (Lower Jurassic) of South Africa and Lesotho. *Zool J Linnean Soc* 145:175–218.
- Butler RJ, Upchurch P, Norman DB. 2008. The phylogeny of the ornithischian dinosaurs. *J Syst Palaeontol* 6:1–40.
- Butler RJ. 2010. The anatomy of the basal ornithischian dinosaur *Eocursor parvus* from the lower Elliot Formation (Late Triassic) of South Africa. *Zoological Journal of the Linnean Society* 160:648–684.
- Cabreira SF, Kellner AWA, Dias-da-Silva S, da Silva LR, Bronzati M, de Almeida Marsola JC, Müller RT, de Souza Bittencourt J, Batista BJA, Raugust T. 2016. A unique Late Triassic dinosauromorph assemblage reveals dinosaur ancestral anatomy and diet. *Curr Biol* 26:3090–3095.
- Carrano MT, Hutchinson JR. 2002. Pelvic and hindlimb musculature of *Tyrannosaurus rex* (Dinosauria: Theropoda). *J Morphol* 253: 207–228.
- Charig AJ. 1984. Competition between therapsids and archosaurs during the Triassic Period; a review and synthesis of current theories. In: Ferguson MWJ, editor. *Symposia of the Zoological Society of London*, Vol. 52. Academic Press, Cambridge, Cambridge University Press. p 597–628.
- Colbert EH. 1989. The Triassic dinosaur *Coelophysus*. *Bull Mus North Ariz* 57:1–174.
- Cope ED. 1869. Synopsis of the extinct Batrachia, Reptilia, and Aves of North America. *Trans Am Philos Soc* 40:1–252.
- Dzik J. 2003. A beaked herbivorous archosaur with dinosaur affinities from the early Late Triassic of Poland. *J Vertebr Paleontol* 23: 556–574.
- Dzik J, Sulej T. 2007. A review of the early Late Triassic Krasiejów biota from Silesia, Poland. *Palaeontologia Polonica* 64:1–27.
- Ezcurra MD. 2006. A review of the systematic position of the dinosauriform archosaur *Eucoelophysus baldwini* Sullivan & Lucas, 1999 from the Upper Triassic of New Mexico, USA. *Geodiversitas* 28:649–684.
- Ezcurra MD. 2010. A new early dinosaur (Saurischia: Sauropodomorpha) from the Late Triassic of Argentina: a reassessment of dinosaur origin and phylogeny. *J Syst Palaeontol* 8:371–425.
- Ezcurra MD. 2016. The phylogenetic relationships of basal archosauriforms, with an emphasis on the systematics of proterosuchian archosauriforms. *PeerJ* 4:e1778. <https://doi.org/10.7717/peerj.1778>.
- Ezcurra MD, Fiorelli LE, Martinelli AG, Rocher S, von Baczko MB, Ezpeleta M, Tabor JR, Hechenleitner EM, Trotteyn MJ, Desojo JB. 2017. Deep faunistic turnovers preceded the rise of dinosaurs in southwestern Pangaea. *Nat Ecol Evol* 1:1477.

- Ferigolo J, Langer MC. 2007. A Late Triassic dinosauriform from south Brazil and the origin of the ornithischian predeontary bone. *Hist Biol* 19:23–33.
- Postowicz-Frelík Ł, Sulej T. 2010. Bone histology of *Silesaurus opolensis* Dzik, 2003 from the Late Triassic of Poland. *Lethaia* 43:137–148.
- Gauthier J. 1986. Saurischian monophyly and the origin of birds. *Mem Calif Acad Sci* 8:1–55.
- Gauthier J, Padian K. 1985. Phylogenetic, functional, and aerodynamic analyses of the origin of birds and their flight. In: Hecht MK, Ostrom JH, Viohl G, Wellnhofer P, editors. *The Beginning of Birds: Proceedings of the International Archaeopteryx Conference*. Freunde des Jura Museums: Eichstätt. p 185–197.
- Goloboff PA, Catalano SA. 2016. TNT version 1.5, including a full implementation of phylogenetic morphometrics. *Cladistics* 32:221–238.
- Goloboff PA, Farris JS, Nixon KC. 2008. TNT, a free program for phylogenetic analysis. *Cladistics* 24:774–786.
- Griffin C. 2018. Developmental patterns and variation among early theropods. *J Anat* 232:604–640.
- Griffin CT, Nesbitt SJ. 2016a. The femoral ontogeny and long bone histology of the Middle Triassic (?late Anisian) dinosauriform *Asilisaurus kongwe* and implications for the growth of early dinosaurs. *J Vertebr Paleontol* e1111224.36.
- Griffin CT, Nesbitt SJ. 2016b. Anomalously high variation in growth is ancestral for dinosaurs but lost in birds. *Proc Natl Acad Sci U S A* 113:14757–14762.
- Holliday CM, Nesbitt SJ. 2013. Morphology and diversity of the mandibular symphysis of archosauriforms. In: Nesbitt SJ, Desojo JB, Irmis RB, editors. *Anatomy, Phylogeny, and Palaeobiology of Early Archosaurs and their Kin*. London, UK: Geological Society Special Volume. p 555–571.
- Hutchinson JR. 2001. The evolution of femoral osteology and soft tissue on the line to extant birds (Neornithes). *Zool J Linnean Soc* 131:169–197.
- Irmis RB. 2011. Evaluating hypotheses for the early diversification of dinosaurs. *Earth Environ Sci Trans R Soc Edinb* 101:397–426.
- Irmis RB, Nesbitt SJ, Padian K, Smith ND, Turner AH, Woody D, Downs A. 2007a. A Late Triassic dinosauriform assemblage from New Mexico and the rise of dinosaurs. *Science* 317:358–361.
- Irmis RB, Parker WG, Nesbitt SJ, Liu J. 2007b. Ornithischian dinosaurs: the Triassic record. *Hist Biol* 18:3–22.
- Juul L. 1994. The phylogeny of basal archosaurs. *Palaeontol Afr* 31:1–38.
- Kammerer CF, Nesbitt SJ, Shubin NH. 2012. The first basal dinosauriform (Silesauridae) from the Late Triassic of Morocco. *Acta Palaeontol Pol* 57:277–284.
- Langer MC. 2003. The pelvic and hind limb anatomy of the stem-sauropodomorph *Saturnalia tupiniquim* (Late Triassic, Brazil). *PaleoBios* 23:1–40.
- Langer MC. 2014. The origins of Dinosauria: much ado about nothing. *Palaeontology* 57:469–478.
- Langer MC, Benton MJ. 2006. Early dinosaurs: A phylogenetic study. *J Syst Palaeontol* 4:309–358.
- Langer MC, Ezcurra MD, Rauhut OWM, Benton MJ, Knoll F, McPhee BW, Novas FE, Pol D, Brusatte SL. 2017. Untangling the dinosaur family tree. *Nature* 551:E1–E3.
- Langer MC, Ferigolo J. 2013. The Late Triassic dinosauriform *Sacisaurus agudoensis* (Caturrita Formation; Rio Grande do Sul, Brazil): anatomy and affinities. In: Nesbitt SJ, Desojo JB, Irmis RB, editors. *Anatomy, Phylogeny, and Palaeobiology of Early Archosaurs and their Kin*. London, UK: Geological Society Special Volume. p 353–392.
- Langer MC, França MAG, Gabriel S. 2007. The pectoral girdle and forelimb anatomy of the stem-sauropodomorph *Saturnalia tupiniquim* (Upper Triassic, Brazil). *Spec Pap Palaeontol* 77:113–137.
- Langer MC, Ezcurra MD, Bittencourt JS, Novas FE. 2010. The origin and early evolution of dinosaurs. *Biol Rev* 85:55–110.
- Langer MC, Nesbitt SJ, Bittencourt JS, Irmis RB. 2013. Early Dinosauriforms. In: Nesbitt SJ, Desojo JB, Irmis RB, editors. *Anatomy, Phylogeny, and Palaeobiology of Early Archosaurs and their Kin*. London, UK: Geological Society Special Volume.
- Madsen JH Jr. 1976. *Allosaurus fragilis*: a revised osteology. *Utah Geol Surv Bull* 109:1–163.
- Marsh AD, Rowe TB. 2018. Anatomy and systematics of the sauropodomorph *Saraksaurus aurifontanalis* from the Early Jurassic Kayenta Formation. *PLoS One* 13:e0204007.
- Martinez RN, Sereno PC, Alcober OA, Colombi CE, Renne PR, Montañez IP, Currie BS. 2011. A basal dinosaur from the dawn of the dinosaur era in southwestern Pangaea. *Science* 331:206–210.
- Martínez RN, Apaldetti C, Alcober OA, Colombi CE, Sereno PC, Fernández E, Malnis PS, Correa GA, Abelin D. 2013. Vertebrate succession in the Ischigualasto Formation. *J Vertebr Paleontol* 32:10–30.
- Müller RT, Langer MC, Bronzati M, Pacheco CP, Cabreira SF, Dias-Da-Silva S. 2018. Early evolution of sauropodomorphs: anatomy and phylogenetic relationships of a remarkably well-preserved dinosaur from the Upper Triassic of southern Brazil. *Zool J Linnean Soc* 184:1187–1248.
- Nesbitt SJ. 2007. The anatomy of *Effigia okeeffeae* (Archosauria, Suchia), theropod convergence, and the distribution of related taxa. *Bull Am Mus Nat Hist* 302:1–84.
- Nesbitt SJ. 2011. The early evolution of Archosauria: relationships and the origin of major clades. *Bull Am Mus Nat Hist* 352:1–292.
- Nesbitt SJ, Flynn JJ, Pritchard AC, Parrish JM, Ranivoharimanana L, Wyss AR. 2015. Postcranial osteology of *Azendohsaurus madagaskarensis* (?Middle to Upper Triassic, Isalo Group, Madagascar) and its systematic position among stem archosaur reptiles. *Bulletin of the American Museum of Natural History* 398:1–126.
- Nesbitt SJ, Sidor CA, Angielczyk KD, Smith RMH, Tsuji LA. 2014. A new archosaur from the Manda beds (Anisian: Middle Triassic) of southern Tanzania and its implications for character optimizations at Archosauria and Pseudosuchia. *Journal of Vertebrate Paleontology* 34:1357–1382.
- Nesbitt SJ, Norell MA. 2006. Extreme convergence in the body plans of an early suchian (Archosauria) and ornithomimid dinosaurs (Theropoda). *Proc R Soc Lond B* 273:1045–1048.
- Nesbitt SJ, Irmis RB, Parker WG. 2007. A critical re-evaluation of the Late Triassic dinosaur taxa of North America. *J Syst Palaeontol* 5:209–243.
- Nesbitt SJ, Irmis RB, Parker WG, Smith ND, Turner AH, Rowe T. 2009a. Hindlimb osteology and distribution of basal dinosauriforms from the Late Triassic of North America. *J Vertebr Paleontol* 29:498–516.
- Nesbitt SJ, Smith ND, Irmis RB, Turner AH, Downs A, Norell MA. 2009b. A complete skeleton of a Late Triassic saurischian and the early evolution of dinosaurs. *Science* 326:1530–1533.
- Nesbitt SJ, Sidor CA, Irmis RB, Angielczyk KD, Smith RMH, Tsuji LA. 2010. Ecologically distinct dinosaurian sister-group shows early diversification of Ornithodira. *Nature* 464:95–98.
- Nesbitt SJ, Butler RJ, Ezcurra MD, Barrett PM, Stocker MR, Angielczyk KD, Smith RMH, Sidor CA, Niedzwiedzki G, Sennikov A, et al. 2017. The earliest bird-line archosaurs and assembly of the dinosaur body plan. *Nature* 544:484–487.
- Nesbitt SJ, Butler RJ, Ezcurra MD, Charig AJ, Barrett PM. 2018. The anatomy of *Teleocrater rhadinus*, an early avemetatarsalian from the lower portion of the Lifua Member of the Manda Beds (~Middle Triassic). In: Sidor CA, Nesbitt SJ, editors. *Vertebrate and climatic evolution in the Triassic rift basins of Tanzania and Zambia. Society of Vertebrate Paleontology Memoir 17. Journal of Vertebrate Paleontology* 37 (6, supplement). p 142–177.
- Novas FE. 1992. Phylogenetic relationships of the basal dinosaurs, the Herrerasauridae. *Palaeontology* 35:51–62.
- Novas FE. 1994. New information on the systematics and postcranial skeleton of *Herrerasaurus ischigualastensis* (Theropoda: Herrerasauridae) from the Ischigualasto Formation (Upper Triassic) of Argentina. *J Vertebr Paleontol* 13:400–423.
- Novas FE. 1996. Dinosaur monophyly. *J Vertebr Paleontol* 16:723–741.
- Olsen PE, Kent DV, Whiteside JH. 2011. Implications of the Newark Supergroup-based astrochronology and geomagnetic polarity time scale (Newark-APTS) for the tempo and mode of the early diversification of the Dinosauria. *Earth Environ Sci Trans R Soc Edinb* 101:201–229.
- Padian K, de Ricqlès AJ, Horner JR. 2001. Dinosaurian growth rates and bird origins. *Nature* 412:405–408.

- Padian K, Horner JR, de Ricqlès A. 2004. Growth in small dinosaurs and pterosaurs: the evolution of archosaurian growth strategies. *J Vertebr Paleontol* 24:555–571.
- Parker WG, Irmis RB, Nesbitt SJ. 2006. Review of the Late Triassic dinosaur record from Petrified Forest National Park, Arizona. *Mus North Ariz Bull* 62:160–161.
- Parrish JM. 1993. Phylogeny of the Crocodylotarsi, with reference to archosaurian and crurotarsan monophyly. *J Vertebr Paleontol* 13: 287–308.
- Peacock BR, Sidor CA, Nesbitt SJ, Smith RMH, Steyer JS, Angielczyk KD. 2013. A new silesaurid from the upper Ntawere Formation of Zambia (Middle Triassic) is among the oldest bird-line archosaur (Avenetatarsalia). *J Vertebr Paleontol* 33:1127–1137.
- Peacock BR, Steyer JS, Tabor NJ, Smith RM. 2018. Updated geology and vertebrate paleontology of the Triassic Ntawere Formation of northeastern Zambia, with special emphasis on the archosauromorphs. In: Sidor CA, Nesbitt SJ, editors. *Vertebrate and climatic evolution in the Triassic rift basins of Tanzania and Zambia. Society of Vertebrate Paleontology Memoir 17. Journal of Vertebrate Paleontology 37 (6, supplement)*. p 8–38.
- Piechowski R, Dzik J. 2010. The axial skeleton of *Silesaurus opolensis*. *J Vertebr Paleontol* 30:1127–1141.
- Piechowski R, Tañanda M, Dzik J. 2014. Skeletal variation and ontogeny of the Late Triassic Dinosauriform *Silesaurus opolensis*. *J Vertebr Paleontol* 34:1383–1393.
- Piechowski R, Niedzwiedzki G, Tañanda M. 2018. Unexpected bird-like features and high intraspecific variation in the braincase of the Triassic relative of dinosaurs. *Hist Biol* 1065-1081.
- Pol D, Garrido A, Cerda I. 2011. A new sauropodomorph dinosaur from the Early Jurassic of Patagonia and the origin and evolution of the sauropod-type sacrum. *PLoS One* 6:e14572>.
- Prieto-Márquez A, Norell MA. 2011. Redescription of a nearly complete skull of *Plateosaurus* (Dinosauria: Sauropodomorpha) from the Late Triassic of Trossingen (Germany). *Am Mus Novit.* 3727, 1–58.
- Rauhut OWM. 2003. The interrelationships and evolution of basal theropod dinosaurs. *Spec Pap Palaeontol* 69:1–213.
- Romer AS. 1923. Crocodilian pelvic muscles and their avian and reptilian homologues. *Bull Am Mus Nat Hist* 48:533–552.
- Romer AS. 1971. The Chañares (Argentina) Triassic reptile fauna. X. Two new but incompletely known long-limbed pseudosuchians. *Breviora* 378:1–10.
- Romer AS. 1972. The Chañares (Argentina) Triassic reptile fauna. XIV. *Lewisuchus admixtus*, gen. et sp. nov., a further thecodont from the Chañares beds. *Breviora* 390:1-13.
- Santa Luca A. 1980. *The postcranial skeleton of Heterodontosaurus tucki (Reptilia, Ornithischia) from the Stromberg of South Africa: South Africa Museum. Annals of the South African Museum, 79.159-211.*
- Sereno PC. 1991. Basal archosaurs: phylogenetic relationships and functional implications. *J Vertebr Paleontol* 10:1–53.
- Sereno PC. 1994. The pectoral girdle and forelimb of the basal theropod *Herrerasaurus ischigualastensis*. *J Vertebr Paleontol* 13:425–450.
- Sereno PC, Arcucci AB. 1994a. Dinosaurian precursors from the Middle Triassic of Argentina: *Lagerpeton chanarensis*. *J Vertebr Paleontol* 13:385–399.
- Sereno PC, Arcucci AB. 1994b. Dinosaurian precursors from the Middle Triassic of Argentina: *Marasuchus lilloensis*, gen. nov. *J Vertebr Paleontol* 14:53–73.
- Sereno PC, Novas FE. 1994. The skull and neck of the basal theropod *Herrerasaurus ischigualastensis*. *J Vertebr Paleontol* 13: 451–476.
- Sereno PC, McAllister S, Brusatte SL. 2005. TaxonSearch: a relational database for suprageneric taxa and phylogenetic definitions. *PhyloInformatics* 8:1-21.
- Sereno PC, Martínez RN, Alcober OA. 2013. Osteology of *Eoraptor lunensis* (Dinosauria, Sauropodomorpha). *J Vertebr Paleontol* 32: 83–179.
- Sidor CA, Nesbitt SJ. 2018. Introduction to vertebrate and climatic evolution in the Triassic rift basins of Tanzania and Zambia. In: Sidor CA, Nesbitt SJ, editors. *Vertebrate and climatic evolution in the Triassic rift basins of Tanzania and Zambia. Society of Vertebrate Paleontology Memoir 17. Journal of Vertebrate Paleontology 37 (6, supplement)*. p 1–7.
- Small B. 2009. A Late Triassic dinosauriform assemblage from the Eagle Basin (Chinle Formation), Colorado, USA. *J Vertebr Paleontol* 29:182A.
- Smith RMH, Sidor CA, Angielczyk KD, Nesbitt SJ, Tabor NJ. 2018. Taphonomy and paleoenvironments of Middle Triassic bone accumulations in the Lifua Member of the Manda Beds, Songea Group (Ruhuhu Basin), Tanzania. In: Sidor CA, Nesbitt SJ, editors. *Vertebrate and climatic evolution in the Triassic rift basins of Tanzania and Zambia. Society of Vertebrate Paleontology Memoir 17. Journal of Vertebrate Paleontology 37 (6, supplement)*. p 65–79.
- Tucker ME, Benton MJ. 1982. Triassic environments, climates and reptile evolution. *Palaeogeogr Palaeoclimatol Palaeoecol* 40:361–379.
- Wilson JA, D’Emic MD, Ikejiri T, Moacdeih EM, Whitlock JA. 2011. A nomenclature for vertebral fossae in sauropods and other saurischian dinosaurs. *PLoS One* 6:e17114. <https://doi.org/10.11371/journal.pone.0017114>.
- Wynd BM, Peacock BR, Whitney MR, Sidor CA. 2017. The first occurrence of *Cynognathus crateronotus* (Cynodontia: Cynognathia) in Tanzania and Zambia, with implications for the age and biostratigraphic correlation of Triassic strata in southern Pangea. *J Vertebr Paleontol* 37:228–239.
- Yates AM. 2007. The first complete skull of the Triassic dinosaur *Melanorosaurus* Haughton (Sauropodomorpha: Anchisauria). *Spec Pap Palaeontol* 77:9–55.
- Zanno LE, Makovicky PJ. 2011. Herbivorous ecomorphology and specialization patterns in theropod dinosaur evolution. *Proc Natl Acad Sci USA* 108:232–237.